JOURNAL OF NATURAL RUBBER RESEARCH

JOURNAL OF NATURAL RUBBER RESEARCH

Contents

Crosslink Distribution in Vulcanised Blends of NR and EPDM

P.S. BROWN* AND A.J. TINKER*

Blends of NR with EPDM and with a chemically modified EPDM have been investigated using a continuous-wave ¹H NMR spectroscopy technique to determine the crosslink density within the NR phase of the blends. In all cases, the observed crosslink density was higher than in a NR control vulcanisate containing the same level of curatives. The modified EPDM gave blends of superior physical properties, but the modification had little effect on the course of sulphur vulcanisation within the blends.

There is ever increasing technological interest in the use of blends of dissimilar rubbers in order to improve specific vulcanisate properties (e.g. ozone resistance, wear). Unfortunately this can often be at the expense of a reduction in other properties (e.g. modulus, tensile strength) of the compound. In the case of accelerated-sulphur-cured blends of polydiene elastomers with rubbers having a low olefin content [ethylene propylene dienemonomer (EPDM) rubber], the poor strength properties are thought to be a consequence of cure rate incompatibility between the two polymers. The polydiene elastomer is assumed to monopolise the curative chemicals added to the mix, resulting in little if any crosslinking of the EPDM.

There is no data to fully support this thesis in the published literature. A recently published paper[1] described how the crosslink density of the individual components in an incompatible blend can be obtained by analysis of the CW-¹H NMR spectrum of the blend. The spectral line widths are found to increase smoothly with crosslink density. The analysis compares a line width measure for both blend components with data from the single polymer vulcanisates to determine the crosslink densities within the phases of the blend. This paper reports the use of the ¹H NMR spectroscopy technique[1] to study blends of natural rubber (NR) with an EPDM and with a chemically modified EPDM shown by Coran[2] to produce

blends with NR possessing superior tensile properties.

EXPERIMENTAL

The rubbers used in this study were SMR L, EPDM [Intolan 155, an ethylidine norbornene (ENB) EPDM, Enichem, described as having a high iodine number which implies a high degree of unsaturation in the context of EPDM] and a modified Intolan 155 produced according to the method of Coran[2] using 2 p.p.h.r. maleic anhydride and 0.2 p.p.h.r. 2,2′ benzothiazole disulphide. Rubber chemicals were standard commercial-grade materials, solvents of AR grade except for the NMR solvents which were of spectroscopic grade, and the maleic anhydride was used as supplied (Koch Light AR).

The olefin content of Intolan 155 was determined by analysis of its solution state ¹H NMR spectrum (General Electric QE 300 MHz), and found to be 0.5 proton% which equates to 2.5 mol% ENB. The ethylene-propylene ratio was determined by infra-red spectroscopy (Perkin Elmer 377)[3] at 6:4 by weight.

Compounding was performed using a BR-size Banbury mixer, a Hampden Shawbury torque rheometer or a two-roll mill, with curatives added on the two-roll mill. The time to reach maximum torque in a Gottfert Elastograph rheometer was used as the cure time.

* Malaysian Rubber Producers' Research Association, Brickendonbury, Hertford, SG13 8NL, United Kingdom

Samples for NMR analysis were extracted for 4 h in a hot Soxhlet apparatus with methanol and dried to constant weight *in vacuo* at room temperature. These samples were stored at room temperature *in vacuo* in the dark until required. Small slivers ($\sim 15 \times 0.5 \times 3$ mm) were pre-swollen to equilibrium uptake in a minimum of $CDCl_3$ for between 36 h and 60 h in the dark before being cut to fit freely into a 5 mm diameter NMR tube. Fresh $CDCl_3$ doped with $CHCl_3$ as an internal marker and HMDS as an internal lock, was added to cover the sample.

The NMR spectra were obtained using a Perkin-Elmer R24E 90 MHz continuous wave spectrometer interfaced to a BBC microcomputer for computer accumulation of the transients (CAT) to improve the signal to noise ratio. The spectrometer was run at an 80 s sweep of 10 p.p.m. width (11 – 1 p.p.m. downfield of TMS) with between forty and eighty transients combined for each spectrum.

Tensile testing was carried out to *ISO 37* standard.

RESULTS AND DISCUSSION

The modified EPDM when used in blends with NR does improve the tensile properties over those of comparable blends containing Intolan 155, in much the same way as observed by Coran in black filled vulcanisates[2]; thus, the tensile strength increased from 19.7 MPa to 24.3 MPa, and the modulus (M300) from 1.60 MPa to 2.19 MPa *(Table 1)*. If the modified EPDM is mixed with zinc oxide and stearic acid *(Table 2, H)*, a soft, thermoplastic material is produced after heating at 160°C. The modulus of this material is reasonable (M300 = 1.41 MPa), but it rises slowly with extension to give a fairly low tensile strength *(Table 1)*. This material is an ionomer produced by zinc ion crosslinking *via* the pendent succinic acid groups introduced during the modification reaction[2] *(Figure 1)*.

Analysis of the ^1H NMR spectrum of any of the NR-EPDM blends yields information on the crosslinking within the NR phase only. The signals arising from the EDPM protons lie together and overlap with the methyl and methylene signals of the NR, the only remote signal in the spectrum being the NR olefin at a chemical shift of *ca* 5.1 p.p.m. *(Figure 2 Spectrum D)*. Analysis[1] of this signal leads to a measure of line broadness H%. H% increases with increasing crosslink density[1], and H%

TABLE 1. PHYSICAL PROPERTIES

Property	Vulcanisate		
	A	B	C
M300 (MPa)	1.60	2.19	1.41
Tensile strength (MPa)	19.7	24.3	3.27
Extension at break (%)	782	737	595

TABLE 2. FORMULATIONS

Compound	Formulation							
	A	B	C	D	E	F	G	H
SMR	70	70	50	50	100	100	100	–
Intolan 155	30	–	50	–	–	–	–	–
Modified Intolan	–	30	–	50	–	–	–	100
Zinc oxide	5.5	5.5	5.5	5.5	5.0	5.0	5.5	5.5
Stearic acid	2.0	2.0	2.0	2.0	2.0	2.0	2.0	2.0
Sulphur	2.0	2.0	0.5	0.5	0.5	1.0	2.0	–
MBS[a]	0.5	0.5	0.5	0.5	0.5	1.0	0.5	–

[a]Morpholino benzothiazole-2-sulphenamide
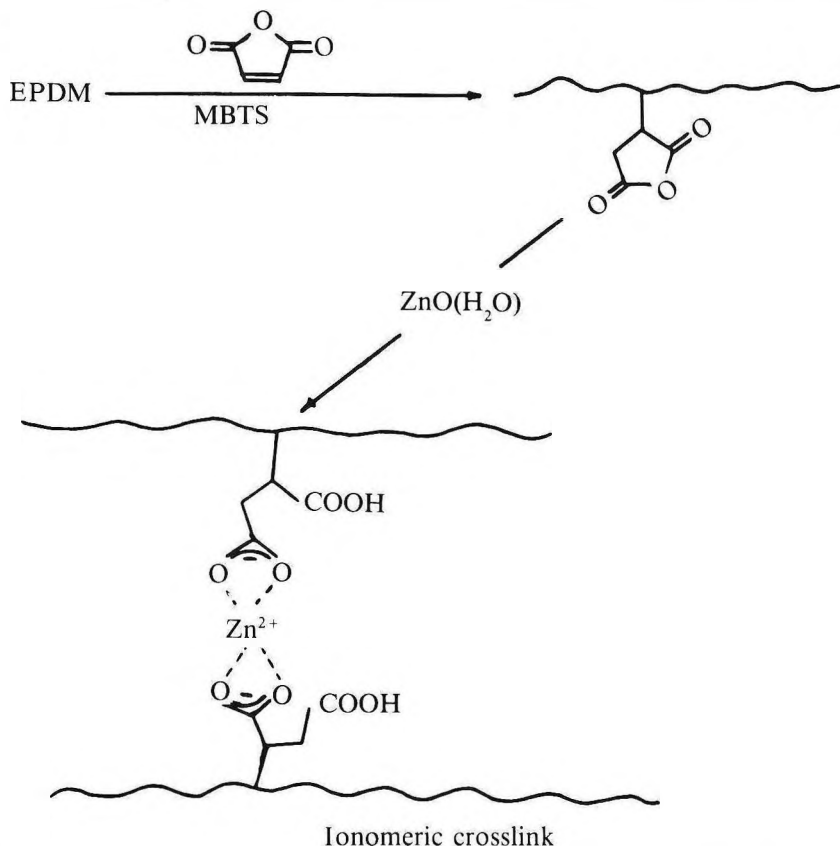
Figure 1. Chemical modification and subsequent ionomer formation in EPDM.

of any of the blends was found to be greater than the H% of the appropriate NR control vulcanisate *(Tables 2* and *3).* H% can be related to the equilibrium volume swelling of the NR, the concentration of physically effective crosslinks or the curative level employed[4]. All NR vulcanisates employing accelerated-sulphur cure systems have been found to have the same H% *Vr* relationship[5,6] so it is possible to equate each H% value observed in vulcanisates to both the crosslink concentration (v) and the amount of sulphur required to produce that crosslink density in a reference cure system *(SV).* The reference system published to-date is sulphur/TMTM (S: TMTM 1:0.4)[4], and both *SV* in terms of this system and v are given in *Table 3. Vulcanisate G,* the NR control vulcanisate for *Blends A* and *B,* is found to have a lower H% value than the blends. The differences represent an increase of 16% and

12% in the crosslink density in the NR phases of *Blends A* and *B* over that in the control. This increase would, for the S/TMTM reference system, represent an increase in curative loading of 22% and 15% respectively.

In NR/NBR blends, the observed uneven crosslink distribution probably arises as a consequence of the solubility parameter difference between the two polymers[4], NBR, the more polar polymer, having a higher concentration of crosslinking intermediates and thus increased crosslink levels. In the NR/EPDM blends, while there are solubility parameter differences possibly favouring NR[2], the major influence on the distribution of crosslinks is probably the concentration of olefin groups in the two polymers (13 530 molm^{-3} for NR *versus* 600 molm^{-3} for the EPDM). The reactivity of the olefin groups of the two polymers is likely

159
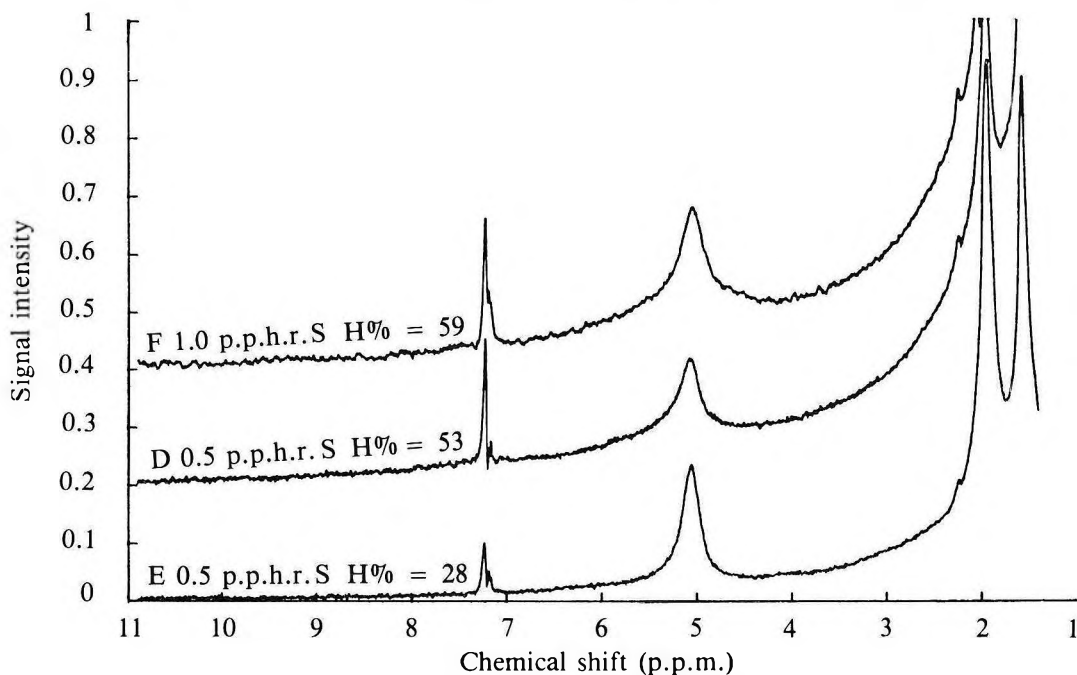
Figure 2. Swollen state ^1H NMR spectrum of Blend D (NR/Mod. EPDM 50:50) and of vulcanisates E and F. The spectra of D and F are offset in intensity for clarity. The signal at 7.2 p.p.m. is the chloroform marker.

to be similar, therefore the rate of crosslinking, and thus the rate of curative utilisation, in the NR phase will be some twenty-two times that in the EPDM phase. This is all the more remarkable since Intolan 155 is described as having a high olefin content. As the NR phase reacts with the crosslinking intermediates their concentration falls, creating a concentration gradient down which cross-linking intermediates formed in the EPDM phase diffuse. Thus, the compounded ingredients are monopolised by the NR components of the blend. In these NR/EPDM blends, the phase sizes were found by phase contrast and differential interference contrast microscopy to be of the order of 1 μ *(Figure 3)* which represents the magnitude of the diffusion distance. Data reported by van Amerongen[7] suggest that the diffusion coefficients *(D)* of the crosslinking agents are likely to be of the order of $10^{-8} cm^2/s$, and the time *(t)* required for the curatives to diffuse X cm is given by:

$$t = (X^2/D) \qquad \qquad ...1$$

Use of *Equation 1* gives $t \backsim 1$ s. This allows ample time for the diffusion of the crosslinking agents from the EPDM to the NR during the vulcanisation of the blends.

Blends A and *B* have a polymer ratio of 7:3 (NR:EPDM), *Blends C* and *D* have a 1:1 polymer ratio and illustrate the consequences of this migration more clearly. NR control *Vulcanisates E* and *F* represent the extreme cases of : 1) no curative migration *(E)* since the curative level is the same as used in the blends; 2) total curative migration to the NR component *(F)* since the curative level is twice that in the blends. Both *Blends C* and *D* show H% values considerably greater than that of the control *Vulcanisate E,* indeed the high values observed are very close to the H% value of control *Vulcanisate F.* The NMR spectra of *Blend D* and vulcanisates *E* and *F* may be compared in *Figure 2.* When these H% values are related to the crosslink concentrations and to the *SV* values, the effect of curative migration is seen to be much more pronounced in *Blends C* and

TABLE 3. NMR DATA

Item	Vulcanisate						
	A	B	C	D	E	F	G
H%	64	62	56	53	28	59	56
ν^a	66.4	64.2	57.3	53.9	25.6	60.7	57.3
SV^b	2.37	2.23	1.93	1.76	1.0	2.10	1.93

[a]Crosslink density mol/m^3 calculated using Equation 2 of Reference 4.

[b]The amount of sulphur required to give the observed H% value if a S/TMTM (1:0.4) system were used, from Figure 3 of Reference 4.
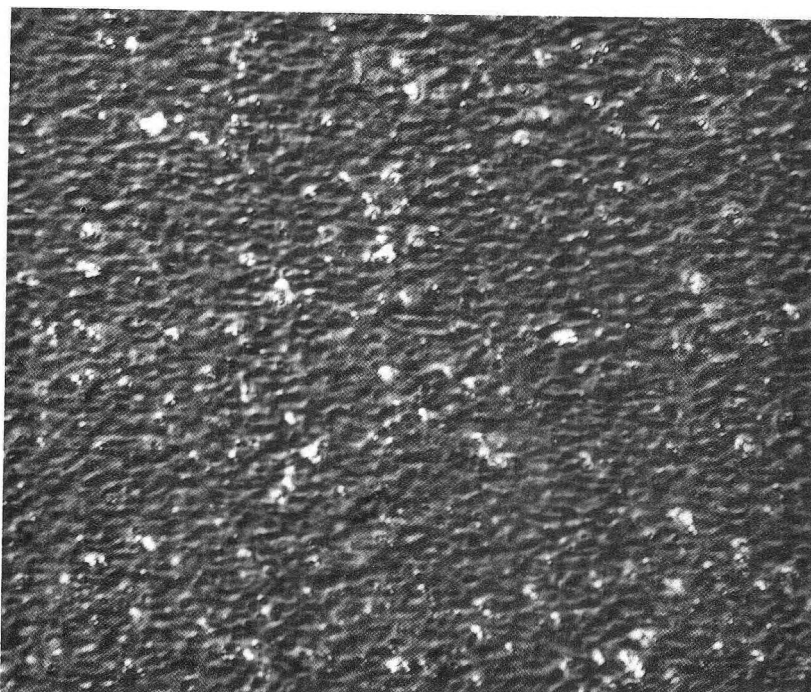
Figure 3. Differential interference contrast light micrograph of Blend A (NR/EPDM 70:30). Field of view 72 × 58 μm. White flecks are zinc oxide particles.

D than in *Blends A* and *B*. The crosslink concentrations in the NR phases of *Blends C* and *D* are actually more than double that in the control *Vulcanisate E*. They are, however, still lower than that in control *Vulcanisate F*. The *SV* values indicate that the NR components of the blends are utilising 84% – 92% of the curatives in the compound, this means that about 80% of the curatives initially located in the EPDM phase are diffusing to the NR phase during vulcanisation.

The higher level of crosslinking attained in the NR phase of an NR/EPDM blend may be undesirable – it can reach levels at which properties in a single polymer vulcanisate would be expected to decline. This should be considered in formulating such blend compounds, and thought should be given to reducing the level of curatives. In order to achieve the degree of crosslinking expected from the level of curatives used, *i.e.* the level that would be obtained in the absence of diffusion of crosslinking agents,

the diffusion of curatives from the EPDM must be considered. If ϕ is the weight fraction of NR in the blend then the proportion of the compounded curatives diffusing from the EPDM is given by the product of this 80% factor and the weight fraction of EPDM $[0.8 \ (1-\phi)]$. This material increases the proportion of the curatives used by the NR phase by $0.8 \ (1-\phi)/\phi$. The increase can be allowed for in compounding if the curative levels are adjusted by a factor of α where:

$$\alpha = 1/\{1 + [0.8 \ (1-\phi)/\phi]\}. \qquad \ldots 2$$

This latter factor may vary with cure system, and should merely be used as a rough guide to the curative levels required. Furthermore, the optimum degree of crosslinking of the NR phase for good physical properties of the blend may lie at a somewhat higher level, due to the near absence of crosslinking in the EPDM phase. Further investigation is required in order to resolve these issues.

At both polymer ratios, the chemical modification of the EPDM results in a small reduction in the observed crosslink levels in the NR phase of the blend, but this is probably too small a reduction to account for the improvement in tensile properties in terms of increased sulphur crosslinking of the EPDM phase. The ionomeric network in the modified EPDM must be responsible for the improvements observed.

CONCLUSIONS

The analysis of swollen rubber vulcanisates, both homopolymer and blends, using ^{1}H NMR spectroscopy has demonstrated the effect of diffusion of crosslinking agents from EPDM to NR during the vulcanisation process. Such diffusion results in elevated crosslink levels in the NR. The magnitude of the effect has been quantified both in terms of the increase in crosslink density within the NR phase (some 14% for a 70:30 NR:EPDM blend, greater than 100% in a 1:1 blend), and in terms of the level of curatives required to produce that amount of crosslinking in a pure NR gum vulcanisate. This latter analysis shows that the NR phase utilises some 80% of the curatives that are expected to reside in the EPDM component. It

is recommended that this factor should be allowed for in compounding such blends, indeed in any blend of polydiene elastomer with an elastomer of low unsaturation. Given such monopolisation of chemicals by one phase, the poor tensile properties of such blends are easily understood.

The use of chemically modified EPDM in NR-EPDM blends results, as reported by Coran[2], in materials of superior tensile properties. The effect of this modification on the vulcanisation chemistry appears to be minimal, at least in terms of the crosslink density observed in the NR component of the blends.

REFERENCES

1. LOADMAN, M.J.R. AND TINKER, A.J. (1989) The Application of Swollen State CW – ^{1}H NMR Spectroscopy to the Estimation of the Extent of Crosslinking in Vulcanized Polymer Blends. *Rubb. Chem. Technol.*, **62**, 234.

2. CORAN, A.Y. (1988) Blends of Dissimilar Rubbers-cure-rate Incompatibility. *Rubb. Chem. Technol.*, **62**, 281.

3. DRUSHEL, H.V. AND IDDINGS, F.A. (1963) Infrared Spectro-photometric Analysis of Ethylene-propylene Copolymers. *Analyt. Chem.*, **35**, 28.

4. TINKER, A.J. (1989) Crosslink Distribution and Interfacial Adhesion in Vulcanized Blends of NR and NBR. Paper 117 presented at a Meeting of the Rubber Division, American Chemical Society, Detroit, Michigan, USA, 1989. *Rubb. Chem. Technol.* (in press).

5. BROWN, P.S. AND TINKER, A.J. (1989) Estimation of the Extent of Crosslinking in the Phases of Vulcanized Rubber Blends by CW – ^{1}H NMR Spectroscopy. Part 2: Scope and Limitations. Presented at International Rubber Conference, Prague, Czechoslovakia 1989.

6. BROWN, P.S. AND TINKER, A.J. (1990) Factors affecting an NMR Technique for the Estimation of Crosslink Density in Rubber Blends. *J. nat. Rubb. Res.*, **5(4)** (in press).

7. VAN AMERONGEN, G.J. (1964) Diffusion in Elastomers. *Rubb. Chem. Technol.*, **37**, 1065.
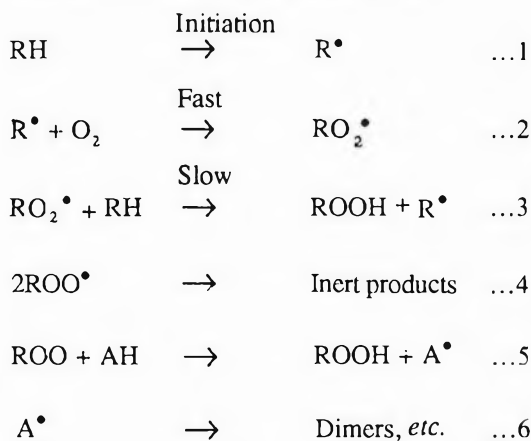
Some New Concepts in the Stabilisation of Polymers

GERALD SCOTT*

Recent research has shown that a variety of antioxidants have the ability to trap alkyl radicals under conditions of rapid radical generation and/or low oxygen pressure [chain-breaking acceptor (CB-A) process]. When the antioxidant has a well characterised oxidised and reduced form, the resulting redox couple may give rise to a catalytic antioxidant effect under certain conditions. Such a CB-A/CB-D catalytic effect has been known to operate in polypropylene during processing and in rubber during fatiguing. It is also believed to account for the high fatigue resistance of sulphur vulcanisates.

The Chain-breaking Mechanism of Antioxidant Action

The classical theory of radical chain anti-oxidation, represented in its simplest form by *Reactions 1–4* suggests that the most important mechanism by which the kinetic chain reaction, *Reactions 2* and *3,* is terminated is by reduction of the alkylperoxyl radical to hydroperoxide by *Reactions 5* and *6* [the chain-breaking donor (CB-D) mechanism]:

$$RH \quad \xrightarrow{\text{Initiation}} \quad R^\bullet \qquad \ldots 1$$

$$R^\bullet + O_2 \quad \xrightarrow{\text{Fast}} \quad RO_2^\bullet \qquad \ldots 2$$

$$RO_2^\bullet + RH \quad \xrightarrow{\text{Slow}} \quad ROOH + R^\bullet \qquad \ldots 3$$

$$2ROO^\bullet \quad \rightarrow \quad \text{Inert products} \qquad \ldots 4$$

$$ROO + AH \quad \rightarrow \quad ROOH + A^\bullet \qquad \ldots 5$$

$$A^\bullet \quad \rightarrow \quad \text{Dimers, } etc. \qquad \ldots 6$$

This mechanism which was originally proposed by Lowry[3] and subsequently elaborated by Bolland and co-workers[4,5] explains many antioxidant processes in liquid substrates at ambient oxygen pressures[6]. However, Bateman[7] in an elegant study of the effect of oxygen pressure on the termination reaction showed that in liquid hydrocarbons such as linoleic esters at low oxygen pressure, *Reaction 7* and even *Reaction 8* may be more important than *Reaction 4:*

$$R^\bullet + ROO^\bullet \quad \rightarrow \quad ROOR \qquad \ldots 7$$

$$2R^\bullet \quad \rightarrow \quad R\text{–}R \qquad \ldots 8$$

Reactions 7 and *8* become increasingly important when the alkyl radical R· is tertiary or is stabilised by electron delocalisation, e.g. in the alkenyl radical (I)[7]:
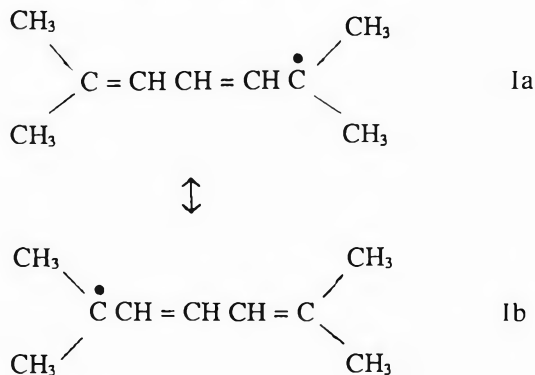
It has been known for many years that some oxidising agents can also be antioxidants[7] and in particular, quinones have been shown to be anti-fatigue agents in rubbers[8]. No entirely satisfactory explanation has been advanced to explain this observation. More recently,

*Department of Chemical Engineering and Applied Chemistry, Aston University, Aston Triangle, Birmingham B4 7ET, United Kingdom

Henman[9] has shown that some oxidation products of the phenolic antioxidant BHT(I) are much more effective than the parent phenol as processing antioxidants for polypropylene. The quinonoid compounds II – IV *(Table 1)* are all formed from BHT under autoxidising conditions and it can be seen that all are much more effective than BHT itself.

Chain-breaking Acceptor (CB-A) Antioxidants

The essential difference between the conditions to which a polymer is subjected during processing and during accelerated heat ageing is that during processing a) the polymer is subjected to high mechanical strain (shear) which leads to scission of a small proportion of the polymer chains, and b) air is deliberately excluded to avoid undue oxidation. Both of these conditions favour termination through alkyl radicals and in a more detailed study of the chemical transformations occurring with one of the above antioxidants, galvinoxyl, (II) Bagheri *et al.* [10,11] observed that galvinoxyl, G·, was substantially reduced to the corresponding phenol during the initial period when the shear in an internal mixer was highest. It was concluded that this was due to oxidation of macroalkyl radicals by galvinoxyl *(Scheme 1)* and indeed it was found that as G· disappeared from the system, GII(V) was formed almost
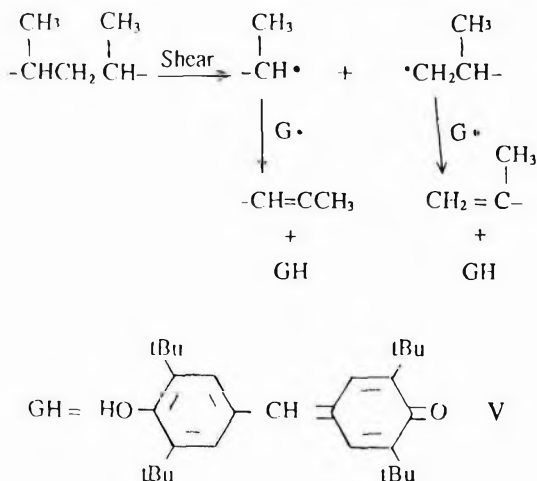
Scheme 1

The chain-breaking acceptor (CB-A) antioxidant mechanism

quantitatively *(Figure 1),* together with olefinic unsaturation *(Figure 2).* However, a surprising feature was the subsequent partial regeneration of G· and the reciprocal disappearance of hydrogalvinoxyl (GH). This suggested that the oxidised and reduced forms of the antioxidant are both relatively stable and are capable of deactivating whichever of the chain propagating radicals is present in highest concentration in the system. This amounts to a catalytic antioxidant process *(Scheme 2)* and by chemical
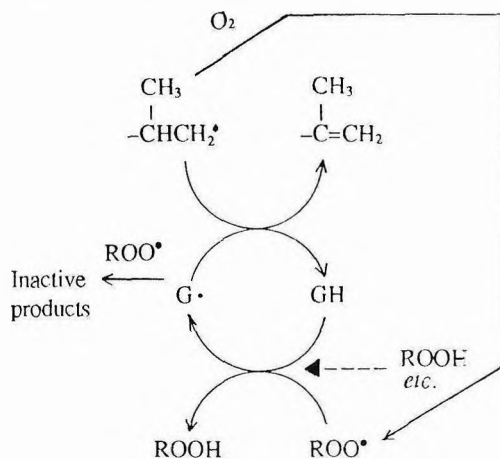
Scheme 2

Catalytic mechanism of galvinoxyl (G·)

measurement of the unsaturation formed in the polymer it was concluded that one galvinoxyl radical is able to deactivate approximately fifty radicals in the polymer melt before it is destroyed by oxidation *(Reaction 9)* and the normal propagation process involving oxygen intervenes:

... 9
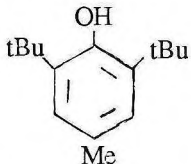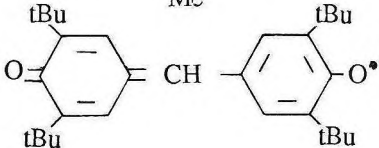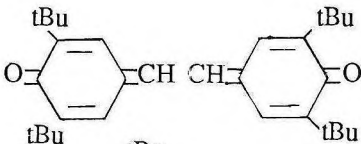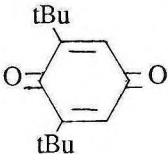
TABLE 1. MECHANO-ANTIOXIDANT EFFECTIVENESS
OF BHT TRANSFORMATION PRODUCTS IN POLYPROPYLENE DURING PROCESSING

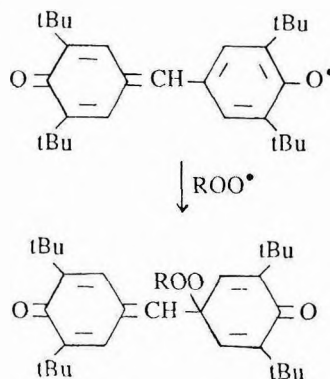| BHT transformation product		ΔMFI (m.mol kg^{-1})	
		4.5	0.5
(structure)	I, BHT	100	270
(structure)	II, G·	45	45
(structure)	III, SQ	50	60
(structure)	IV, BQ	55	65

An interesting consequence of the above complementary oscillation of the concentration of oxidised and reduced species during the processing operation is that the heat ageing activity of the antioxidant depends on processing time[12]. The stability of the polymer is linearly related to the concentration of GH after processing. It therefore also oscillates with processing time. From this, it can be concluded that G· itself has relatively poor thermal antioxidant activity and that the CB-D antioxidant process due to GH predominates. The most likely reason for this is that G· cannot compete with oxygen for alkyl radicals when the latter is present in large excess in polypropylene *(Reaction 10)*:

$$R\bullet \begin{array}{c} \nearrow \ O_2 \ RO\dot O \quad \text{Propagation} \\ \searrow \ G\bullet \ C=C + GH \quad \text{Inhibition} \quad \ldots 10 \end{array}$$
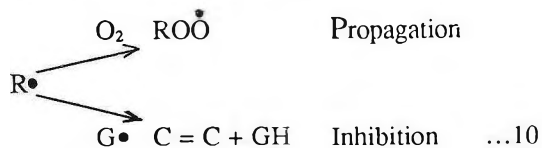
It may also be destroyed directly by oxygen.

Nitroxyl Radicals as Catalytic Antioxidants

Other redox systems with stable oxidised and reduced states can act as melt stabilisers for polyolefins during processing[13]. *Table 2* shows that the inorganic redox systems, Cu^{2+} / Cu^+ and $I\cdot/I^-$ are effective processing stabilisers. They have limited practical utility, however, since the former is a powerful catalyst for oxidation of polymers under oven-ageing conditions (copper ions catalyse the radical decomposition of hydroperoxides and I_2 and HI are readily lost by volatilisation). However, CuI is an effective thermal antioxidant for polyamides and it seems likely that both the copper and the iodine are participating as catalytic chain-breaking antioxidants in this system. Nitroxyl radicals are much more important catalytic antioxidants in polymers[13,14]. Not only are they effective melt stabilisers for polypropylene[13-17] *(Table 2)* but they are also photo-antioxidants[14,16] and the aromatic nitroxyls are anti-fatigue agents for
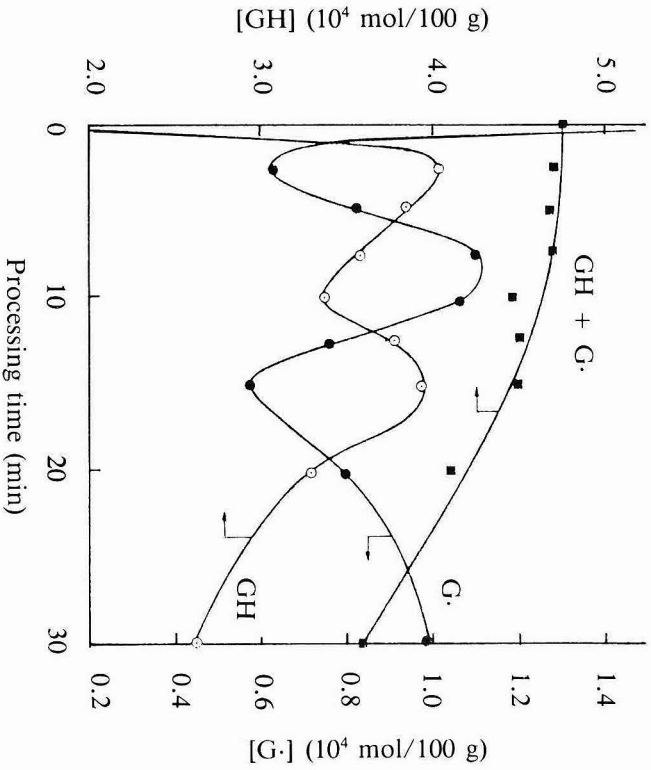
Figure 1. Changes in G· and GH concentrations in polypropylene during processing at 200°C. Initial G· = 4.74 × 10⁻⁴ mol/100 g. (After References 10 and 11)
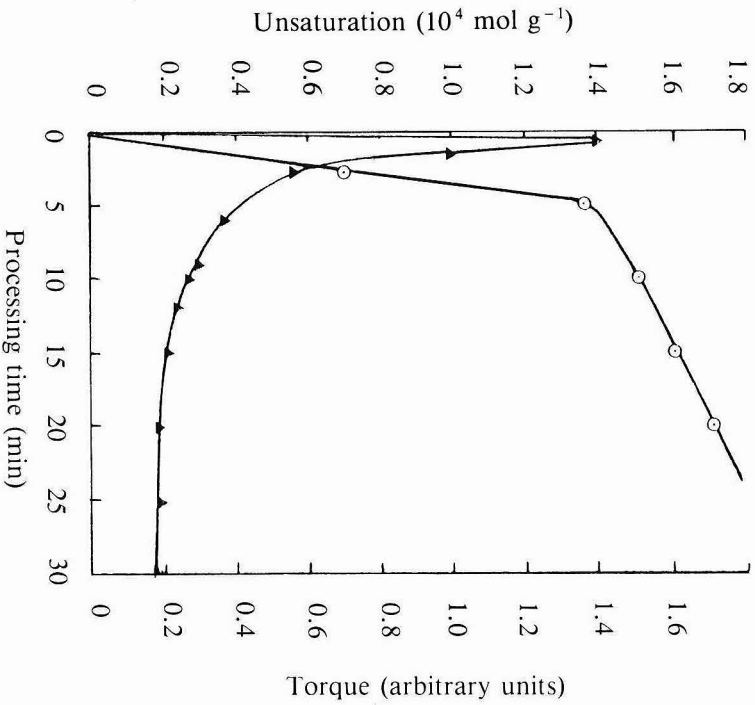
Figure 2. Relationship between the formation of unsaturation and the applied torque during processing of polypropylene at 200°C. Initial G· = 4.75 × 10⁻⁴ mol/100 g. (After References 10 and 11)

natural rubber[14,18]. Hindered piperidinoxyls (e.g. VI) undergo the same kind of complementary oscillation reactions with the conjugate hydroxylamine in polypropylene as does galvinoxyl *(Scheme 3)*[13-17]
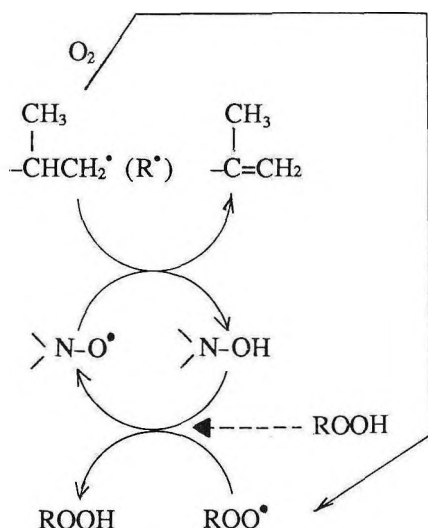
Scheme 3

Catalytic mechano-antioxidant activity of nitroxyls

and again the nitroxyl is ineffective in the presence of excess air[16]. The oscillatory cycle can be reproduced by computer simulation by introducing the appropriate rate constants for the individual steps and assuming a low rate of oxygen ingress to the mixer[13]. *Table 2* shows that the aromatic nitroxyls (VII) are also effective melt stabilisers for polypropylene and a study of a variety of nitroxyls in model systems by Berger and co-workers[19] has shown that they all have catalytic activity, their effectiveness depending on the structure of the autoxidising medium. In general, the more oxidisable the substrate, the higher is the stoichiometric inhibition coefficient f^*, in the system.

Nitroxyl Radicals as Anti-fatigue Agents for Rubbers

Aromatic p-phenylene diamines (VIII) are the longest established and most widely used
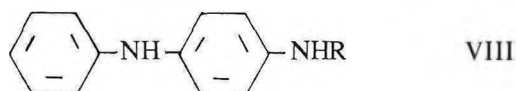
class of antioxidants in vulcanised rubbers. Their success derives from the fact that they are not only heat ageing antioxidants but they are also effective anti-fatigue agents and anti-ozonants[20]. The reason for their almost unique activity under conditions of mechanical stress has been in the past a cause of considerable puzzlement to antioxidant chemists, although it has been recognised that fatigue differs from thermal oxidation processes in that a small but mechanically significant number of rubber chains are subjected to stresses in excess of those required to break carbon-carbon bonds in the polymer backbone[21,22] *(Reaction 11)*. This gives rise to macroalkyl radicals in the polymer substrate:
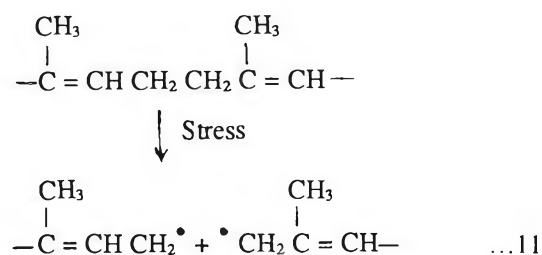
Under conditions of oxygen saturation the macroalkyl groups produced in *Reaction 11* will be converted rapidly to alkylperoxyl, *Reaction 12* and then to hydroperoxides

167
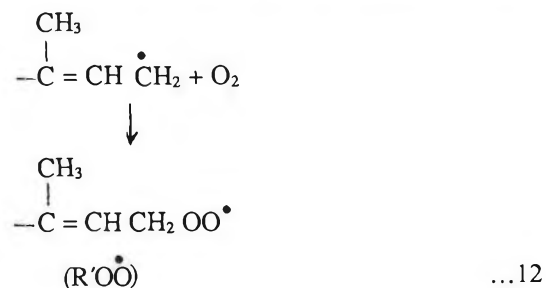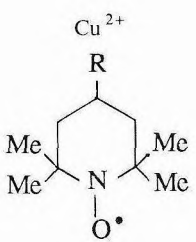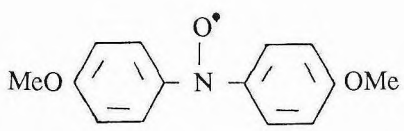
TABLE 2. REDOX SYSTEMS AS MECHANO-ANTIOXIDANTS FOR
POLYPROPYLENE DURING PROCESSING[13]

CB-A	CB-D	MFI (m.mol kg^{-1})	
		4.5	0.5
I$^{\bullet}$	HI	45	50
Cu^{2+}	Cu$^+$	40	80
VI	>N–OH	–	55
VII	>N–OH	–	45
BHT		100	270

by the parent amine *(Scheme 4).* The resulting arylaminyl radicals, IX, are highly reactive and can undergo two alternative reactions giving either oligomers (e.g. Xa,
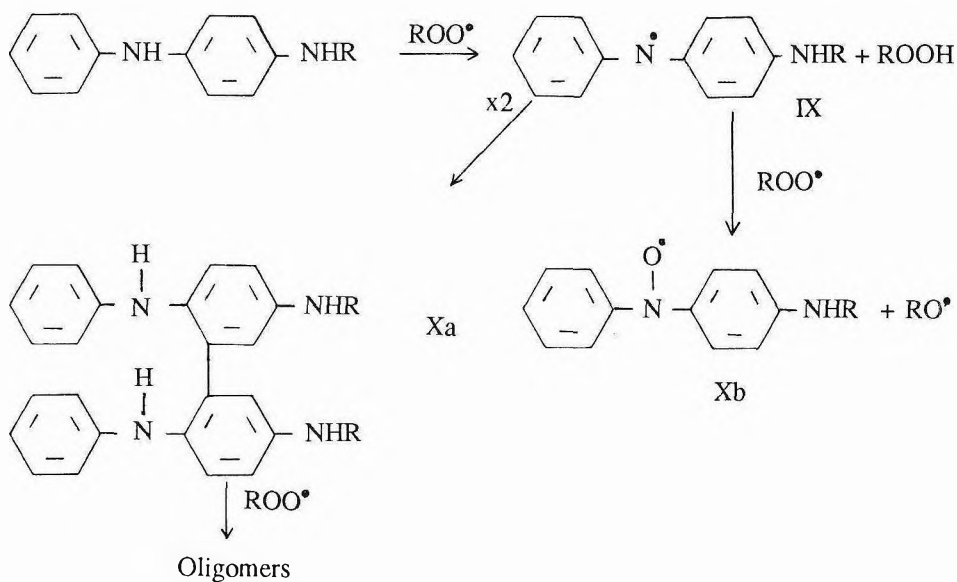
Scheme 4

Alternative transformation products of N-alkyl-p-phenylene diamines in the presence of alkylperoxyl radicals

Scheme 4) or the corresponding nitroxyl radical (Xb)[23].

Katbab and Scott[24] studied the formation of radicals in vulcanised NR by ESR. Both alkylperoxyl radicals and nitroxyl radicals are formed rapidly under dynamic stress in a Monsanto fatigue to failure tester *(Figure 3)*. The peak in the alkylperoxyl concentration occurs before substantial amounts of nitroxyl are present, confirming the sequence of events given in *Scheme 4*. The nitroxyl concentration also goes through a maximum, decaying away to a stationary state.

If, instead of arylamine, a nitroxyl (XI, R = O·) was used, this was substantially unreacted after compounding but after vulcanisation only about 1% could be detected[25]. The remainder was transformed to a mixture of the free hydroxylamine, XI, R = OH and the parent amine (XI, R = H):

$$MeO-\langle\ \rangle-\underset{N}{\overset{R}{|}}-\langle\ \rangle-OMe$$

XI
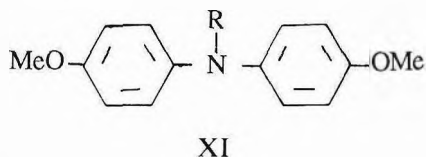
The nitroxyl concentration in the rubber remained sensibly constant during fatiguing but only a small fraction of nitroxyl originally added could be measured until the failure of the rubber sample, when it increased rapidly and the arylamine and hydroxylamine concentrations decayed. It appears then that the amine (XI, R = H), the nitroxyl (XI, R = O·) and the hydroxylamines, XI, R = OH and R = OP (where P is the polymer)
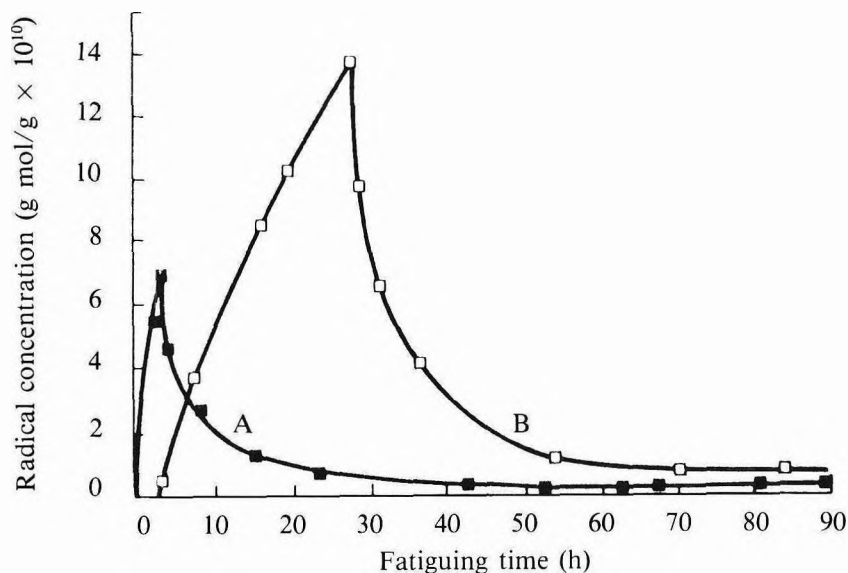
Figure 3. Formation of alkylperoxyl (A) and nitroxyl (B) during the fatiguing of NR in the presence of IPPD.
(After Reference 24)

are interconvertable during fatiguing although not indefinitely so due to side

reactions[25]. The cyclical mechanism proposed is summarised in *Scheme 5*.
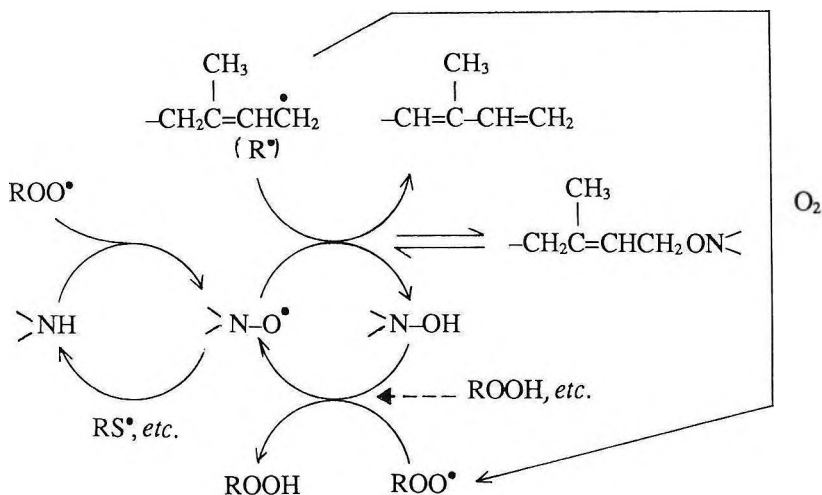
Scheme 5

Oxidation and reduction mechanisms involved in the anti-fatigue activity of aromatic amines (NH)

The analogy to the catalytic mechanism of nitroxyl radicals in polypropylene discussed above is obvious. It should follow from *Scheme 5* that the nitroxyl (>N-O·) and hydroxylamine (>NOH) should be as effective as the parent amine as anti-fatigue agents. *Table 3* compares the activity of some typical aromatic amines and their oxidation products.
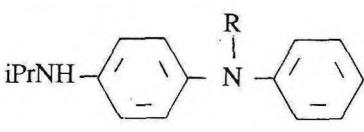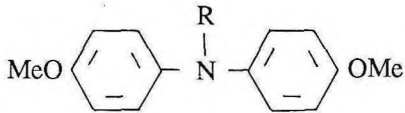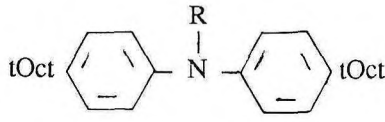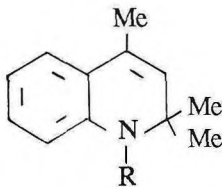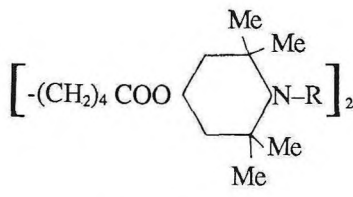
Only nitroxyls and hydroxylamines derived from amines with high anti-fatigue agents were found to be effective anti-fatigue agents themselves and indeed these were more effective than the amines from which they were derived, indicating that side reactions may reduce conversion to anti-fatigue-active agents compared to the nitroxyls themselves. Nevertheless, the reduction of the nitroxyls to the corresponding amines appears to play an essential part in the mechanism of the anti-fatigue activity of the nitroxyls since amines

without antioxidant activity (notably XIV, R = H) and their derived nitroxyls (R = O·)

XIV
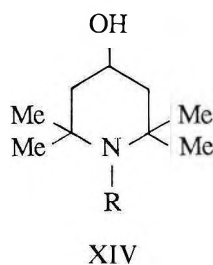
have no significant anti-fatigue activity[26] *(Table 3)* although the nitroxyls are effective mechano-antioxidants in unvulcanised rubber[24]. It was concluded that the sulphur species present in vulcanised rubber reduce the nitroxyls to the corresponding amines which unlike the aromatic amines are not antioxidants and cannot participate in *Scheme 5*.

TABLE 3. FATIGUE LIVES OF NR VULCANISATES CONTAINING AMINES
AND THEIR DERIVED OXIDATION PRODUCTS[25,26]

Additive		Fatigue life (h)		
		R = H	O·	OH
iPrNH—⟨ ⟩—N(R)—⟨ ⟩	VIII	273	337	–
MeO—⟨ ⟩—N(R)—⟨ ⟩—OMe	XI	207	411	55[a]
tOct—⟨ ⟩—N(R)—⟨ ⟩—tOct	XII	83	88	107
(quinoline structure with Me, Me, Me, N–R)	XIII	53	56	55
[-(CH₂)₄COO— ⟨ ⟩ N–R]₂ (with Me, Me, Me, Me)		25	30	
Control (no additive)			21	

[a] Insoluble in rubber. Bloomed to the surface.

Oxidation of *cis*-polyisoprenyl radicals by nitroxyl to give unsaturated conjugation *(Reaction 13)* appears to take place even at ambient temperatures[27].

$$-\overset{\overset{\displaystyle CH_3}{|}}{C}=CH\ \overset{\bullet}{C}H\ CH_2\ \overset{\overset{\displaystyle CH_3}{|}}{C}=CH- \quad \xrightarrow{>NO^\bullet} \quad -\overset{\overset{\displaystyle CH_3}{|}}{C}=CH\ CH=CH\ \overset{\overset{\displaystyle CH_3}{|}}{C}=CH- \ +\ >NOH \qquad ...13$$
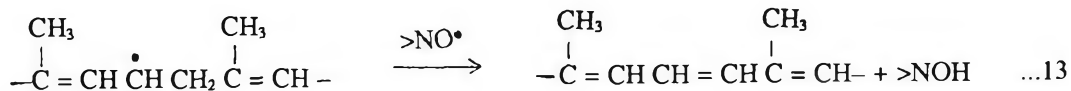
This reaction is driven by the conjugation energy generated by loss of the hydrogen and this reaction is much more facile than that involved in polyolefins where the main reaction at ambient temperatures is believed to be radical pairing.

Spin Traps as Anti-fatigue Agents

A variety of spin traps, which give rise to nitroxyl radicals in the presence of alkyl radicals, have been found to be effective mechano-antioxidants (processing stabilisers) for polyolefins[15, 28]. Typical are the nitroso-tert-alkanes (e.g. XV), aromatic nitroso compounds (e.g. XVI) and the nitrones (e.g. XVII).

All of them give rise to nitroxyl radicals in polypropylene during processing and it was considered by analogy that they should have anti-fatigue activity in rubbers[15]. Variation of the structure XVII showed that when X = H and R_1 = alkyl, the nitrones are devoid of significant activity. When X = OH, however, significant activity was found although not as high as the 4-alkylaminodiphenyl nitroxyls *(Table 4)*[29]. Although all of the additives in *Table 4* gave nitroxyl radicals during processing in NR, they were not chemically attached to the polymer. This coupled with the lack of anti-fatigue activity of the nitrones without hydroxyl groups suggests that the mechanism of formation of nitroxyl involves oxidation of the phenolic group by alkylperoxyl rather than reduction by alkyl;

$$(CH_3)C - N = O$$

XV

XVI

XVII

XVIII

$$\downarrow ROO^{\bullet}$$
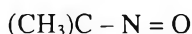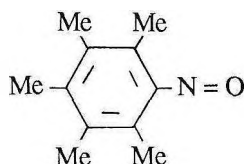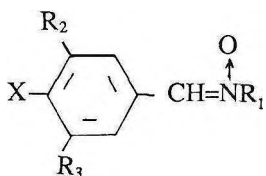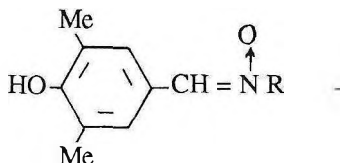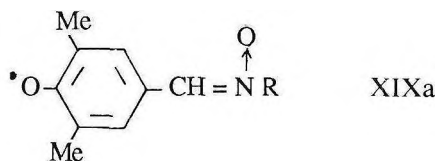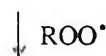
  XIXa

$$\updownarrow$$
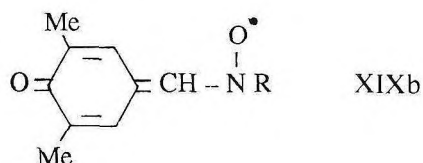
  XIXb

TABLE 4. ANTI-FATIGUE ACTIVITY OF BENZALNITRONES (XVII)

XVII				Time to fatigue failure, JIS average (h)
X	R₁	R₂	R₃	
H	tBu	H	H	26
OH	tBu	H	H	30
Cl	iPr	H	H	37
OMe	iPr	H	H	33
OH	tBu	Me	Me	110
OH	iPr	Me	Me	130
OH	Et	Me	Me	93
OH	Me	Me	Me	80
H	Me	H	H	29
IPPD				270
Control				20

However, no phenoxyl radicals were detected by ESR indicating that the radical produced is more correctly represented by XIXb than XIXa. However, there seems little doubt that the same cyclic mechanism is involved as in the case of the aromatic nitroxyls *(Scheme 6)*[18,29].
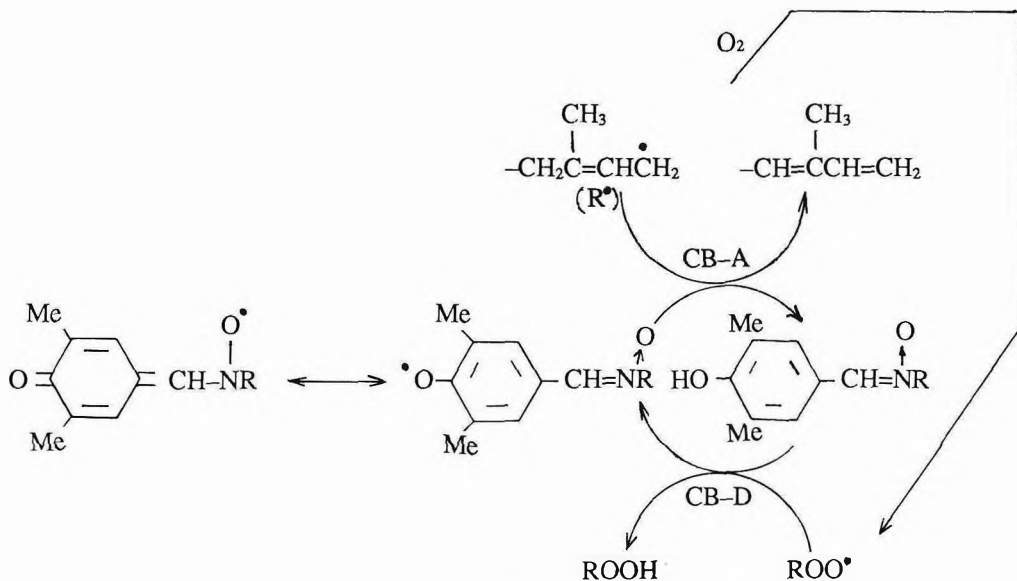
Scheme 6

Proposed anti-fatigue mechanism for the 4-hydroxy benzalnitrones (XVIII) in NR[29].

As might be expected, the aliphatic nitroso compounds provide little anti-fatigue activity but the aromatic nitroso compounds are more effective. In particular 4-nitroso-diphenylamine
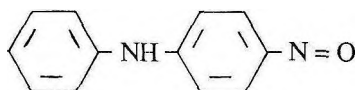
XX

(XX) has been shown to give a high level of bound nitroxyl under certain conditions and this adduct imparts anti-fatigue activity to NR. Furthermore, it is resistant to solvent extraction or loss by migration from the rubber and under these conditions it is much more effective than IPPD as an anti-fatigue agent.[30].

'Stable' Sulphur Radicals as Anti-fatigue Agents

The ability of sulphur vulcanisates to resist fatigue has been recognised for many years but the reason for this has not so far been clarified. It has been proposed[31,32] that under the influence of strain, S-S cross-links can undergo scission with subsequent recombination and shortening of the polysulphide cross-link. This explanation does not, however, adequately explain the effects of sulphur compounds added to a peroxide vulcanisate[8,18,33]. *Table 5*

shows that low molecular weight mono- and disulphides, DLTP and DLPDS are very effective anti-fatigue agents when added to a peroxide vulcanisate[33].

$$(C_{12} H_{25} O CO CH_2 CH_2)_2 S$$

DLTP

$$(C_{12} H_{25} O CO CH_2 CH_2 S)_2$$

DLPDS

$$(C_{12} H_{25} O CO CH_2 CH_2)_2 S-O$$

DLSP

The former is oxidised readily by hydroperoxides to the corresponding sulphoxide, DLSP, and then was found to be more effective than DLTP. Sulphoxides are known to be thermally unstable and break down to give sulphinic acids and olefins[34,35]. It seems likely then that alkyl sulphides, whether part of a rubber vulcanisate or added as additives give rise to sulphinyl radicals which are known traps for macro-alkyl radicals[36], thus inhibiting the conventional radical chain reaction *(Scheme 7)*. Although the sulphinyl radical is continuously reformed in *Scheme 7*, the overall process is not very efficient because sulphinyl radicals can disappear in other ways, particularly by

TABLE 5. FATIGUE LIVES OF PEROXIDE CURED NR WITH
ADDED SULPHUR COMPOUNDS

Additive concentration (g/100g)	Improvement in fatigue life relative to control (%)		
	DLTP	DLSP	DLPDS
0.5	95	105	133
1.0	127	157	293
2.0	166	209	380

dimerisation to thiosulphinates *(Scheme 7)*. However, in a sulphur vulcanisate there is a large reservoir of sulphides and hence of

sulphuryl radicals. They are also formed readily from partially oxidised polysulphides by further oxidation and thermolysis[37].
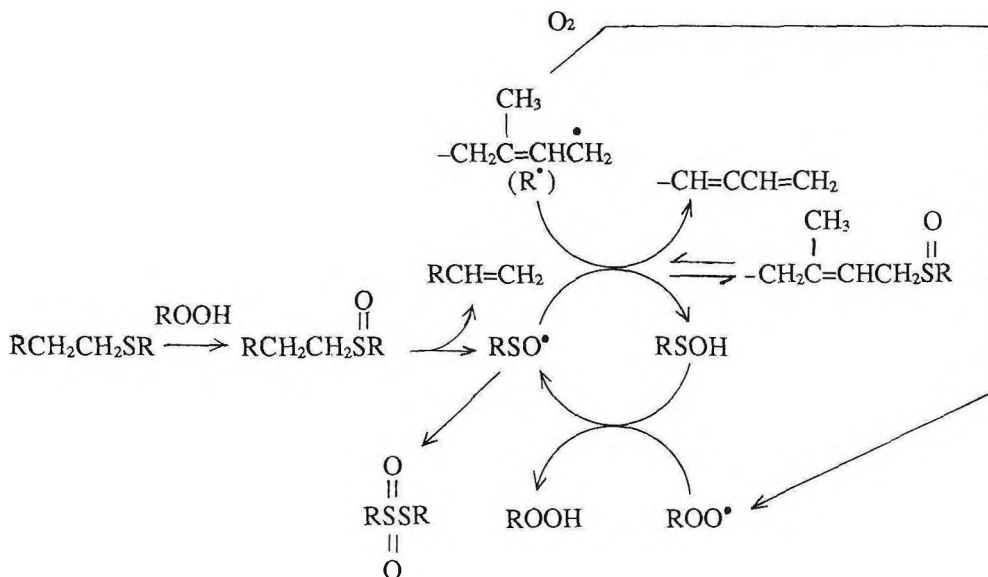
Scheme 7

Proposed mechanism for fatigue inhibition by sulphur compounds.

CONCLUSION

The concept that some antioxidants could act both as chain-breaking donors and chain breaking acceptors in a catalytic mechanism arose simultaneously in three quite different areas of polymer technology. The idea proved to be seminal and further work has shown the essential unity of the mechanism in the stabilisation of thermoplastics in the melt during processing, in the photo-stabilisation of the thermoplastics and in fatigue prevention in rubbers.

Polymer stabilisation technologists have in the past tended to believe that their own medium is unique and that stabilisation data can rarely be transferred between technologies. The studies reviewed above indicate that, provided certain basic similarities and differences are recognised, of which the most important are oxygen concentration at the site

of oxidation and the chemical structure of the substrate, then the common chemistry of catalytic antioxidant action can be transferred across technological boundaries to the ultimate benefit of all polymer technologies[10].

It seems likely then that other examples of the CB-A/CB-D catalytic mechanism will be recognised and exploited in the future in rubbers. The potential application of the mechanism to sulphur vulcanisates has been mentioned in this review, but the possibility of optimising it remains unexplored. It seems likely that the sulphide cross-links found in conventional sulphur vulcanisates are not the ideal structures to give optimum antioxidant activity. A fundamental re-appraisal of the sulphur-accelerator curing system from the standpoint of both heat aging and fatigue could be very beneficial. In the long-term, it may be necessary to consider removing sulphur from

the cross-link altogether and replacing it by sulphur-containing and other antioxidants with catalytic activity in order to independently control the cross-linking and antioxidant processes.

Date of receipt: January 1990
Date of acceptance: April 1990

REFERENCES

1. GRASSIE, N. AND SCOTT, G. (1985) *Polymer Degradation and Stabilisation*, p. 120. Cambridge University Press.

2. LOWRY, C.D. (1936) *J. Electrochem.*, **69**, 185.

3. LOWRY, C.D., EGLOFF, G., MORRELL, J.G. AND DRYER, C.G. (1933) Correlation of Inhibiting Action and Oxidation-reduction Potential. *Ind. Engng Chem.*, **25**, 804.

4. BOLLAND, J.L. AND TEN HAVE, P. (1947) The Inhibitory Effect of Hydroquinone on the Thermal Oxidation of Ethyl Linoleate. *Trans. Faraday Soc.*, **43**, 201.

5. BOLLAND, J.L. AND TEN HAVE, P. (1947) The Inhibitory Effect of Phenolic Compounds on the Thermal Oxidation of Ethyl Linoleate. *Discuss. Faraday Soc.*, **2**, 252.

6. SCOTT, G. (1965) *Atmospheric Oxidation and Antioxidants*, Chap. 4. Elsevier.

7. BATEMAN, L. (1954) *Q. Rev.*, **8**, 147.

8. KATBAB, A.A., OGUNBANJO, A. AND SCOTT, G. (1985) *Polym. Deg. and Stab.*, **12**, 333.

9. HENMAN, T.J. (1979) *Developments in Polymer Stabilisation-1 (Scott, G. ed.)*. Applied Science Publisher.

10. BAGHERI, R., CHAKRABORTY, K.B. AND SCOTT, G. (1980) Mechanisms of Antioxidant Action: the Role of Galvinoxyl as a Melt Stabiliser for Polypropylene. *Chemy Ind.*, 865.

11. BAGHERI, R., CHAKRABORTY, K.B. AND SCOTT, G. (1983) *Polym. Deg. and Stab.*, **5**, 145.

12. BAGHERI, R., CHAKRABORTY, K.B. AND SCOTT, G. (1983) *Polym. Deg. and Stab.*, **5**, 197.

13. SCOTT, G. (1989) *Makromol. Chem., Macromol. Symp.*, **27**, 1.

14. SCOTT, G. (1984) *Developments in Polymer Stabilisation-7 (Scott, G. ed.)*, p.65. Elsevier Applied Science.

15. CHAKRABORTY, K.B. AND SCOTT, G. (1984) *J. Polym. Sci. (Polym. Sci. ed.)*, **22**, 553.

16. BAGHERI, R., CHAKRABORTY, K.B. AND SCOTT, G. (1982) *Polym. Deg. and Stab.*, **4**, 1.

17. AL-MALAIKA, S., OMIKOREDE, E.O. AND SCOTT, G. (1986) *Polym. Comm.*, **27**, 173.

18. SCOTT, G. (1985) A Review of Recent Developments in the Mechanisms of Anti-fatigue Agents. *Rubb. Chem. Technol.*, **58**, 269.

19. BERGER, H., BOLSMAN, T.A.B.M. AND BROUWER, D.M. (1983) *Developments in Polymer Stabilisation-6 (Scott, G. ed.)*, p.1. Applied Science Publisher.

20. SCOTT, G. (1965) *Atmospheric Oxidation and Antioxidants*, Chap. 10. Elsevier.

21. POTTER, W.D. AND SCOTT, G. (1971) *Eur. Polym. J.*, **7**, 489.

22. KUZMINSKY, A.S. (1981) *Developments in Polymer Stabilisation-4 (Scott, G. ed.)*, p.7. Applied Science Publisher.

23. POSPISIL, J. (1984) *Developments in Polymer Stabilisation-4 (Scott, G. ed.)*, p.1. Elsevier Applied Science.

24. KATBAB, A.A. AND SCOTT, G. (1980) Mechanisms of Antioxidant Action: Nitroxyl Radicals in the Stabilisation of Rubber against Mechano-chemical Degradation. *Chemy Ind.*, 573.

    KATBAB, A.A. AND SCOTT, G. (1981) *Polym. Deg. and Stab.*, **3**, 221.

25. DWEIK, H.S. AND SCOTT, G. (1984) Mechanisms of Antioxidant Action: Aromatic Nitroxyl Radicals and their Derived Hydroxylamines as Anti-fatigue Agents for Natural Rubber. *Rubb. Chem. Technol.*, **57**, 735.

26. NETHSINGHE, L.P. AND SCOTT, G. (1984) Mechanisms of Antioxidant Action: Complementary Chain-breaking Mechanisms in the Mechano-stabilisation of Rubbers. *Rubb. Chem. Technol.*, **57**, 918.

27. NETHSINGHE, L.P. AND SCOTT, G. (1984) The Role of Nitroxyl Radicals as Chain-breaking Acceptor Antioxidants in the Mechano-degradation of Rubber. *Eur. Polym. J.*, **20(3)**, 213.

28. CHAKRABORTY, K.B., SCOTT, C. AND YAGHMOUR, H. (1985) *J. appl. Polym. Sci.*, **30**, 189.

29. NETHSINGHE, L.P AND SCOTT, G. (1984) Mechanisms of Antioxidant Activity of 'Spin-traps' in Rubber. *Rubb. Chem. Technol.*, **57**, 779.

30. NOUSHIN, H. AND SCOTT, G. Unpublished Data.

31. KUZMINSKY, A.S. (1981) *Developments in Polymer Stabilisation-4 (Scott, G. ed.)*, p.92. Applied Science Publisher.

32. RUSSELL, R.M. (1969) Changes in the Chemical Structure of Natural Rubber Tyre Vulcanisates in Service. *Br. Polym. J.*, **1**, 53.

33. COKER, M.S.S. SCOTT, G. AND SWEIS, H.A.A. (1982) *Polym. Deg. and Stab.,* **4,** 333.

34. SCOTT, G. (1981) *Developments in Polymer Stabilisation-4 (Scott, G. ed.),* p.1. Applied Science Publisher.

35. SCOTT, G. (1983) *Developments in Polymer Stabilisation-6 (Scott, G. ed.),* p.29. Applied Science Publisher.

36. ARMSTRONG, C. AND SCOTT, G. (1971) *J. Chem. Soc. B.,* 1747.

37. ARMSTRONG, C., HUSBANDS, H.J. AND SCOTT, G. (1979) Mechanisms of Antioxidant Action: Antioxidant-active Products formed from the Dialkyl Thiodipropionate Esters. *Eur. Polym. J.,* **15,** 241.

Slow Crystallisation of Natural Rubber Latex

G.D. WATHEN* AND A.N. GENT**

Samples of natural rubber latex (with ethylene glycol added to prevent freezing) did not crystallise to a measurable extent on standing for one week at - 29°C. In contrast, coagulated latex rubber has a half-life of crystallisation of only about 2 h at this temperature and purified solid rubber has a half-life of only about 8 h. It is concluded that latex rubber particles, about 0.5 μm in diameter, crystallise more than one hundred times slower than solid rubber, probably because crystal nuclei are relatively scarce in rubber, with a concentration of less than one nucleus in fifty latex particles or in 10^6 rubber molecules.

In a classical experiment, Cormia *et al.*[1] showed that relatively few drops of molten polyethylene, about 3 – 5 μm in diameter, crystallised on cooling to 100°C. Under the same circumstances, bulk polyethylene crystallises rapidly. They deduced that crystallisation is initiated by nuclei that are relatively scarce and thus unlikely to be found in small isolated drops of the polymer. This observation suggests a method of measuring the concentration of crystal nuclei and hence inferring something of their nature, a still rather obscure aspect of polymer crystallisation. But, as far as the present authors are aware, no comparable observations have been reported for other polymers. Some experiments with natural rubber (*cis*-1, 4-polyisoprene) are described here.

The exact nature of crystal nuclei is unclear. It has been suggested that particularly long molecules crystallise first in pure polymers, and then serve as nuclei for the rest[2]. In most cases, it seems likely that foreign inclusions act as nuclei[3,4]. For example, it has been shown that natural rubber usually contains crystallisation catalysts, and that small amounts of stearic or linoleic acid have the same effect, accelerating crystallisation by a factor of about five at the temperature[5] where crystallisation is fastest, - 25°C. Particles of various solids are reported to increase the number of crystal nuclei in nylon 6, by factors of three to ten[6].

A successful nucleating agent must have several attributes. It must be solid, wetted by the polymer but not soluble. Also, it must be crystalline, with at least one crystal face similar in lattice spacing to the polymer crystal so that the polymer molecules can employ the foreign particle as a base for crystallisation.

On the other hand, the mechanism of homogeneous nucleation is not at all clear. In this case, spontaneous aggregation of polymer molecules into a crystalline assembly occurs by chance. The question arises whether crystallisation in pure polymers is ever homogeneous or if it is always catalysed by some unknown nucleation agent. Observations of the new locations at which crystals appear after melting[3], and the time-dependence of crystallisation[5], have suggested that, at least in some instances (including natural rubber) the process is homogeneous.

Some experiments on the crystallisation of natural rubber latex are reported here.

EXPERIMENTAL DETAILS

Samples of ammonia-stabilised natural rubber latex, containing 62.5% by weight of solids,

* The Goodyear Tire & Rubber Company, Akron, Ohio, 44316, U.S.A.

** The University of Akron, Akron, Ohio, 44325-0301, U.S.A.

Figure 2. Wide-angle x-ray scattering photograph for a sample of natural rubber latex with 40 parts of ethylene glycol added, stored for one week at − 29°C.

Figure 1. Wide-angle x-ray scattering photograph for a sample of natural rubber latex, stored for one week at − 29°C. The inner diffraction rings, from crystalline rubber, are indicated by arrows. The outer rings are from ice.

were obtained from P.T. Goodyear Sumatra Plantation Company, Indonesia. The particle sizes were found to be rather disperse with two clear peaks, corresponding to diameters of 0.25 μm and 0.56 μm. The average diameter is taken here as 0.5 μm. One latex sample was diluted with an equal amount of ethylene glycol, one with a lesser amount, and one was used as received. They were placed in 2 mm diameter quartz tubes and stored at $-29°$C for one week. At the end of this time, the tubes were transferred to a Rigaku DMax wide-angle x-ray spectrometer, care being taken to maintain the samples at $-29°$C or below during transfer and x-ray examination. Wide-angle x-ray scattering (WAXS) transmission Polaroid photographs were taken using point focus copper radiation (40 kV, 30 mA), a nickel filter and a 1 mm diameter pinhole collimator.

RESULTS AND DISCUSSION

Particle size measurements by sedimentary field flow fractionation showed almost no change on adding ethylene glycol to natural rubber latex. The peaks corresponded to particle diameters of 0.25 μm and 0.56 μm with ethylene glycol present, compared to 0.24 μm and 0.56 μm originally, indicating little if any swelling of the rubber particles by ethylene glycol.

WAXS transmission photographs showed typical amorphous halo patterns at room temperature for both specimens. Indeed, they were virtually identical. However, after storage at $-29°$C for one week, sharp differences were apparent. The unprotected natural rubber latex gave typical Debye-Scherrer patterns *(Figure 1)*, with crystalline rings for both *cis*-1,4-polyisoprene and ice. The degree of crystallisation of the rubber was estimated to be 39% by comparing the intensity of peaks attributed to rubber lattice spacings with the intensity of the amorphous halo. On the other hand, the natural rubber latex with ethylene glycol added gave an unchanged amorphous WAXS pattern *(Figure 2)*, with no evidence of crystallisation. As the lowest detectable amount

by this method is about 2%, it is concluded that the degree of crystallisation of the sample protected with ethylene glycol was 2% or less.

A rubber coagulum was found on warming the unprotected sample to room temperature. It was concluded that, as a result of the freezing of the water serum, the rubber particles had coalesced together and crystallised as a solid mass on standing at $-29°$C. On the other hand, the protected sample was found to remain in the latex phase on warming to room temperature and the particle size distribution was found to be unchanged. In this case, therefore, it was inferred that the individual particles remained isolated at low temperatures. They did not crystallise because of a paucity of crystal nuclei. Apparently, crystal nuclei in rubber are not present as frequently as one per latex particle, or even one per fifty latex particles. Therefore, they are probably foreign inclusions. Crystallisation appears to be homogeneous in purified natural rubber[5] but the high rate of crystallisation in comparison with that observed here in latex implies that nucleation in bulk rubber, even when purified, is not homogeneous but seeded in some way.

CONCLUSIONS

The particle size of natural rubber latex is sufficiently small that the chance of a single particle containing a crystallisation nucleus is remote. As a result, rubber latex does not crystallise, even after long periods at $-29°$C, provided that the serum itself is prevented from crystallising. From the measured particle size, it is inferred that the density of crystal nuclei is less than one in fifty particles, or less than one in 10^6 molecules.

ACKNOWLEDGEMENTS

REFERENCES

1. CORMIA, R.L., PRICE, F.P. AND TURNBULL, D. (1962) Kinetics of Crystal Nucleation in Polyethylene. *J. chem. Phys.* **37**, 1333.

2. KELLER, A. (1968) Polymer Crystals. *Rep. Prog. Phys.*, **31(2)**, 623.

3. SHARPLES, A. (1966) *Introduction to Polymer Crystallization.* New York: St. Martin's Press.

4. BINSBERGEN, F.L. (1977) Natural and Artificial Heterogeneous Nucleation in Polymer Crystallization. *J. Polym. Sci.: Polym. Symp.*, **59**, 11.

5. GENT, A.N. (1954) Crystallization in Natural Rubber II. The Influence of Impurities. *Trans. Instn Rubb. Ind.*, **30**, 139.

6. INOUE, M. (1963) Nucleating Effect on the Kinetics of Crystallization and the Spherulites of Nylon 6. *J. Polym. Sci.*, **A1**, 2013.

The Mooney Viscosity of Raw Natural Rubber

G.M. BRISTOW*

Non-standard Mooney test parameters have been derived for a range of raw natural rubber grades in an attempt to obtain information other than a simple assessment of viscosity. Increasing the pre-heat time to 5 min and observing the torque–time relation over 1–4 min give readings which prove characteristics of the source materials used in the production of the sample and can distinguish therefore between samples of latex grade (e.g. SMR L) and field coagulum grade (e.g. SMR 10) rubbers.

The potential use of the standard Mooney viscometer to provide more information on raw natural rubber than $ML1 + 4$, $100°C$, a simple measure of viscosity, has been noted recently[1]. Such information can be derived from four features:

- The overall shape of the torque-time relation during a test of perhaps 5 min

- A special aspect of the above feature; the extent of the initial stress overshoot as evinced in a maximum torque

- The influence of temperature on the above two features

- Relaxation of torque following cessation of rotor movement at the conclusion of the 4-min test time.

For the effective use of the first three features, to a lesser extent the last feature, the initial pre-heat time must be sufficient to allow the rubber to attain the test (platen) temperature. A period of 5 min, rather than the conventional 1-min pre-heat, has been found to be adequate[1]. This is the only difference to the standard test procedure. As has been shown previously[1], the parameters derived in tests of this type are dependent on the grade (or rather production route) of the rubber in question. Furthermore, the information obtained clearly relates to the rheological characteristics of

the rubber and hence inevitably to the processing behaviour noted by the end-user. Although the information is not immediately expressable in terms of basic material properties, consistency in the various Mooney parameters would nevertheless be expected to be indicative of consistency in processing behaviour. The potential practical utility of such parameters is therefore obvious.

The Mooney viscometer was first developed some fifty years ago and has been in continual use ever since. Not surprisingly, therefore, observations relating to the above points have been made in the past, although there seem to have been no systematic studies and certainly no attempt to relate these factors to the production route used for raw natural rubber. The studies reported here have, of course, been stimulated by the current pressure on elastomer producers to supply materials, including natural rubber, with *consistent* processing behaviour in the end-user's factory. As noted above, in practice such *consistency* should be achievable without the need to specify a wide range of fundamental rheological parameters.

In this paper, data for Mooney torque as a function of running time (0–4 min) over a range of temperatures are reported for samples of various grades of natural rubber. Relaxation of torque at the conclusion of the test, is not considered but will be the subject of a subsequent publication.

*Malaysian Rubber Producers' Research Association, Brickendonbury, Hertford SG13 8NL, United Kingdom

EXPERIMENTAL

The samples used were, in the main, normal commercial materials obtained from consumers' stocks. In all cases, before testing the bale rubber was blended and homogenised using the two-roll mill procedure specified for the testing of SMR[2]. A standard Mooney viscometer fitted with a pen recorder was used. As noted above, the rubber was pre-heated in the machine for 5 min and then the torque–time trace recorded over the period 0-4 min. Values of the initial torque, ML_{max}, and torque after 4 min, $ML (5 + 4)$ were obtained from this trace.

RESULTS

Representative torque–time traces for three samples each of SMR L, SMR CV and SMR 10 are given in *Figures 1, 2* and *3* respectively While, in general, torque at a given time usually decreases with temperature, as would be expected, there are much more complex variations in the shape of the torque–time plot. The most obvious feature is the consistency in shape, including the temperature dependence, between the three samples for each grade and the clear differences in shape between the grades. The shape is in essence a 'finger print' of the grade, albeit a qualitative one, and therefore a sample not displaying the appropriate finger print would be suspect. Such complex effects can only result from the interplay of several factors probably having different temperature coefficients, and at this stage a detailed analysis has not proved possible. It should be noted however that an essentially empirical analysis of the torque–time relation of a black-filled system has been proposed by Turner[3]. Further analysis of the data obtained is therefore restricted to a consideration of the parameters ML_{max} and $ML(5 + 4)$ noted above, together with $R = ML_{max}/ML(5 + 4)$ obtained at 70°C – 110°C. Data of this type for a wide range of samples, including those of *Figures 1, 2* and *3*, are given in *Tables 1–5*.

It should be noted perhaps that, while the 4-min test time has been adopted in conformity with conventional practice, the torque or 'viscosity' observed at the 4-min stage is not necessarily an equilibrium value and certainly not an intrinsic material parameter. (Conventionally a 1-min pre-heat, rather than the 5 min adopted here, is used.) Previous studies[1] have shown that, at 100°C at least, the torque falls over the subsequent 4-60-min period at a rate which suggests that oxidation may be a factor. Furthermore, inspection of *Figures 1, 2* and *3* suggests that the proximity of the 4-min torque to an equilibrium or 'true' value almost certainly depends on the temperature of the test.

Examination of *Tables 1–5* reveals that the 'equilibrium' torque or viscosity , $ML(5 + 4)$, decreases with increasing temperature from 70°C to 90°C, as would be expected. At higher temperatures, however, the 'viscosity' is constant or increases. While such an increase might reflect the minor incursion of some crosslinking process, this seems improbable under the conditions of time and temperature involved. It is more likely that the increase is spurious and simply reflects the non-equilibrium nature of the $ML(5 + 4)$ values. The rapid increase in viscosity below *ca* 90°C is paralleled by similar effects noted previously in capillary flow measurements[4]. Representative data for two samples each of the latex grade SMR L and field coagulum grade SMR 10 are plotted in *Figure 4*. The overall dependence of viscosity on temperature for the two grades is broadly similar, including the rise in viscosity above 90°C. There is, however, a tendency for the viscosity increase below 90°C to be more rapid for the latex material. Here again, this is consistent with capillary flow data. The trend is quantified by the grade mean values given in *Table 6*. It is to be noted that the relative increase in viscosity at lower temperatures is particularly marked for the CV grade.

The initial maximum torque, ML_{max} is a more interesting parameter. The dependence of the ratio R [$= ML_{max}/ML(5 + 4)$] on natural rubber grade has been noted previously[1]. More extensive data are presented here in *Tables 1–5*. Unlike $ML(5 + 4)$, ML_{max} shows
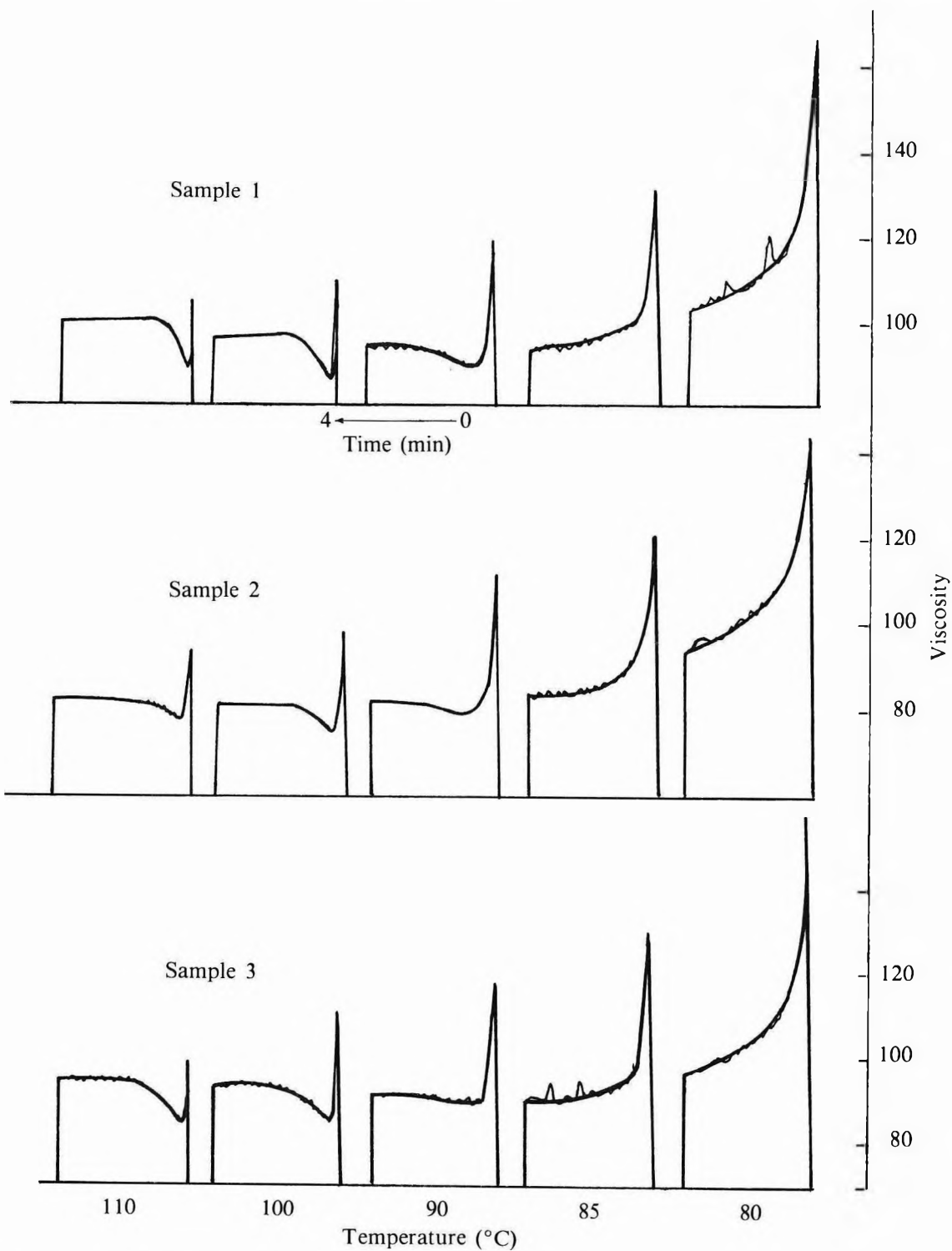
Figure 1. Mooney viscosity as a function of time (0–4 min) after 5-min pre-heat at 80°C–110°C for three samples of SMR L.
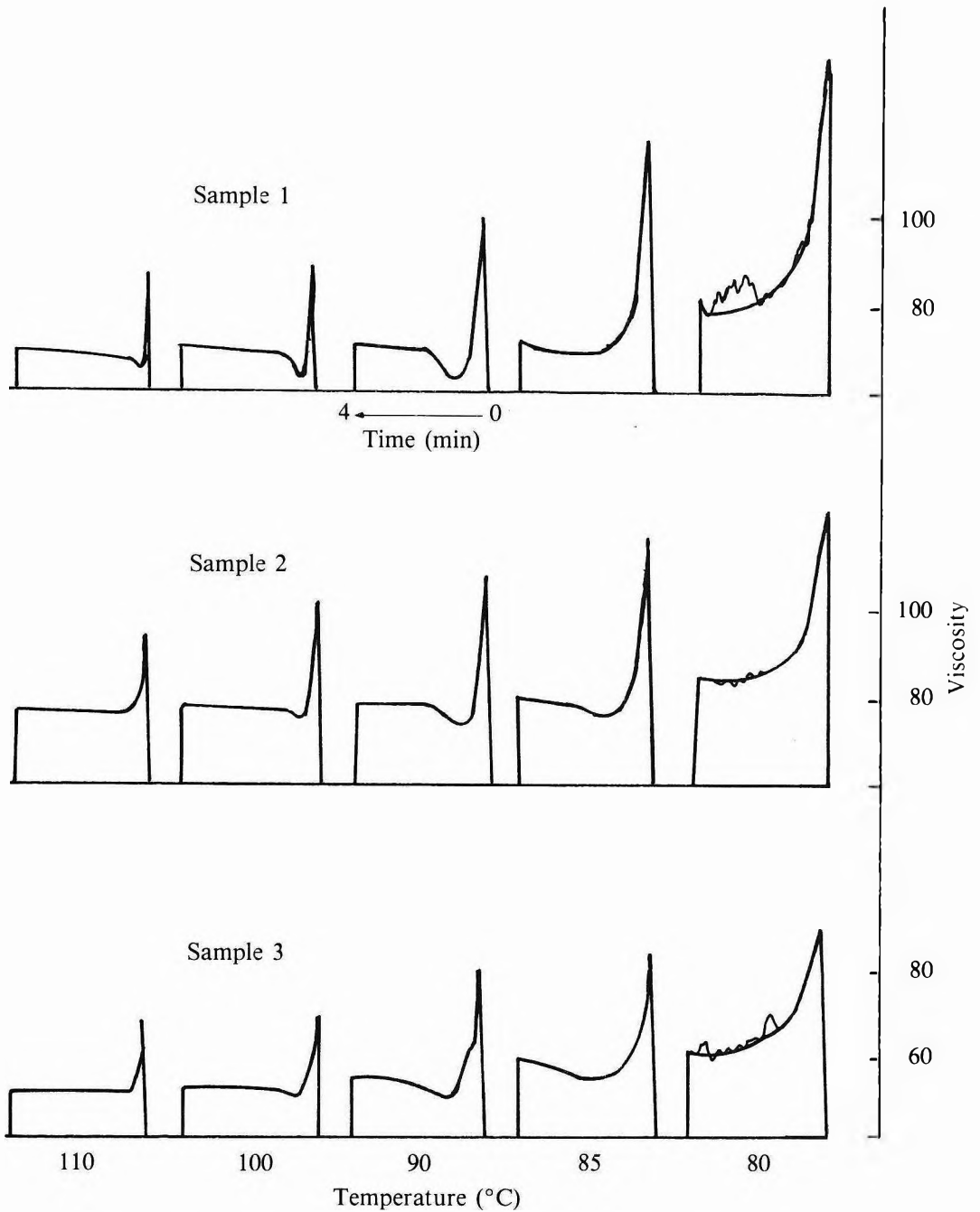
Figure 2. Mooney viscosity as a function of time (0–4 min) after 5-min pre-heat at 80°C–110°C for three samples of SMR CV.
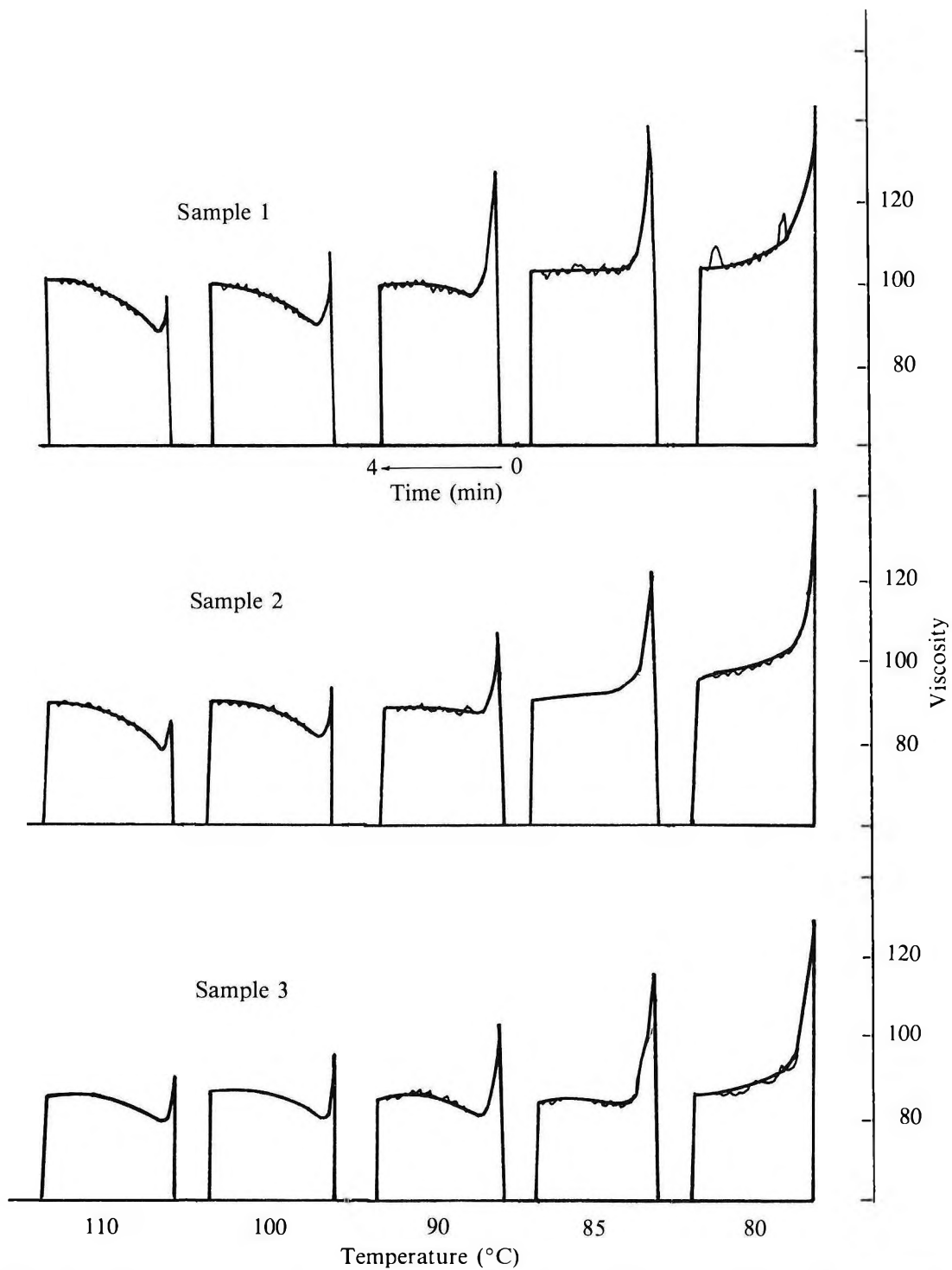
Figure 3. Mooney viscosity as a function of time (0–4 min) after 5-min pre-heat at 80°C–110°C for three samples of SMR 10.

TABLE 1. MOONEY DATA AT 75°C–110°C FOR EIGHT SAMPLES OF SMR L

Temp. (°C)	Sample 1			Sample 2			Sample 3			Sample 4		
	Mx	4'	R	Mx	4'	R	Mx	4'	R	Mx	4'	R
110	99.5	94.5	1.05	90.5	86.5	1.05	95	83	1.14	86	87	0.99
100	108.5	93	1.17	97	87	1.11	99.5	82	1.21	90.5	88	1.03
90	129	90.5	1.43	102.5	85.5	1.20	112	82.5	1.36	98	86	1.14
85	131	91	1.44	111.5	85.5	1.35	121	84	1.44	104.5	84	1.24
80	158.5	98.5	1.61	125	86	1.45	143.5	94	1.53	117.5	83.5	1.41
75	186	118	1.58	144	101	1.43	166.5	111	1.50	132.5	87	1.52
70	>200	143	–	183	121	1.51	195	133	1.47	164.5	105	1.57

TABLE 1. MOONEY DATA AT 75°C–110°C FOR EIGHT SAMPLES OF SMR L (Contd.)

Temp. (°C)	Sample 5			Sample 6			Sample 7			Sample 8		
	Mx	4'	R	Mx	4'	R	Mx	4'	R	Mx	4'	R
110	95.5	84	1.14	85	81	1.05	105	100.5	1.04	101	85.5	1.18
100	100	82.5	1.21	88	82	1.07	111	97.5	1.14	110.5	86	1.29
90	116.5	81.5	1.43	96.5	79.5	1.21	120	95.5	1.26	136	86	1.58
85	120	82	1.46	104	80	1.30	132	94	1.40	150	90	1.67
80	145	91	1.59	118.5	82	1.45	167	104	1.61	180	102	1.77
75	176	116	1.52	132	92.5	1.43	186	125	1.49	>200	122	–
70	>200	144	–	158	112	1.41	>200	150	–	–	–	–

Mx = Initial maximum torque

4' = ML(5 + 4)

R = Mx/ML(5 + 4)

TABLE 2. MOONEY DATA AT 75°C–110°C FOR ELEVEN SAMPLES OF TSR 10

Temp. (°C)	Sample 1			Sample 2			Sample 3			Sample 4		
	Mx	4'	R	Mx	4'	R	Mx	4'	R	Mx	4'	R
110	99.5	101.5	0.98	109	106.5	1.02	90	92.5	0.97	89	86	1.03
100	108	99	1.09	120	105	1.14	96	93	1.03	94	86.5	1.09
90	121	96.5	1.26	138	104.5	1.32	109	91	1.20	102	85.5	1.19
85	131	96	1.36	149.5	108	1.38	119	92	1.29	116.5	85	1.37
80	145	99	1.46	173	112.5	1.54	132	96	1.39	129	86	1.50
75	178	109	1.63	191	123.5	1.55	149	101	1.48	173	91	1.90
70	>200	127	–	204	142	1.44	181	118	1.52	200	101.5	1.97

TABLE 2. MOONEY DATA AT 75°C–110°C FOR ELEVEN SAMPLES OF TSR 10 (Contd.)

Temp. (°C)	Sample 5			Sample 6			Sample 7			Sample 8		
	Mx	4'	R	Mx	4'	R	Mx	4'	R	Mx	4'	R
110	96	98.5	0.97	97.5	98.5	0.99	113.5	106.5	1.07	93.5	100	0.94
100	105.5	98	1.08	100.5	99	1.02	126.5	107.5	1.18	100	101	0.99
90	121	97	1.25	108	97	1.11	153.5	108	1.42	112.5	98	1.15
85	130.5	98	1.33	120	99	1.21	153	110	1.39	119	100	1.19
80	142	101.5	1.40	128	101.5	1.26	191.5	120	1.60	122	100	1.22
75	176	111	1.59	152.5	111	1.37	>200	135.5	–	146	109	1.34
70	198.5	126	1.58	188	129	1.46	>200	151.5	–	169	117.5	1.44

TABLE 2. MOONEY DATA AT 75°C–110°C FOR ELEVEN SAMPLES OF TSR 10 (Contd.)

Temp. (°C)	Sample 9			Sample 10			Sample 11		
	Mx	4′	R	Mx	4′	R	Mx	4′	R
110	92	94.5	0.97	100.5	103	0.98	87	91.5	0.95
100	102	95	1.07	110	101.5	1.08	95	91	1.04
90	109.5	92	1.19	128	100	1.28	108	90.5	1.19
85	128	93	1.38	139	102	1.36	123	92	1.34
80	141	96	1.47	144	105.5	1.36	132	96.5	1.37
75	154	106.5	1.45	171.5	114	1.50	149	107	1.39
70	184.5	125	1.48	>200	131	–	178	123	1.45

Mx = Initial maximum torque

4′ = ML(5 + 4)

R = Mx/ML(5 + 4)

TABLE 3. MOONEY DATA AT 75°C–110°C FOR TEN SAMPLES OF TSR 20

Temp. (°C)	Sample 1			Sample 2			Sample 3			Sample 4			Sample 5		
	Mx	4'	R	Mx	4'	R	Mx	4'	R	Mx	4'	R	Mx	4'	R
110	83	87	0.95	92	93.5	0.98	105.5	99.5	1.06	92	85.5	1.08	80	83	0.96
100	87	87	1.00	101.5	93.5	1.09	117	98	1.19	96	86.5	1.11	86	89.5	0.96
90	101.5	88	1.15	118	92.5	1.28	138	99	1.39	109	86.5	1.26	95	90.5	1.05
85	109.5	86	1.27	130.5	94	1.39	151.5	104	1.46	121	89.5	1.35	100	91.5	1.09
80	116.5	87	1.34	144	98	1.47	182	111	1.64	136	94	1.45	105	90	1.17
75	134	96	1.40	169.5	107	1.58	>200	123	–	172	106	1.62	125	92.5	1.35
70	168.5	107	1.57	195	121	1.61	>200	140	–	>200	130	–	138	95	1.45

TABLE 3. MOONEY DATA AT 75°C–110°C FOR TEN SAMPLES OF TSR 20 (Contd.)

Temp. (°C)	Sample 6			Sample 7			Sample 8			Sample 9			Sample 10		
	Mx	4'	R	Mx	4'	R	Mx	4'	R	Mx	4'	R	Mx	4'	R
110	94	96	0.98	77	83	0.93	79.5	80.5	0.99	91	95.5	0.95	73	82	0.89
100	99.5	97	1.03	84	88	0.95	85.5	82.5	1.04	94.5	97	0.97	77.5	83	0.93
90	119	98.5	1.21	91.5	89	1.03	94	84	1.12	110	96.5	1.14	83.5	84	0.99
85	124	99	1.25	94	89	1.06	101	85	1.19	118	96.5	1.22	89.5	84.5	1.06
80	136	105	1.30	107.5	89.5	1.20	107	86	1.24	132	99	1.33	93.5	84.5	1.11
75	169	115	1.47	123.5	91	1.36	126	94	1.34	160	106	1.51	103.5	86	1.20
70	192	127.5	1.51	144.5	96	1.51	140.5	104	1.35	187.5	119	1.58	116.5	92	1.27

Mx = Initial maximum torque
4' = ML(5 + 4)
R = Mx/ML(5 + 4)

TABLE 4. MOONEY DATA AT 75°C–110°C FOR FIVE SAMPLES OF RSS-CV[a]

Temp. (°C)	Sample 1			Sample 2			Sample 3			Sample 4			Sample 5		
	Mx	4'	R	Mx	4'	R	Mx	4'	R	Mx	4'	R	Mx	4'	R
110	76	57	1.33	80	64.5	1.24	106	90	1.18	77	59	1.31	92	75.5	1.22
100	79	58.5	1.35	84	65.5	1.28	114	90	1.27	78	59.5	1.31	97.5	75	1.30
90	87.5	60.5	1.45	92.5	66	1.40	138	89.5	1.54	86.5	60	1.44	113	75.5	1.50
85	96	62	1.55	95.5	68	1.40	151	91.5	1.65	93	61.5	1.51	129	76.5	1.69
80	111.5	63.5	1.76	118	70	1.69	191.5	101.5	1.89	101	62.5	1.62	141	84	1.68
75	126	82	1.54	129	86	1.50	>200	125	-	124	76	1.63	184	107	1.72

[a]Monoclonal samples (cf Reference 5)
Mx = Initial maximum torque
4' = ML(5 + 4)
R = Mx/ML(5 + 4)

TABLE 5. MOONEY DATA AT 75°C–110°C FOR FIVE SAMPLES OF SMR CV[a]

Temp. (°C)	Sample 1			Sample 2			Sample 3			Sample 4			Sample 5		
	Mx	4'	R	Mx	4'	R	Mx	4'	R	Mx	4'	R	Mx	4'	R
110	68	52	1.31	76	58	1.31	107.5	85.5	1.26	67	53.5	1.25	88	71	1.26
100	70	53.5	1.31	83.5	58.5	1.43	115.5	86	1.34	71.5	54	1.32	90	71	1.27
90	80.5	55.5	1.46	88.5	59.5	1.49	137	86.5	1.58	78	55	1.42	100.5	71	1.42
85	84	≷57.5	1.46	97.5	61	1.60	162	88	1.84	82.5	56	1.47	120	72	1.67
80	90	61	1.48	103.5	65	1.59	191.5	101	1.90	89.5	57	1.57	134.5	79	1.70
75	114	77	1.48	121	83	1.46	>200	128	–	93.5	62	1.51	162	100	1.62

[a]Monoclonal samples (cf Reference 5)
Mx = Initial maximum torque
4' = ML(5 + 4)
R = Mx/ML(5 + 4)

Figure 4. Temperature dependence of ML(5 + 4) for samples of SMR L and SMR 10.

TABLE 6. GRADE MEAN VALUES OF
ML(5 + 4)75°C/ML(5 + 4)100°C

Grade	No	Mean	sd
SMR L	8	1.25	0.15
TSR 10	11	1.13	0.06
TSR 20	10	1.13	0.08
SMR CV	5	1.38	0.13
RSS CV	5	1.36	0.06

a monotonic dependence on temperature over the whole range 70°C–110°C and this dependence is large enough to offset small changes in $ML(5 + 4)$ so that the ratio, R, shows a similar temperature dependence. As would be expected, ML_{max} depends upon $ML(5 + 4)$. The ratio R, measured at 100° C, has been noted previously as discriminating between latex and cup lump natural rubber grades. This discrimination is confirmed by the data of *Table 7* which shows further that a

196

TABLE 7. GRADE MEAN VALUES OF $R = ML_{max}/ML\,(5 + 4)$ at $75°C$-$100°C$

Temp. (°C)	SMR L 8 samples		TSR 10 11 samples		TSR 20 10 samples		RSS CV 5 5 samples		SMR CV 5 samples	
	Mean	sd	Mean	sd	Mean	sd	Mean	sd	Mean	sd
110	1.08	0.07	0.99	0.04	0.98	0.06	1.26	0.06	1.27	0.05
100	1.15	0.08	1.07	0.05	1.03	0.08	1.30	0.03	1.33	0.06
90	1.33	0.15	1.22	0.09	1.16	0.12	1.47	0.05	1.47	0.07
85	1.41	0.13	1.33	0.07	1.23	0.14	1.56	0.12	1.61	0.16
80	1.55	0.12	1.42	0.11	1.33	0.16	1.73	0.10	1.65	0.16
75	1.50	0.05	1.48	0.10	1.43	0.13	–	–	–	–

similar pattern of behaviour is evident at temperatures other than 100°C. However, normalisation of the data to give the values recorded in *Table 8* shows that improved discrimination cannot be achieved by testing at temperatures other than 100°C.

All the grades tested show considerable within-grade scatter, with coefficients of variation of typically 3%-8%. Such variability clearly limits the use of R as a discriminating test parameter and the source of the scatter is therefore of some interest. The samples tested were commercial materials, for which the precise details of production procedure or even source materials, are unknown. It could well

be, therefore, that the value of R is influenced by production factors other than the basic latex or cup lump nature of the source material, such as maturation time of a latex coagulum or time and temperature of drying. This could only be determined using special materials produced by very well characterised procedures.

Variability, or rather apparent variability, also could arise because of the very simple analytical approach adopted. Though ML_{max} clearly must be dependent on $ML\,(5 + 4)$, there is no physical basis for a simple proportionality, and hence no such basis for a constant value of $R = ML_{max}/ML\,(5 + 4)$ for samples of one grade differing in viscosity. More generally, $R*$

TABLE 8. VALUES OF R RELATIVE TO THE MEAN VALUE AT ONE TEMPERATURE

Temp. (°C)	Mean R	R relative to mean				
		SMR CV	RSS CV	SMR L	TSR 10	TSR 20
110	100	114	113	97	89	88
100	100	113	111	98	91	88
90	100	111	111	100	92	87
85	100	113	109	99	93	86
80	100	107	113	101	92	87

TABLE 9. ANALYSIS OF VARIATION OF ML_{max} WITH ML (5 + 4)

Rubber	Temp. 80°C			Temp. 100°C		
	x	Coeff.[a] corr.	coeff.[b] var. (%)	x	Coeff.[a] corr.	Coeff.[b] var. (%)
SMR L	1.00	0.97	7.6	1.00	0.60	7.3
8 samples	1.67	0.98	3.7	0.83	0.59	1.1
TSR 10	1.00	0.85	8.1	1.00	0.88	5.0
11 samples	1.26	0.82	7.6	1.32	0.88	4.5
TSR 20	1.00	0.92	12.1	1.00	0.79	8.0
10 samples	1.97	0.91	7.8	1.46	0.80	3.0
SMR CV	1.00	0.99	9.8	1.00	0.98	4.5
5 samples	1.39	0.99	3.1	0.97	0.98	4.4
RSS CV	1.00	0.99	6.0	1.00	0.99	2.4
5 samples	1.20	0.99	4.1	0.73	0.82	3.3

[a]Between ML_{max} and $[ML(5 + 4)]^*$ for x = 1 or rms value

[b]For $R = ML_{max}/ML(5 + 4)$ or $R^* = ML_{max}/[ML(5 + 4)]^*$

could be equated to $ML_{max}/[ML(5 + 4)]^x$ with x determined by the best fit for a constant value of R^*. The results of such an analysis, which for the data obtained at 80°C and 100°C are given in *Table 9*, are disappointing. While variability in R^* is in many, but not all, cases much less than in R, the values of x required do not conform to any regular pattern and are too variable to be indicative of a viable interpretation of the data.

CONCLUSIONS

The data discussed here were obtained using a standard Mooney 'viscometer' but with 5-min rather than 1-min pre-heating of the test sample. The shape of the torque *versus* time relation over the period 1 min to 4 min and its dependence on temperature has been found to be dependent on the overall process history of the material. Latex rubber (SMR L) and field coagulum (SMR 10) show quite different responses. Quantitative analysis has been restricted to the dependence of viscosity, $ML(5 + 4)$, on temperature; and, the relation between initial maximum torque or stress-

overshoot and $ML(5 + 4)$. Both these features appear to depend on the grade. Considerable scatter in behaviour is evident between the several samples of each grade. It is envisaged that this scatter could stem, at least in part, from differences in the detailed process history, such as in the drying temperature. Since the samples studied were normal commercial materials, such differences are quite likely to have been present.

REFERENCES

1. BRISTOW, G.M. AND SEARS, A.G. (1987) The Use of Novel Parameters in the Assessment of Natural Rubber Processability. *J. nat. Rubb. Res,* **2(1)**, 15.

2. RUBBER RESEARCH INSTITUTE OF MALAYA (1970) RRIM Test Methods for Standard Malaysian Rubbers. *SMR Bull. No. 7.*

3. TURNER, D.M. (1979) Private Communication. Avon Rubber Co. Ltd., Melksham, U.K.

4. BRISTOW, G.M. (1985) Capillary Flow of Raw Natural Rubber, *NR Technol.* **16**, 76.

Adherence, Friction and Contact Geometry of a Rigid Cylinder Rolling on the Flat and Smooth Surface of an Elastic Body (NR and SBR)

M. BARQUINS*

Static equilibrium conditions, the contact geometry and the rolling friction force of a hard cylinder in adhesive contact with an elastic body are studied using classic thermodynamics, the concepts of fracture mechanics, such as the stress intensity factor or the strain energy release rate and the plane elasticity theory. It is shown that the rolling resistance, the contact geometry and the pressure are linked to the three interfacial quantities: Dupre's energy of adhesion and the dissipative forces resisting the rupture and the formation of the contact. Experiments carried out with polymethyl-methacrylate (PMMA) and stainless steel cylinders rolling on smooth NR and SBR surfaces confirm all the theoretical predictions, in particular, one can observe that the experimental value of the contact length, which increases with the rolling speed, remains perfectly between the theoretical values deduced from the measured rolling resistance and the extreme values of the dissipative force resisting the formation of the contact. Moreover, it is shown that, due to the intervention of molecular attraction forces, a light rigid cylinder rolls under an inclined NR surface and it is found that the rolling speed is the same when the cylinder rolls on the same inclined surface. It has been verified that if a flat rubber substrate, with an adequate length, is rotated at constant angular velocity, a light stainless steel cylinder rolls alternately on and under the rubber surface without dropping.

Previous work[1-4] has shown that an approach derived from Griffith's theory allows one to describe the evolution of the contact area between a hard punch or substratum and an elastic solid for different geometries such as plane[1] and axisymmetric[2] peeling experiments or contacts of plane[1], spherical[1,3] or cylindrical[4] hard punches. The edge of the contact area is assumed to be a crack tip which propagates in the interface, moving backwards or forwards as the applied load is increased or decreased. This approach which takes into account the strain energy release rate G and its derivative $\delta G/\delta A$ with respect to the area of contact A, enables the determination of the elastic adherence force, to study the kinetics of the crack propagation speed v and predict the evolution of the system whatever the

geometry of contact and loading conditions. It has been shown that, in a wide range of crack propagation speed v, the strain energy release rate varies as a power function of the crack speed as follows:

$$G = kv^n \qquad \ldots 1$$

Although more complicated geometries like rolling[4-9] and sliding[10-13] friction conditions have already been widely studied, it appears that their theoretical analyses are incomplete. This paper aims to show that the thermodynamical approach which generalises Griffith's theory[14] together with the plane elasticity theory[15] allows us to solve problems of adherence and rolling of a hard cylinder in adhesive contact with an elastic solid, such as a rubber-like material[16].

---

*Laboratoire de Physique et Mecanique des Milieux Heterogenes (URA 857), ESPCl 10, rue Vauquelin, 75231 Paris Cedex 05, France

THEORY

Thermodynamical Approach

Let us consider a long and rigid cylinder with weight W, radius R and length L in contact with the flat and smooth surface of an elastic body, characterised by Young's modulus E and Poisson ratio ν, and let $E^* = E/(1 - \nu^2)$. All the forces, like normal applied loads or rolling resistances, are expressed per unit axial length of cylinder.

When a sphere or a cylinder rolls upon a rubber surface[4-9], the edges of the contact area, perpendicular to the motion, can be considered as two crack tips propagating in the same direction, with the same speed but they behave differently: there is a closing crack in the front region and an opening crack at the rear where the major part of the energy is dissipated by a peeling mechanism, so that a large extension is observed at the trailing edge. This is the reason for considering an asymmetrical contact *(Figure 1)*.

At a given time t, the relative position of the two solids in contact is determined by the elastic displacement δ and abcissas X_0, X_1 and X_2 of the cylinder axis, the trailing and leading edges of the contact area, respectively *(Figure 1)*. According to the second principle of thermodynamics, evolution of the system is only possible if:

$$P\dot\delta + F\dot{X_0} + df/dt \geq 0 \qquad \ldots 2$$

where P and F are respectively the normal force and rolling resistance per unit axial length, $\dot\delta = d\delta/dt$, $\dot{X_0} = dX_0/dt$ and f is the component of the free energy that depends on the stored elastic energy U_E together with Dupre's energy of adhesion w, a function of the contact size *(Figure 1)*, so that:

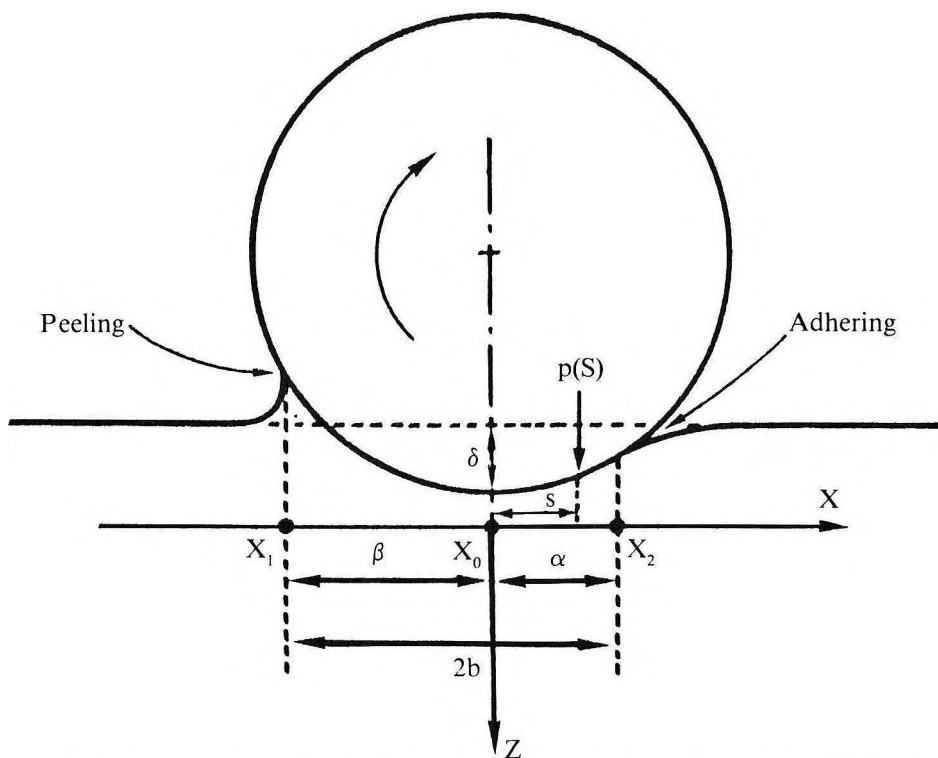$$f = U_E(\delta, \alpha, \beta) - w(X_2 - X_1) \qquad \ldots 3$$

Figure 1. Contact geometry of a rigid cylinder rolling on an elastic solid.

with $\alpha = X_2 - X_0$ and $\beta = X_0 - X_1$. Taking into account the two strain energy release rates G_α and G_β at the leading and trailing edges respectively:

$$G_\alpha = \partial U_E / \partial \alpha \qquad \ldots 4$$

$$G_\beta = \partial U_E / \partial \beta \qquad \ldots 5$$

Equation 1 can be written as:

$$(P - \partial U_E / \partial \delta)\,\dot{\delta} + (F + G_\alpha - G_\beta)\,\dot{X}_0 +$$

$$(G_\alpha - w)\dot{X}_1 + (w - G_\beta)\dot{X}_2 \geq 0 \qquad \ldots 6$$

This condition means that a sum of terms, each one being equal to the product of variables of type of force, by evolution velocities of the system cannot be smaller than zero. *Equation 6* is satisfied using the normal principle of dissipation and assuming that every force is equal to the partial derivative of a function Ω, called dissipative function, with respect to the associated evolution speed:

$$\Omega = \omega(\dot{X}_1) + \omega(-\dot{X}_2) \qquad \ldots 7$$

where ω is a derivable function, which can be possibly discontinuous at zero and which verifies the condition:

$$X\omega'(X) \leq 0 \qquad \ldots 8$$

So, the behaviour law of the system is defined by the four relations:

$$P = \partial U_E / \partial \delta \qquad \ldots 9$$

$$F = G_\beta - G_\alpha \qquad \ldots 10$$

$$G_\alpha = w + \omega'(-\dot{X}_2) \qquad \ldots 11$$

$$G_\beta = w + \omega'(\dot{X}_1) \qquad \ldots 12$$

so that the rolling resistance is:

$$F = \omega'(\dot{X}_1) - \omega'(-\dot{X}_2) \qquad \ldots 13$$

For the simple case of a static contact under a normal applied load, obviously one has $F = 0$, hence $G_\beta = G_\alpha$ and $\alpha = \beta = b$. Regarding rolling conditions at constant speed v, as noted earlier, the leading and trailing edges of the contact area move at the same velocity $\dot{X}_1 = \dot{X}_2 = v \geq 0$. Taking into account *Equations 9 – 12,* the rolling resistence is equal to the sum of two positive terms which are

the dissipative components $[\omega'(\dot{X}_1)]$ and $[-\omega'(-\dot{X}_2)]$ of molecular attraction forces acting during the detachment of the elastic solid at the trailing edge of the contact area and during the re-adhering in the front part, respectively. As the energy release rate is always positive (or equal to zero) and as $\omega'(-\dot{X}_2) \leq 0$ from *Equation 8*, one deduces, according to experimental results obtained by Kendall[5] for plane peeling conditions:

$$0 \leq G_\alpha \leq w \qquad \ldots 14$$

$$-w \leq \omega'(-\dot{X}_2) \leq 0 \qquad \ldots 15$$

So, it can be predicted that the front half-length α is smaller than the rear one β, as confirmed by rolling ball experiments[6,7,9].

Plane Elasticity Theory Application and Contact Geometry

Let us consider the asymmetrical contact, shown in *Figure 1*, between a hard cylinder and an incompressible elastic half-space ($v = 0.5$), such as a rubber-like material. This particular two-dimensional problem in which displacements are specified over the interval $-\beta \leq X \leq \alpha$ can be easily written from general equations[15] in the following form:

$$\int_{-\beta}^{\alpha} [p(S)/(X - S)]\,dS = \pi E^* X / 2R \qquad \ldots 16$$

where $p(S)$ is the normal pressure and R the cylinder radius. Inverting *Equation 16*, the pressure at distance X from the cylinder axis is:

$$p(X) = [1/\pi(X + \beta)^{1/2}(\alpha - X)^{1/2}]$$

$$\{-P + (E^*/2R)\int_{-\beta}^{\alpha}[(S + \beta)^{1/2}(S - \alpha)^{1/2}/$$

$$(X - S)]dX\} \qquad \ldots 17$$

To simplify calculations, one symmetrises the contact area, with the length $2b = \alpha + \beta$, by choosing the axis origin at the centre of the loaded region; distances are thus changed from X to $r = X - (\alpha - \beta)/2$ and from

S to $s = S - (\alpha - \beta)/2$. Thus *Equation 17* becomes:

$$p(r) = [1/\pi(b^2 - r^2)^{1/2}]\{-P + (E^*/2R)$$
$$\int_{-b}^{b}[(b^2 - s^2)^{1/2}(s + (\alpha - \beta)/2)/$$
$$(r - s)]ds\} \qquad \ldots 18$$

as proposed by Johnson[15] with some misprints. The integration is easier if displacements r and s are expressed in terms of b:

$$p(r) = [1/(b^2 - r^2)^{1/2}]\{-P/\pi + (E^*/2R)$$
$$[r^2 + r(\alpha - \beta)/2) - b^2/2]\} \qquad \ldots 19$$

The stress intensity factor K_α at the leading edge of the contact area, calculated as follows:

$$K_\alpha = \lim_{r \to +b} \{p(r)[2\pi(b - r)]^{1/2}\} \qquad \ldots 20$$

is equal to:

$$K_\alpha = -P/(\pi b)^{1/2} + E^*(3\alpha - \beta)(\pi b)^{1/2}/8R \qquad \ldots 21$$

At the trailing edge, the corresponding stress intensity factor K_β takes the similar form:

$$K_\beta = -P/(\pi b)^{1/2} + E^*(3\beta - \alpha)(\pi b)^{1/2}/8R \qquad \ldots 22$$

For a plane strain state, the strain energy release rate is linked to the stress intensity factor by:

$$G_i = K_i^2/2E^* \qquad \ldots 23$$

in which the factor $(1/2)$ is introduced in order to take into account the cylinder rigidity.

So, the relation linking the normal applied load P per unit axial length, the half-length b of the contact area and the strain energy release rates G_α and G_β in the front and rear parts of the contact zone can be easily deduced from *Equations 21, 22* and *23*:

$$P = \pi E^* b^2/4R - (\pi E^* b/2)^{1/2}[(G_\alpha)^{1/2} + (F + G_\alpha)^{1/2}] \qquad \ldots 24$$

where F is the rolling resistance per unit axial length of the cylinder *(Equation 10)*.

Static Contact

For an equilibrium static contact, without rolling *i.e.* $F = 0$ and $G_\alpha = w$, *Equation 24* takes the simple form:

$$P = \pi E^* b^2/4R - (2\pi E^* bw)^{1/2} \qquad \ldots 25$$

as already proposed by Barquins[4]. This equilibrium relationship is represented on *Figure 2*, in which forces and lengths are normalised as:

$$|P| = P/(\pi E^* w^2 R/16)^{1/3} \qquad \ldots 26$$
$$|b| = b/(2wR^2/\pi E^*)^{1/3} \qquad \ldots 27$$

Figure 2 clearly shows that molecular attraction forces, which act through Dupre's energy of adhesion w, increase the length of the contact area for the same normal applied load (the non-adhesive contact case, $w = 0$, is given for comparison). Due to this intervention of surface energy effects, an equilibrium contact area exists under zero and negative applied loads, the ultimate value that corresponds to the limit of stability of the contact, $(\partial G/\partial b)p = 0$ with $G = w$, is $|P_c| = -3$, and the associated smallest stable contact area is $|b_c| = 1$.

Rolling Contact

Rolling conditions are defined by the general *Equation 24* in which the value of G_α, is narrowly limited by virtue of *Equation 14*. *Equation 24* clearly shows that an increase in rolling resistance F, at an increasing speed without change in normal load P, involves an increase in contact area length. From *Equations 22* and *23*, the size of the contact area is given by:

$$\beta = 3b/2 - (2R/\pi E^* b)[P + (2\pi E^* bG_\alpha)^{1/2}] \qquad \ldots 28$$

$$\alpha = 2b - \beta \qquad \ldots 29$$

so that at an increasing rolling speed, a large extension of the rear part of the contact area can be easily predicted.
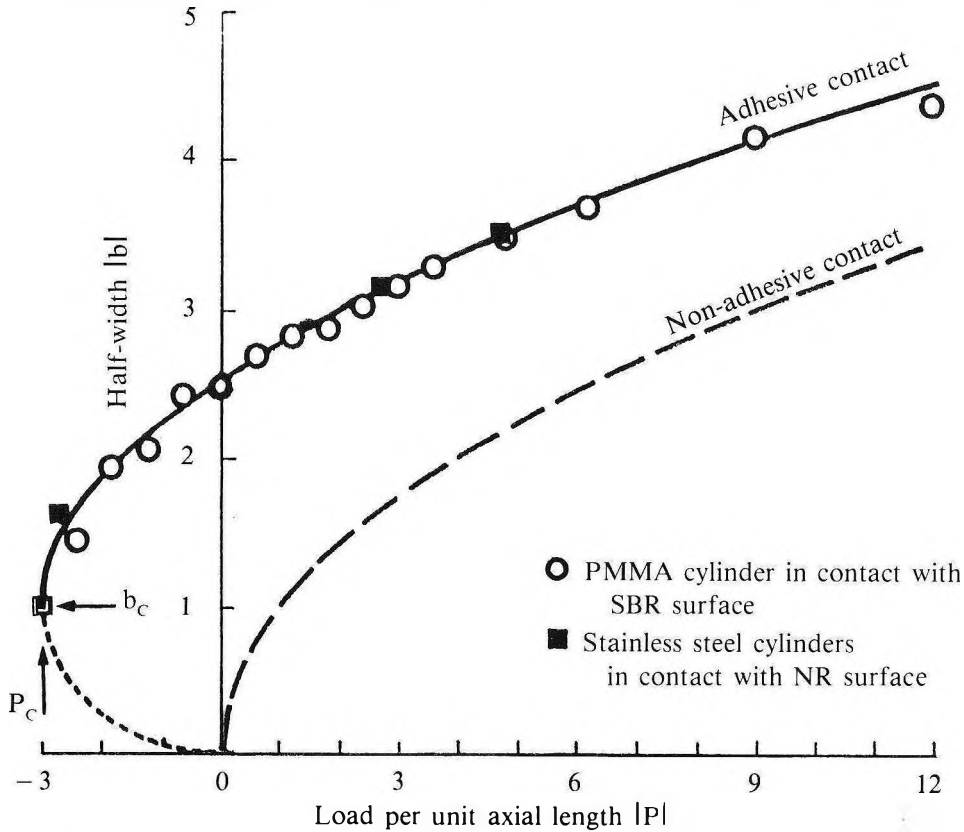
Figure 2. Half-width of the equilibrium contact area between a rigid cylinder and smooth surface of an elastic solid as a function of the normal applied load per unit axial length, in reduced coordinates. The curve deduced from the classical theory (non-adhesive contact) is given for comparison.

RESULTS AND CONCLUSION

Apparatus and Solids in Contact

The experimental device is fundamentally the same as the one used by Barquins *et al.*[6] to study the rolling friction of a glass ball in contact with a rubber plate. The ball is replaced by a PMMA cylinder, 6.3 mm long, with a radius of curvature $R = 2.5$ mm. This cylinder has a brass horizontal axis which is guided by two micro ball bearings; it is placed against the smooth surface of a soft rubber-like material plate with the help of a balance arm, as schematically shown in *Figure 3*. The elastic specimen is a transparent plate, 2 mm thick, of an unfilled SBR vulcanised with 2% dicumyl peroxide ($E = 4.7$ MPa). The area of contact and its immediate vicinity are observed in reflexion through the specimen with a low-power microscope equipped with a video camera. For rolling experiments, the specimen is translated above the cylinder with a screw-nut motor system linked to elastic springs calibrated in force in order to measure the rolling resistance. Of course, for static contact experiments, the elastic translator system is clamped. Some similar experiments were carried out using two stainless steel cylinders of radius 5 mm and lengths 10 mm and 18 mm, in contact on an inclined unfilled NR surface cured with 2% dicumyl peroxide ($E = 0.9$ MPa), with
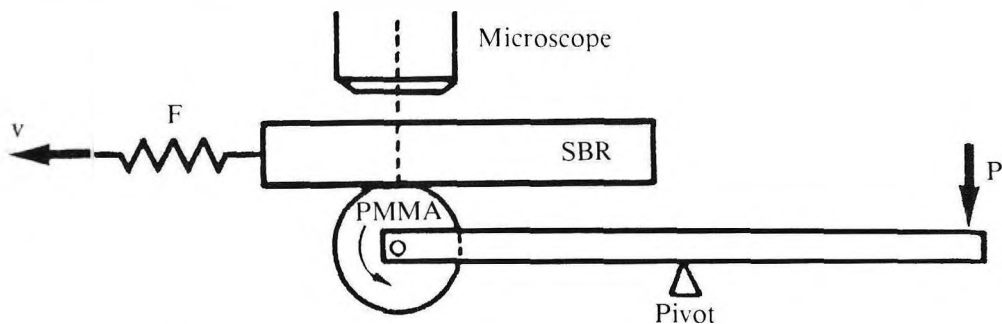
Figure 3. Schematic diagram of the experimental device used to record simultaneously rolling forces and corresponding areas of contact.

normal loads -6.81 N.m^{-1}, 6.81 N.m^{-1} and 12.25 N.m^{-1}. In all the experiments, temperature (23°C) and humidity ratio (52%) were controlled.

Equilibrium Static Contact Results

In a first set of experiments, the PMMA cylinder is placed for 10 min against the SBR plate under several normal loads varied corresponding to forces per unit axial length in the range -6.228 M.m^{-1} to $+31.143$ M.m^{-1}. For every load and associated contact length, the corresponding value of Dupre's energy of adhesion w is computed from *Equation 25*. From the average value $w_{pmma} = 75$ mJ.m^{-2}, experimental data are normalised following *Equations 26* and *27* and plotted in *Figure 2* where all the points fall in the immediate vicinity of the theoretical equilibrium curve (heavy line) confirming the validity of hypotheses. In a second set of experiments, carried out using stainless steel cylinders, the corresponding points *(Figure 2)* verify the theoretical predictions, using the average value $w_{steel} = 121$ mJ.m^{-2}, which is greater than that of w_{pmma} probably due to the less rough surfaces of stainless steel cylinders that increase the adherence force as clearly shown by Briggs and Briscoe[17].

Rolling Contact

Rolling resistances are measured at various speeds in the range 5 μm.s^{-1} to 1 cm.s^{-1}, the PMMA cylinder being placed against the SBR

plate under the normal force $P = 3.114$ N.m^{-1}; the evolution with the speed of the rolling resistance per unit axial length is shown in *Figure 4*, in log-log coordinates. Beyond the speed $v = 100$ μm.s^{-1}, variation of the rolling friction as a power function of the celerity $F = kv^n$ is found again[1,4] with $n = 0.54$ for the SBR-PMMA contact and $n = 0.55$ for the NR-stainless steel contact if steel cylinders roll on an inclined rigid substrate overlapped by a natural rubber trip[4] *(Figure 5)*.

Lengths of contact area between the PMMA cylinder and SBR plate, at various speeds, are shown in *Figure 6*. Every point represents the average value of ten measurements at constant speed along a rolling distance 15 mm long, *i.e.* for about one cylinder rotation. As already observed with ball rolling experiments[6,7,9], the contact length strongly increases at increasing speed, with a marked extension of the rear part of the contact area, according to *Equation 28*. *Figure 6* also shows the two theoretical curves that can be deduced from *Equation 25* for the extreme values of the strain energy release rate at the leading edge of the contact area, $G_\alpha = 0$ and $G_\alpha = w = 75$ mJ.m^{-2}, taking into account measured values of the rolling resistance F plotted in *Figure 4*.

The very good position of experimental data between the two theoretical curves mainly shows that the increase in the rolling contact length together with the increase in the rolling resistance at increasing speeds are two concomitant consequences of the viscous
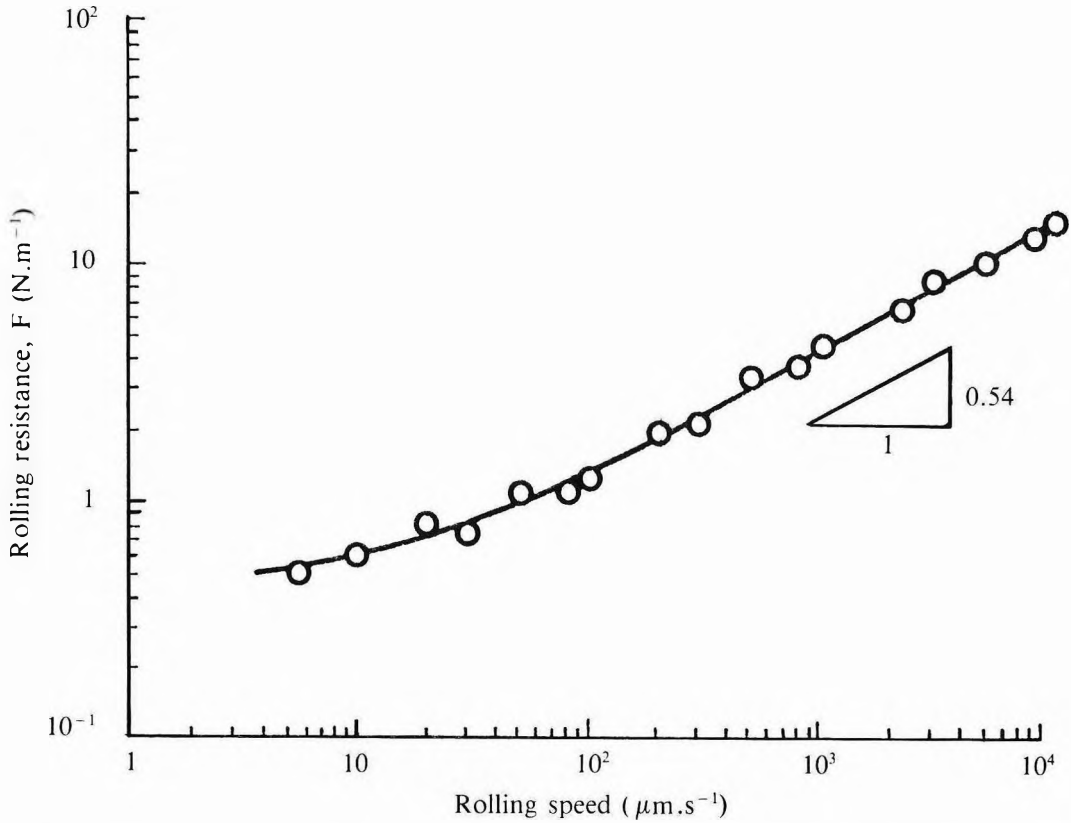
Figure 4. Rolling resistance per unit axial length versus speed for a PMMA cylinder in contact with a flat and smooth surface of SBR plate.
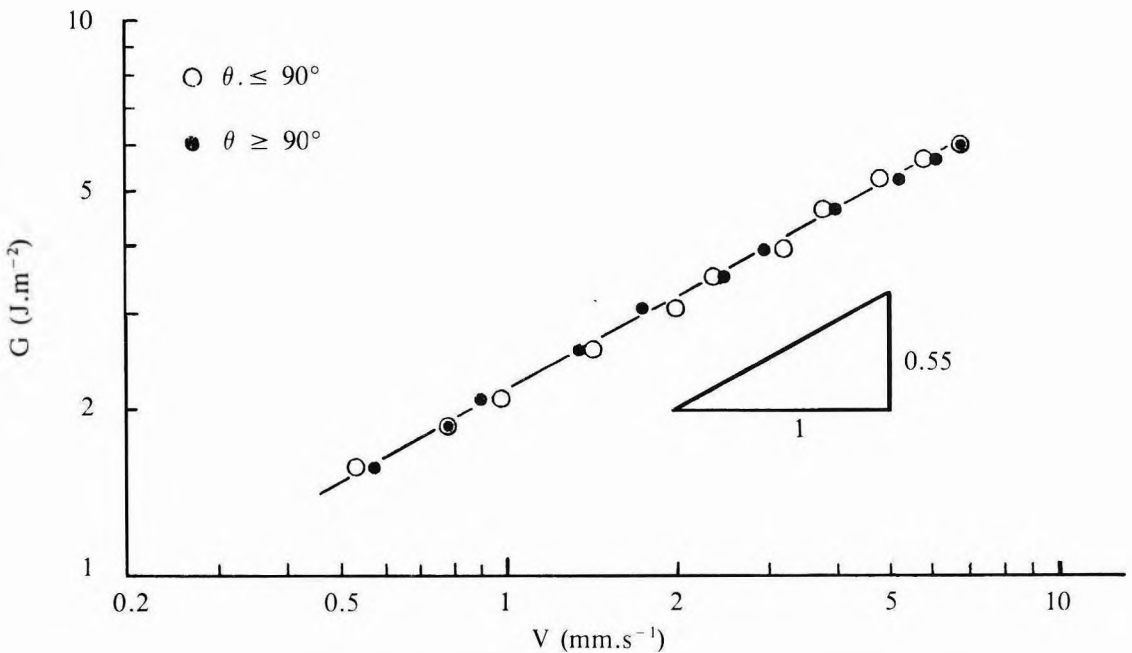
Figure 5. G strain energy release rate versus v rolling speed of a stainless steel cylinder along an inclined soft natural rubber flat surface.
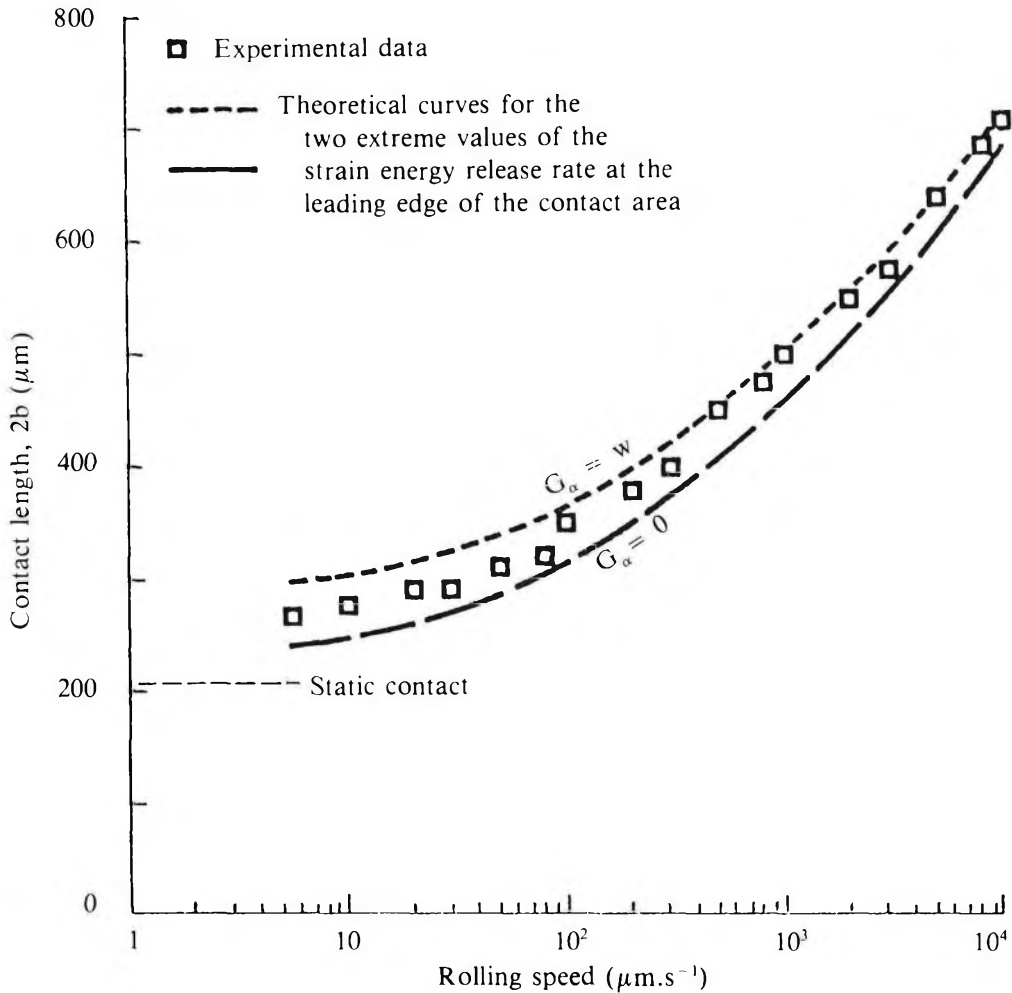
Figure 6. *Total contact length versus rolling speed.*

energy dissipated during separation of the rubber at the trailing edge of the contact area.

As the rolling friction can be seen as a particular form of a $\pi/2$ peeling test[5,11], and because, whatever the peeling angle the relation between the peeling force and the crack propagation speed does not depend on the length of the not peeled trip or on the area of contact in a rolling experiment, the rolling speed of a stainless steel cylinder in contact with a natural rubber strip was studied for various incline angles θ in the range 0° to 180° with respect to the horizontal.

If the weight P of the cylinder per unit axial length is smaller than 3 (absolute value of the adherence force P_c), firstly, the cylinder rolls under the inclined rubber trip and, secondly, the rolling speed takes the same value as if the cylinder is in contact with the same inclined rubber surface *(Figure 7)*. Experimental data obtained with a stainless steel cylinder, weighing 122.5 mN and 20 mm long, are shown in *Figure 5*, in which the strain energy release rate G is calculated following the simple form[5,11]:

$$G = P\sin\theta \qquad \ldots 30$$
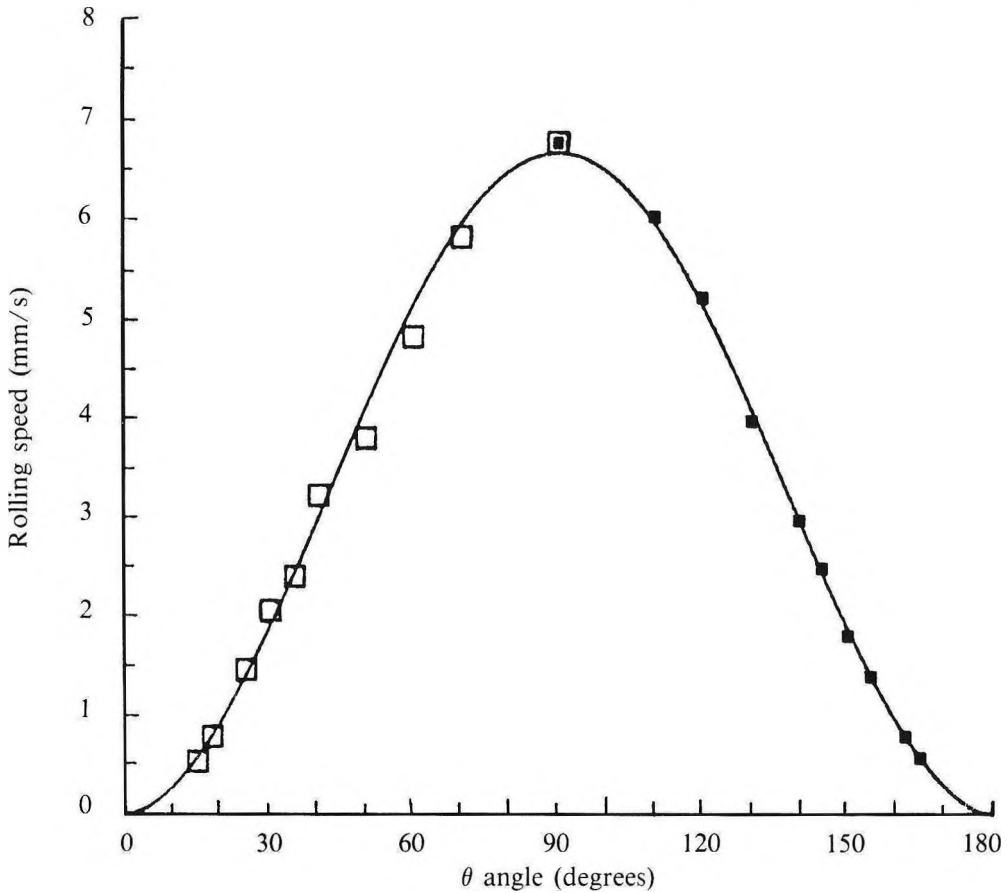
Figure 7. Variations in rolling speed v of stainless steel cylinders, according to angle θ of the inclined natural rubber surface.

Figure 5 clearly proves that G is computable by *Equation 30* for every slope ($0° \leq \theta \leq 180°$) of the cylinder trajectory, so that the energy dissipated by rolling arises solely from the work of tensile stresses at the trailing edge of the contact area, independent of the weight of the cylinder, provided that this weight is smaller than the absolute value of the elastic adherence force. Moreover *Figure 7* shows that G varies as the power function of the crack propagation speed:

$$G = k v^{0.55} \qquad \dots 31$$

with $k = 96.5$ SI units. Thus, using *Equations 30* and *31*, one can compute the variation in the rolling speed v *versus* the incline angle θ; the corresponding curve is recorded in *Figure 7* and confirms experimental data.

FURTHER INVESTIGATIONS

Due to the non-excessive value of the maximum rolling speed measured when $\theta = 90°$ ($v = 6.7$ $mm.s^{-1}$), experiments were carried out in which the incline angle θ was linearly varied with time, using an electric motor imposing a constant half-turn and the rolling distance was measured, as schematically described in *Figure 8*. Various slow angular velocities were tested and *Figure 9* illustrates the variations in rolling distances L according to the speed of rotation. As expected, the rolling distance decrease with an increase in rotation speed.
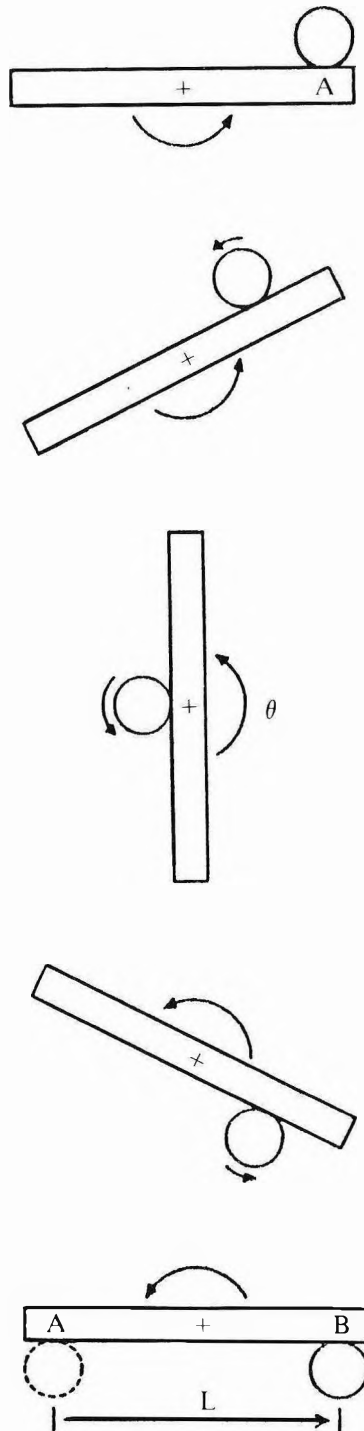
Figure 8. Schematic diagram showing the rolling of a rigid cylinder in adhesive contact with an elastic substrate turned round at constant angular velocity.
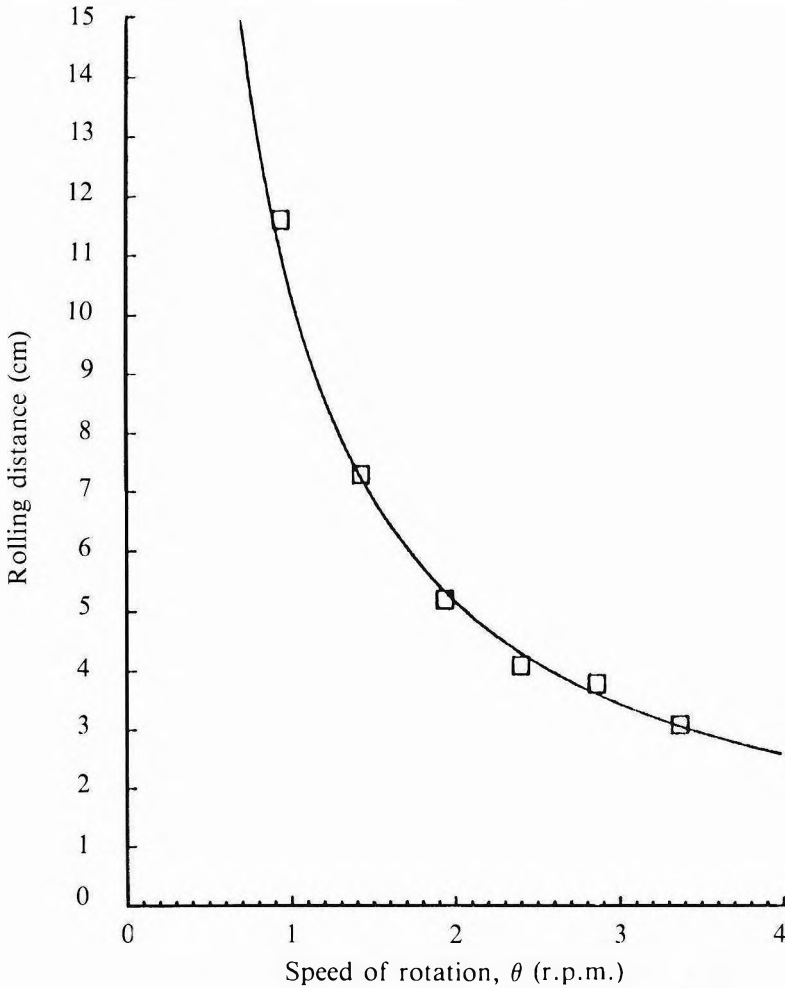
Figure 9. Rolling distance L variations according to the angular velocity $\dot{\theta}$ (computed curve and experimental data for a stainless steel cylinder in contact on a flat and smooth surface of natural rubber).

By numerical integration of kinetics, *Equation 31* with $k = 96.5$ SI units and G deduced from *Equation 30*, we have simulated the rolling distance L *versus* angular speed $\dot{\theta}$. The corresponding curve *(Figure 9)* appears to be in very good agreement with the experimental data. These results allow one to explain the following attractive experiment: when the substrate overlapped by the rubber trip is turned round continuously, the stainless steel cylinder rolls alternately on and under the rubber surface, unceasingly without dropping provided the length of the trip is greater than the rolling distance L corresponding to the imposed angular velocity.

REFERENCES

1. MAUGIS, D. AND BARQUINS, M. (1980) Fracture Mechanics and Adherence of Viscoelastic Solids, *Adhesion and Adsorption of Polymers (Lee, L.H. ed.)*, **A**, 203. New York: Plenum Publ. Corp.

2. BARQUINS, M. AND FELDER, E. (1989) Adherence and Friction of Rubber-like Materials: Some New Observations. *Proc. 5th Int. Conf. Tribology, Helsinki*, **3**, 295.

3. MAUGIS, D. AND BARQUINS, M. (1983) Adhesive Contact of Sectionally Smooth-ended Punches on Elastic Half-spaces: Theory and Experiment. *J. Phys. D: Appl. Phys.*, **16**, 1843.

4. BARQUINS, M. (1988) Force d'adherence et cinetique de roulement d'un cylindre rigide en contact adhesif avec la surface plane et lisse d'un materiau elastique souple (caoutchouc naturel). *C.R. Acad. Sci. Paris*, serie II, **306**, 509.

5. KENDALL, K. (1975) Rolling Friction and Adhesion between Smooth Solids. *Wear*, **33**, 351.

6. BARQUINS, M., MAUGIS, D., BLOUET, J. AND COURTEL, R. (1978) Contact Area of a Ball Rolling on an Adhesive Viscoelastic Material. *Wear*. **51**. 375.

7. ROBERTS, A.D. (1979) Looking at Rubber Adhesion. *Rubb. Chem. Technol.*, **52**, 23.

8. FULLER, K.N.G. AND ROBERTS, A.D. (1981) Rubber Rolling on Rough Surfaces. *J. Phys. D: Appl. Phys.*, **14**, 221.

9. ROBERTS, A.D. (1989) Rubber Adhesion at High Rolling Speeds. *J. nat. Rubb. Res.*, **3(4)**, 239.

10. BARQUINS, M. AND COURTEL, R. (1975) Rubber Friction and the Rheology of Viscoelastic Contact. *Wear*, **32**, 133.

11. ROBERTS, A.D. AND THOMAS, A.G. (1975) The Adhesion and Friction of Smooth Rubber Surfaces. *Wear*, **33**, 45.

12. SAVKOOR, A.R. AND BRIGGS, G.A.D. (1977) The Effect of Tangential Force on the Contact of Elastic Solids in Adhesion. *Proc. R. Soc.*, **A346**, 103.

13. BARQUINS, M. (1987) Adherence, frottement et usure des elastomeres. *Kautschuk Gummi Kunststoffe*, **40**, 419.

14. FELDER, E. (1988) Approche thermodynamique de l'adhesion et du frottement entre corps solides. Etude des films mices interfaciaux et de l'anisotropie de frottement. *Thesis of Sciences Doctorate*, University of Lyon, France.

15. JOHNSON, K.L. (1985) *Contact Mechanics*. Cambridge: Cambridge University Press.

16. FELDER, E. AND BARQUINS, M. (1989) Adherence, frottement et geometrie de contact d'un cylindre rigide roulant sur la surface plane et lisse d'un massif elastique. *C. R. Acad. Sci. Paris*, serie II, **309**, 1101.

17. BRIGGS G.A.D. AND BRISCOE, B.J. (1977) The Effect of Surface Topography on the Adhesion of Elastic Solids. *J. Phys. D: Appl. Phys.*, **10**, 2453.

Nitrogen Removal from Latex Concentrate Effluent Using the Anoxic/Oxidation Ditch Process: A Laboratory Study

NORDIN BIN AB. KADIR BAKTI*

Existing oxidation ditches treating rubber effluent can effectively remove organics and ammonia if fully aerated but they do not easily achieve denitrification of the nitrate formed from ammonia. A laboratory study was carried out to investigate the possibility of improving nitrogen removal and lowering the energy requirements for oxygenation in the oxidation ditch system by incorporating a pre-anoxic reactor and recycling of the nitrified effluent. The hydraulic retention time (HRT) of the anoxic reactor was varied from 0.98 days to 1.54 days, the mean cell retention time (MCRT) of the oxidation ditch from 4.43 days to 6.59 days and the ratio of effluent recycle to raw effluent flow rate (r) from 1.25 to 6.0. Under the best conditions investigated (anoxic reactor HRT of 0.98 days oxidation ditch MCRT of 6.59 days and r of 3.5), the laboratory unit was capable of removing 99% biochemical oxygen demand, 99% ammonium nitrogen and 86% total nitrogen [comprises both the total Kjeldahl nitrogen (TKN) and the total oxidised nitrogen]. A mathematical model for the process was developed and model coefficients evaluated. The model coefficients, except for those pertaining to TKN removal in the anoxic reactor, were statistically significant at probability level < 0.1. Malodour due to sulphate reduction to hydrogen sulphide in the anoxic reactor was not a problem because nitrate was preferentially utilised.

Latex concentrate effluent contains a high level of nitrogen, mainly in the form of ammonium ion, resulting from ammonia used in preserving the latex. Experience has shown that adequate removal of organics from the effluent can be achieved but removal of nitrogen is poor[1]. Laboratory studies have demonstrated the applicability of the oxidation ditch process to remove ammonium nitrogen[2,3]. However, full-scale aeration systems including the oxidation ditch system were found to be not effective in removing the nitrogen from the latex concentrate effluent[4]. The main reason for the poor nitrogen removal from the aeration systems is the inadequate supply of dissolved oxygen for the ammonium ion oxidation (nitrification) process.

Existing aeration systems, such as the oxidation ditch, if properly operated with adequate supply of dissolved oxygen, can remove organics and ammonium ion. Nitrate formed from the oxidation of ammonium ion is not removed. Because nitrate is also a pollutant, the ammonium ion removal through nitrification resulting in a high level of nitrate does not provide the complete solution. Although a regulatory standard for nitrate in rubber effluent is yet to be formulated, the removal of nitrate should be given due consideration. The presence of nitrate in drinking water has been associated with methemoglobinemia in infants[5].

A feasible approach to remove both forms of nitrogen (ammonia and nitrate) is to use a system where both the nitrification and denitrification processes occur in separate reactors[6,7]. In this system (*Figure 1*), the first reactor is the denitrification or anoxic (nitrate instead of oxygen is the oxidant) reactor and the second reactor is the aeration tank, such as,

---

*Rubber Research Institute of Malaysia, P.O. Box 10150, 50908 Kuala Lumpur, Malaysia
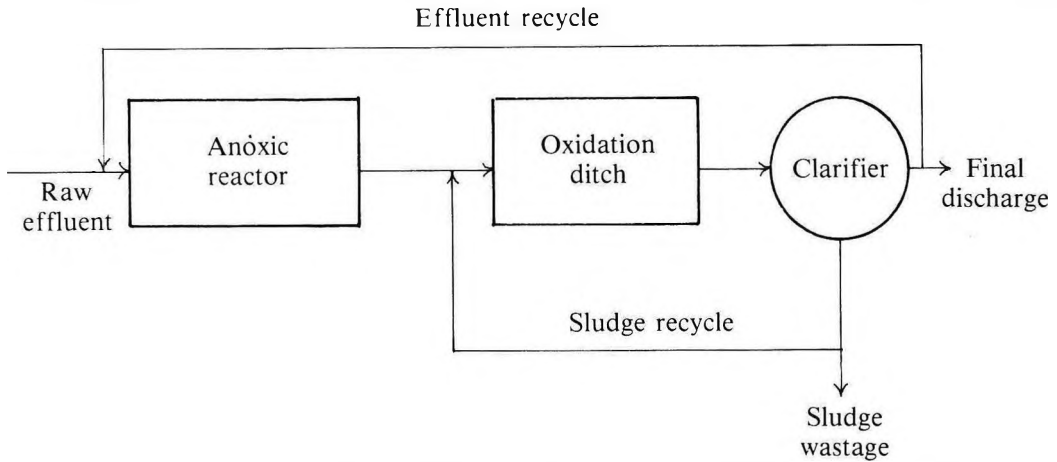
Effluent recycle

Figure 1. Process flow diagram for the anoxic/oxidation ditch system.

the oxidation ditch. A fraction of the nitrified aeration tank effluent is recycled to the anoxic reactor. This results in several aerobic/anoxic cycles for the wastewater before discharge. A substantial amount of biochemical oxygen demand (BOD) is removed in the anoxic reactor through the denitrification process, thus lowering the microbial oxygen demand in the subsequent aeration process. Also, malodour resulting from reduction of sulphate to sulphide will not occur in the anoxic reactor because nitrate is preferentially utilised instead of sulphate in the oxidation of organics[8].

The anoxic/oxidation ditch (ANOD) process can provide a modification required to improve the nitrogen removal in the existing oxidation ditch process. It can significantly lower the energy requirements for oxygenation to satisfy the carbonaceous and the nitrogenous oxygen demands in the oxidation ditch. Although there is a need to put up an additional reactor for the denitrification process, the total cost of the process can be lower than that of the existing oxidation ditch system with nitrification because in the ANOD process nitrate replaces part of the oxygen demand associated with microbial oxidation of organics.

This report presents the results of laboratory experiments using the ANOD process and the evaluation of kinetic coefficients used in the mathematical modelling of the process.

MODEL DEVELOPMENT

Considering the mass balance on a continuous flow, completely-mixed system operated under steady-state conditions, the equation describing soluble chemical oxygen demand (COD) removal in the anoxic reactor *(Figure 1)*, receiving both raw and recycled effluent, can be stated as:

$$Q_F S_{FC} + Q_R S_{RC} - (Q_F + Q_R) S_{AC}$$
$$= k_{Cl} V_A S_{AC} \qquad \dots 1$$

Letting $r = Q_R/Q_F$ and $\theta_A = V_A/Q_F$, *Equation 1* can be rearranged as:

$$\frac{1}{\theta_A} \cdot S_{FC} + \frac{r}{\theta_A} \cdot S_{RC} - \frac{(1 + r)}{\theta_A} S_{AC} = k_{Cl} S_{AC} \qquad \dots 2$$

where Q_F and Q_R = raw and recycled effluent flow rates (litre/day), respectively,

S_{FC}, S_{RC} and S_{AC} = COD concentration in raw, recycled and anoxic effluent (mg/litre), respectively,

k_{Cl} = first-order COD removal rate coefficient in the anoxic reactor (day^{-1})

V_A = volume of the anoxic reactor (litre).

The COD removal in the anoxic reactor was assumed to be first order with respect to the COD concentration in the anoxic reactor effluent based more on empirical fit to

experimental data than on any fundamental considerations. The rate coefficient k_{C1} is dependent on the reactor configuration and the type of packing medium used.

The equation describing soluble COD removal in the oxidation ditch *(Figure 1)* can be stated as:

$$(Q_F + Q_R) S_{AC} - (Q_F + Q_R) S_{RC}$$
$$= k_{C2} X_S S_{RC} V_B \qquad \qquad ...3$$

Letting $r = Q_R / Q_F$ and $\theta_B = V_B / Q_F$, *Equation 3* can be rearranged as:

$$\frac{(1 + r)}{\theta_B} \frac{(S_{AC} - S_{RC})}{X_S} = k_{C2} S_{RC} \qquad ...4$$

where k_{C2} = first-order COD removal rate coefficient in the oxidation ditch (litre/mg-day)

X_S = volatile suspended solids (VSS) in the oxidation ditch (mg/litre)

V_B = volume of the oxidation ditch (litre).

All other terms in this equation are as defined earlier. The selection of this rate equation was based on the ability to obtain a practical solution. The use of Monod's continuous function[9] to describe the kinetics using the data obtained in this study did not yield a satisfactory solution. The rate term in *Equation 3* is a special case of the Monod's function, that is, pertaining to the situation where the COD concentration is very much lower than the half-velocity coefficient in the Monod's function. The reaction in *Equation 3* is also first order with respect to the VSS concentration in the oxidation ditch. The VSS approximates the biomass concentration[9,10] and the distinction between active and inert biomass is neglected[11].

The mass balance for the total Kjeldahl nitrogen (TKN), which is composed of the ammonium and the organic nitrogen, in the anoxic reactor can be stated as:

$$Q_F S_{FA} + Q_R S_{RA} - (Q_F + Q_R) S_{AA}$$
$$= C_1 k_{C1} S_{AC} V_A - C_2 V_A \qquad ...5$$

Rearranging *Equation 5* gives:

$$\frac{1}{\theta_A} \cdot S_{FA} + \frac{r}{\theta_A} \cdot S_{RA} - \frac{(1 + r)}{\theta_A} S_{AA}$$
$$= C_1 k_{C1} S_{AC} - C_2 \qquad ...6$$

where S_{FA}, S_{RA} and S_{AA} = soluble TKN concentrations in the raw, recycled and anoxic reactor effluent (mg/litre)

C_1 = biosynthetic nitrogen uptake coefficient for the anoxic reactor, a product of nitrogen fraction in biomass and microbial growth yield in the anoxic reactor, dimensionless

C_2 = rate coefficient of soluble TKN release due to microbial decay in the anoxic reactor (mg/litre-day).

The TKN release due to microbial decay is a function of the biomass concentration. However, determining biomass concentration in the partially attached growth anoxic reactor is extremely difficult. Thus, the C_2 coefficient is dependent on the reactor configuration and type of packing medium.

The TKN mass balance in the oxidation ditch can be stated as:

$$(Q_F + Q_R) [S_{AA} - S_{RA}]$$
$$= C_3 (Q_F + Q_R) [S_{AC} - S_{RC}]$$
$$+ k_N X_S V_B - C_4 X_S V_B \qquad ...7$$

Rearranging *Equation 7* gives:

$$\frac{(S_{AA} - S_{RA})}{X_S} = \frac{C_3 (S_{AC} - S_{RC})}{X_S} + \frac{(k_N - C_4) \theta_B}{(1 + r)}$$
$$...8$$

where C_3 = biosynthetic nitrogen uptake coefficient for the oxidation ditch dimensionless

C_4 = rate coefficient of soluble TKN release due to microbial decay in the oxidation ditch (day^{-1})

k_N = nitrification rate coefficient (day^{-1})

The nitrification rate was assumed to be zero order with respect to the TKN concentration in the oxidation ditch because experimentally determined values of Monod's function half-velocity coefficient for nitrification are much

smaller than the ammonium nitrogen concen-
trations usually found in waste-water[12]. It was
assumed that the variation of the fraction of
nitrifying organisms in the mixed liquor VSS
is negligible in order that the nitrification rate
can be directly related to the mixed liquor VSS.
This simplifying assumption was made because
determining the fraction of nitrifying organisms
in mixed liquor VSS has not been well
established[12].

The mass balance for the total oxidised
nitrogen (NO_x – N) which is composed of
nitrate and nitrite nitrogen, in the oxidation
ditch can be stated as:

$$(Q_F + Q_R) [S_{AN} - S_{RN}] = k_N X_S V_B \quad ...9$$

Rearranging *Equation 9* to include r and θ_B
gives:

$$\frac{(S_{AN} - S_{RN})}{X_S} = \frac{-k_N \theta_B}{(1 + r)} \quad ...10$$

where S_{AN} and S_{RN} = NO_x - N concentrations
in the anoxic reactor effluent and the oxidation
ditch effluent, respectively. The other terms are
as defined earlier.

Equations 2, 4, 6, 8 and *10* form the
mathematical model for the ANOD system
operated under steady-state conditions and thus
could be used to predict the performance of the
system under various operating conditions.

MATERIALS AND METHODS

Description and Operation of Laboratory Unit

A schematic diagram of the laboratory
anoxic/oxidation ditch unit is shown in
Figure 2. The anoxic tank, fabricated from
aluminium sheets, measured 30 cm in length,
30 cm in width and contained water to a depth
of about 50 cm. The upper 35 cm of the anoxic
tank was packed vertically with 128 pieces of
polyvinyl chloride (PVC) tubes. Each tube had
an internal diameter of 2.3 cm, a wall thickness
of 2 mm and a length of 35 cm. The tubes
provided the surface for bacterial attachment
and growth and they were vertically placed to
minimise clogging. The specific surface area of
the packing was 234 m^2/m^3. A paddle,

measuring 23 cm horizontally and 5 cm
vertically, was centrally attached to a vertical
shaft at about 42 cm below the water surface
in the anoxic tank. The centrally-located shaft
was driven by a 0.75 kW motor. The paddle
provided mixing of the influent and kept solids
in suspension. The paddle speed was kept
constant at about 35 r.p.m.

The oxidation ditch basin, also fabricated
from aluminium sheets, was 25 cm high,
61 cm wide and 244 cm long. It contained a
baffle which was 1.2 m long and symmetrically
situated in the middle of the basin. The depth
of liquid in the basin was about 20 cm. The
liquid in the basin circulated around the baffle
with the aid of a rotor. The rotor, measuring
23 cm in length and 25 cm in diameter, consisted
of four 'comb-like' sweepers placed longitudi-
nally and symmetrically along the shaft.

Raw effluent in a holding tank was pumped
into the anoxic reactor at a constant rate using
a peristaltic pump (Watson-Marlow Model
MHRE 200). The discharge from the anoxic
reactor flowed by gravity into the oxidation
ditch basin. A portion of the clarified oxidation
ditch effluent, after solids settling, was recycled
to the anoxic reactor using a peristaltic pump
(Watson-Marlow Model MHRE 200).

In the first run, the oxidation ditch rotor
speed was 24 r.p.m. However, in subsequent
runs, the rotor speed was increased to 30 r.p.m.
to prevent the solids from settling in the basin.
The rotor speed was maintained at this low level
in order to effect mixing just sufficient to keep
the solids in suspension. Oxygenation was thus
mainly by diffused aeration. Diffused aeration
was provided by compressed air from a
portable air compressor (Hydrovane Model 5),
supplied through a fine-bubble porous stone
diffuser. The air flow rate was maintained
constant at 480 ml/min.

Five runs were carried out. *Table 1* gives the
flow rates and retention times for the five runs.
For the first four runs, the rate of effluent
recycle from oxidation ditch to the anoxic
reactor was maintained constant at
24.5 litres/day. In the last run, this recycle rate
was increased to 35 litres/day. Also, for the

View from above

Side view
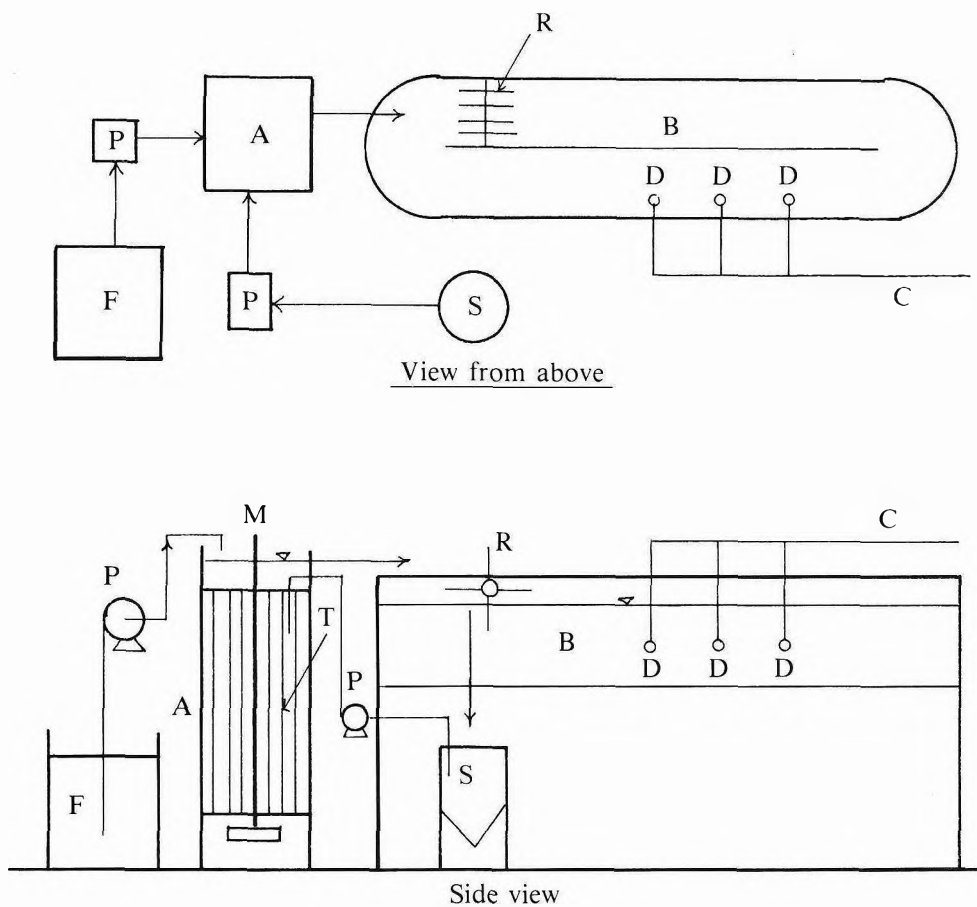
A   Anoxic reactor   M   Slow speed mixer
B   Oxidation ditch   P   Peristaltic pump
C   Compressed air   R   Rotor
D   Porous stone diffuser   S   Solids settling tank
F   Feed tank   T   PVC tubes

Figure 2. Schematic diagram of laboratory-scale anoxic/oxidation ditch system.

TABLE 1. FLOW RATES AND RETENTION TIMES OF EXPERIMENTAL RUNS

Run	Influent flow rate (litre/day)	Effluent recycle rate (litre/day)	Hydraulic retention time[a] (day), anoxic reactor oxidation ditch	
1	19.50	24.5	1.00	4.43
2	12.25	24.5	1.20	5.31
3	6.13	24.5	1.44	6.37
4	4.08	24.5	1.54	6.82
5	10.00	35.0	0.98	4.33

[a]Considering both the influent flow and effluent recycle

first four runs, solids from the oxidation ditch sedimentation tank were not recycled to the oxidation ditch. However, in the last run, solids recycle was practised (both approaches are acceptable in practice). In this run, about 5.23 g VSS/day was recycled.

Due to nitrification in the oxidation ditch which contributed to the acidity of the mixed liquor, a source of alkalinity had to be added to maintain the pH of the mixed liquor to around neutral. Thus, for the third and fourth runs, a certain amount of 1 M NaOH solution was added batch-wise daily to the oxidation ditch. But, due to the batch addition, pH in the ditch was not at a constant level. To improve the situation, in the last run, 120 ml/day of 100 g/litre $NaHCO_3$ solution was added continuously to the oxidation ditch to give a constant pH of about 7 in the ditch.

The laboratory unit was located indoors. Averaged mean, minimum and maximum ambient temperatures were 29.0°C, 24.5°C and 35.0°C, respectively. Averaged mean, minimum and maximum liquid temperatures were 26.7°C, 24.0°C and 29.0°C, respectively.

Feed Preparation

Skimmed serum, obtained from a local latex concentrate factory, was diluted with tap water to give a chemical oxygen demand (COD) of about 3000 mg/litre in the feed. This COD value approximates the value in latex concentrate factory effluent. Lime was used to adjust the pH of the feed to a value of about 7.

Sampling and Analysis

Raw, anoxic reactor and oxidation ditch effluent samples were collected twice at weekly intervals and analysed for pH, suspended solids (SS), volatile suspended solids (VSS), chemical oxygen demand (COD), biochemical oxygen demand of three days' incubation at 30°C (BOD), total organic carbon (TOC), total Kjeldahl nitrogen (TKN), ammonium nitrogen (AN), nitrate nitrogen (NO_3N), nitrite nitrogen (NO_2N), phosphorus (P), total alkalinity (Alk) and sulfate (SO_4). Except for SS and VSS, all analyses were on filtered samples. The dissolved oxygen (DO) of the oxidation ditch mixed liquor was also monitored twice a week.

RESULTS AND DISCUSSION

Steady-state conditions in the reactors were assumed after operating each experimental run for a period exceeding twice the hydraulic retention time of the oxidation ditch (*Table 1*). Although it was known that microbial populations may attain steady-state very slowly or may not attain it at all[13], the assumption of steady-state conditions was necessarily based on practical considerations. A summary of the experimental data for each run obtained during the assumed steady-state period is given in the *Appendix*.

Substrate Removal Efficiencies

Table 2 gives the overall removal efficiencies of COD, BOD, TKN, AN and TN

TABLE 2. REMOVAL OF ORGANICS AND NITROGEN IN THE LABORATORY-SCALE ANOXIC/OXIDATION DITCH PROCESS TREATING RUBBER EFFLUENT

Run	Removal efficiency (%)				
	COD	BOD	TKN	AN	TN[a]
1	98.2	99.7	83.0	81.6	64.5
2	97.4	99.5	84.8	83.8	76.4
3	98.7	99.7	83.6	83.3	59.4
4	98.6	99.9	97.7	98.9	79.8
5	97.9	99.6	98.7	99.0	86.2

[a]TN = TKN + NO_x-N

(TKN + NO_x-N) from the ANOD system for the five experimental runs. The COD and BOD removals were extremely good (> 97%) for all the runs. The TKN and AN removals were above 80% and in the last run the removals were greater than 98%. The TN removal ranged from 59.4% *(Run 3)* to 86.2% *(Run 5)*. The variation in the nitrogen removal was mainly attributed to the ratio of effluent recycle to influent flow rate, mixed liquor pH, mixed liquor VSS and influent flow rate (governing the hydraulic retention times of the reactors). The low mixed liquor pH [pH of 4.28 before the batch NaOH addition *(Appendix)*] in *Run 3* could be the main factor for the low TN removal in this run because other factors (effluent recycle ratio = 4, mixed liquor VSS = 379 mg/litre and influent flow rate = 6.13 litres/day) were favourable to the TN removal. In *Run 4,* the low mixed liquor VSS and pH could be affecting the TN removal in the system. The introduction of continuous addition of $NaHCO_3$ in *Run 5* to maintain a constant pH level of about 7 could be the main factor contributing to the improvement in the TN removal.

Evaluation of Kinetic Coefficient

Linear regression analysis was used to determine the values of the various kinetic coefficients in *Equations 1 – 10,* using the experimental data given in the *Appendix.* The results of the statistical analysis are summarised in *Table 3.*

The variation in the experimental data could be generally explained by the mathematical models, except that of *Equation 6* where only 36.83% of the total variation in the data was explained by the model (R^2 = 0.3683). *Equation 6* pertains to the TKN removal in the anoxic reactor. The mathematical relationship could not satisfactorily explain the variation in the data partly because the solids concentration in the anoxic reactor was not determined and thus the rate of TKN release from microbial lysis as a function of solids concentration was not incorporated in the model. Determining solids concentration in the anoxic reactor was difficult because of the existence of both attached and suspended microbial growth.

In order to find out the ability of the model to predict values, linear regression analyses of predicted *versus* observed values for COD and TN (TKN + NO_x-N) concentrations in the final discharge were carried out *(Figures 3* and *4)*. Predicted values were obtained from solving a simultaneous set of equations *(Equations 2, 4, 6, 8* and *10)*, using the experimental data given in *Table 1,* the *Appendix* and the values of model coefficients given in *Table 2.* A perfect agreement between the predicted and the observed values is reached when the slope of the regression line is equal

TABLE 3. STATISTICAL ANALYSIS TO EVALUATE COEFFICIENTS IN THE PRESENT MODEL

Coefficient	Value	t-statistics	Equation	R^2
k_{C1}	2.6618***	12.560	2	0.8875
k_{C2}	0.0024*	3.728	4	0.7485
C_1	0.0445 (P<0.3)	– 1.323	6	0.3683
C_2	23.8817 (P<0.4)	1.201	6	0.3683
C_3	0.6352**	4.653	8	0.9552
$k_N - C_4$	0.0411 (P<0.1)	2.123	8	0.9552
k_N	0.0701**	5.731	10	0.6818

* Significant at probability level (P) < 0.05

** Significant at P < 0.01

*** Significant at P < 0.001

R^2 = Square of correlation coefficient for the relevant equation

Predicted COD value (mg/litre)

- 100
- 80
- 60
- 40
- 20
- 0
- − 20
- − 40

o——o Observed data

——— Regression line with $R^2 = 0.891$,
slope = 1.815 and y-intercept = −51.39

Observed COD value (mg/litre)
0 10 20 30 40 50 60 70 80
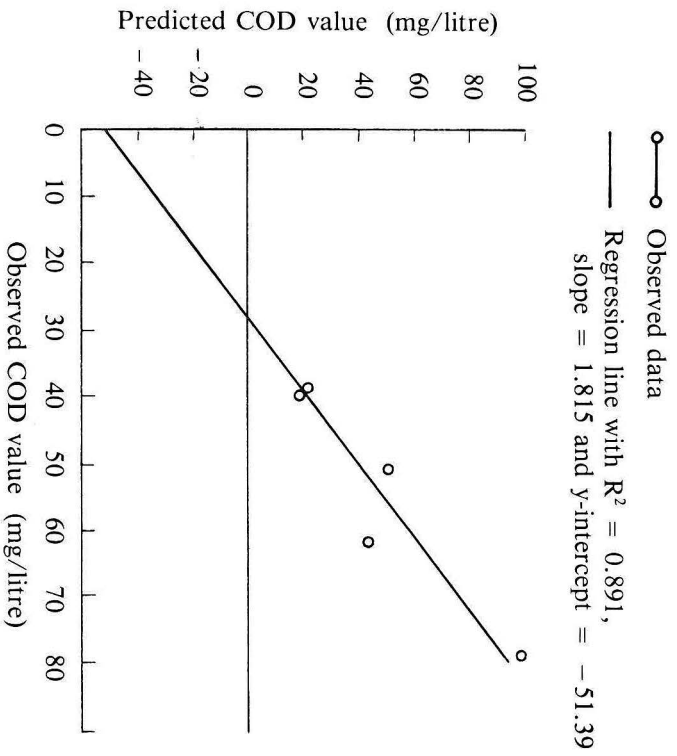
Figure 3. Linear least-squares plot of predicted versus observed COD of oxidation ditch effluent.

Predicted total nitrogen (mg/litre)

- 300
- 250
- 200
- 150
- 100
- 50
- 0

– – – Regression line for a complete model

■ Observed data for this regression (complete model)

——— Regression line for a model neglecting Equation 6

o——o Observed data for this regression (model neglecting Equation 6)

R^2	= 0.014
slope	= 0.205
y-intercept	= 172.49

R^2	= 0.850
slope	= 1.085
y-intercept	= 12.13

Observed total nitrogen (mg/litre)
0 50 100 150 200

Figure 4. Linear least-squares plots of predicted versus observed total nitrogen ($TKN + NO_x\text{-}N$) of oxidation ditch effluent.

to unity, the y-intercept is zero and the square of correlation coefficient (R^2) has a value of one. However, due to unavoidable experimental errors and inadequacies in the model, perfect agreement between the predicted and observed values is rarely achieved.

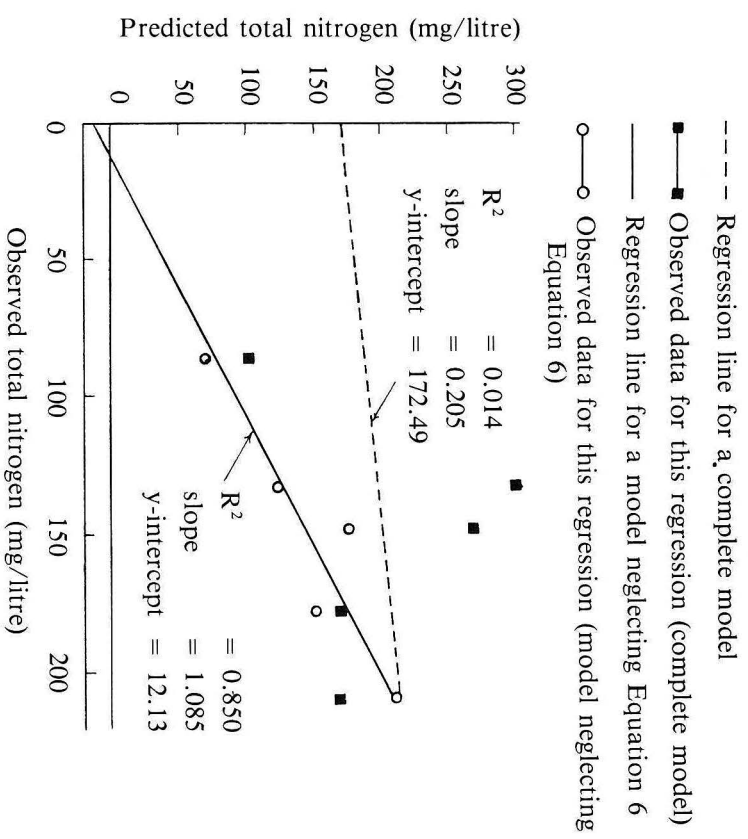In *Figure 3,* it can be seen that the agreement between the predicted and the observed COD of oxidation ditch effluent is reasonably good as indicated by a good correlation ($R^2 = 0.891$) between the variables. However, the model could not fully explain the variation in the experimental data as indicated by the significant deviations in the values of the y-intercept and the slope of the regression line from those of the ideal relationship explained in the preceding paragraph.

In *Figure 4,* agreement between the predicted and observed TN values was poor if a complete model was considered ($R^2 = 0.014$). This agreement however significantly improved if *Equation 6* was not included in the model ($R^2 = 0.85$).

Sulphate Reduction

The relationship between rate of sulphate reduction and rate of total oxidised nitrogen (NO_x-N) reduction in the anoxic reactor is given in *Figure 5.* The rate of sulphate reduction is seen to be higher at lower NO_x-N, reduction rates. In the present study, NO_x-N, mainly nitrate, was completely utilised in all the experimental runs (the NO_x-N concentrations in the anoxic reactor effluent ranged from 0.3 mg/litre to 2.9 mg/litre), whereas, sulphate was only partially utilised (SO_4 concentrations in the anoxic reactor effluent ranged from 864 mg/litre to 1479 mg/litre). It should also be noted that the mean energy yields[8] for the transfer of a molar equivalent of electrons from an organic compound to nitrate and sulphate are 18.0 kcal and 2.4 kcal, respectively. This favours nitrate to be used as an electron acceptor (oxidant) in preference to sulphate. Thus, sulphate reduction is dependent on nitrate reduction as indicated in *Figure 5.* This means a lower rate of hydrogen sulphide production with a higher rate of nitrate reduction. Thus,
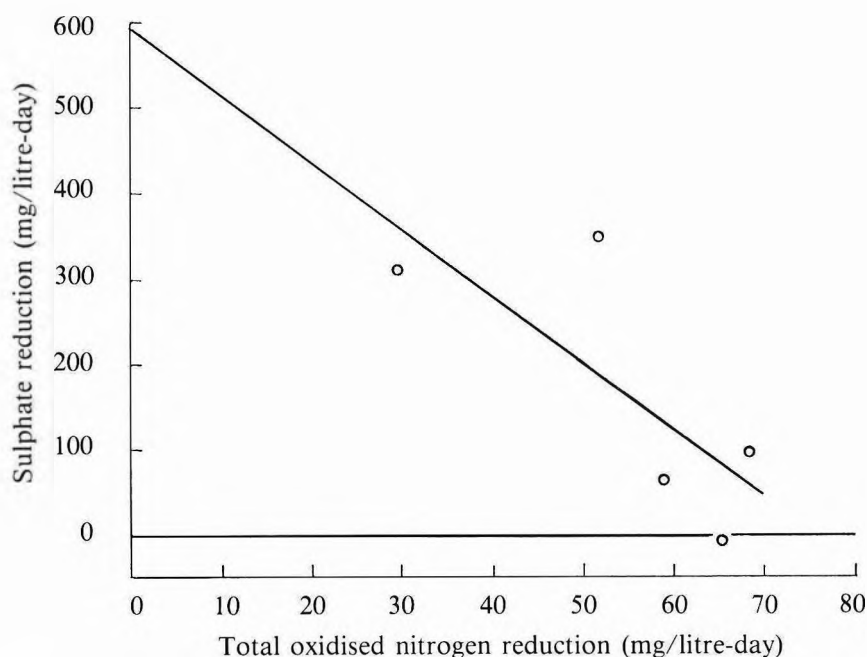

Figure 5. Relationship between sulphate reduction and total oxidised nitrogen reduction in the anoxic reactor.

a well-operated anoxic reactor with sufficient nitrate in the recycled effluent will not pose a problem with malodour due to hydrogen sulphide and other anaerobic biodegradation processes.

Process Parameters

Parameters governing the nitrification and the denitrification processes in the ANOD system include the COD to TKN ratio, pH, dissolved oxygen level, hydraulic retention time, mean cell retention time and ratio of effluent recycle to raw effluent flow rate.

In the present study, the raw effluent COD to TKN ratio ranged from 4.2 to 5.8. The values are above the theoretical ratio for denitrification[14] which is 2.95. The results indicate that, for the rubber effluent, total denitrification theoretically can be achieved.

The optimum pH for heterotrophic and autotrophic nitrifying growth[10] is generally about 7. Rubber effluent is acidic and thus a source of alkalinity has to be added. Nitrification process in the oxidation ditch also contributes to the acidity of the effluent. In the present study, about 0.27 g of $NaHCO_3$ per litre of effluent was added to maintain a pH of about 7 in the ditch.

In the present study, the dissolved oxygen (DO) level in the anoxic reactor was extremely low (0.2 mg/litre) and was favourable to the denitrification process. The low DO level was mainly the result of the lack of aeration and the oxygen-consuming reaction of facultative bacteria on the waste entering the reactor. The DO level in the oxidation ditch was sufficiently high (generally above 2.0 mg/litre) and was not inhibiting the nitrification process. The lowest DO level[15] at which nitrification can occur is 0.3 mg/litre.

In the present study, the HRT of the anoxic reactor ranged from 0.98 days to 1.54 days, and that of the oxidation ditch ranged from 4.33 days to 6.82 days. It would not be cost effective to have higher HRT values.

The mean cell retention time (MCRT) is an important process parameter for suspended-growth systems because of its basic relationship to bacterial growth rate. In the first four runs of the present study, the MCRT in the oxidation ditch was equal to the HRT because sludge was not recycled. In the final run, the MCRT was 6.59 days, higher than the corresponding HRT which was 4.33 days, due to sludge recycle. The present results indicate that the MCRT in the oxidation ditch should be at least 6 days to achieve the total nitrogen (TN) removal greater than 80%.

A fraction of the nitrified oxidation ditch effluent was recycled to the anoxic reactor to allow denitrification. The ratio of effluent recycle to raw effluent flow rate (r) was varied from 1.25 to 6.0. Increasing r theoretically enhances the rate of denitrification. The present results indicate that the r value of at least 2 should be used to give the TN removal greater than 75%.

Commercial Application

The laboratory study has indicated the possibility of using the ANOD system to remove both the reduced and oxidised forms of nitrogen and with this modification the energy inputs for oxygenation in the oxidation ditch can be lowered. However, there is a need for an additional reactor, namely, the anoxic reactor. But the cost of the anoxic reactor can be high if PVC tubes, used in this study, were to be used. Further investigation to lower the cost of anoxic reactor packing is required before the ANOD system can be commercially applied.

CONCLUSION

The laboratory study has demonstrated the possibility of improving the nitrogen removal in the oxidation ditch system by incorporating the anoxic reactor and effluent recycle. The process provides the opportunity for the nitrate formed in the aeration system to be also removed. Under the best conditions investigated, the laboratory unit of the modified oxidation ditch process was capable of removing 98% COD, 99% BOD, 99% TKN, 99% AN

and 86% TN. The TN comprises both the TKN and the total oxidised nitrogen.

A mathematical model for the process was developed and model coefficients evaluated. The model coefficients, except for those pertaining to the nitrogen removal in the anoxic reactor, were statistically significant at probability level < 0.1.

The sulphate reduction rate was observed to be lower at higher nitrate reduction rates. With sufficient nitrate in the recycled effluent, the production of hydrogen sulphide is suppressed and thus malodour will not arise in a well-operated anoxic system.

With PVC tubes providing surfaces for microbial growth, the cost of the anoxic system may be prohibitive. Further investigation is required to find cost-effective anoxic reactor packings.

REFERENCES

1. AHMAD IBRAHIM AND NORDIN BIN AB. KADIR BAKTI (1981) Nitrogen Removal from Latex Concentrate Effluent through Biological Nitrification and Ammonia Desorption. *Proc. Rubb. Res. Inst. Malaysia Plrs' Conf. Kuala Lumpur 1981*, 389.

2. PONNIAH, C. D. (1975) Treatment of Acidified Skim Serum by a Laboratory Scale Oxidation Ditch. *Proc. Agro-Ind. Wastes Symp.*, 94.

3. AHMAD IBRAHIM (1980) A Laboratory Evaluation of Removal of Nitrogen from Rubber Processing Effluent Using the Oxidation Ditch Process. *J. Rubb. Res. Inst. Malaysia*, **28(1)**, 26.

4. AHMAD IBRAHIM AND JOHN, C. K. (1986) Aeration Systems for the Treatment of Effluent from Latex Concentrate Factories. *Proc. Int. Rubb. Conf. 1985 Kuala Lumpur*, 202.

5. SAWYER, C. N. AND McCARTY, P. L. (1978) *Chemistry for Environmental Engineering* (3rd edition). New York: McGraw-Hill Inc.

6. VAN HAANDEL, A. C., EKAMA, G. A. AND MARAIS, G. V. R. (1981) The Activated Sludge Process. 3. Single Sludge Denitrification. *Wat. Res.*, **15**, 1135.

7. BATCHELOR, B. (1982) Kinetic Analysis of Alternative Configurations for Single-sludge Nitrification/Denitrification. *J. Wat. Pollut. Control Fed.*, **54**, 1493.

8. PAINTER, H. A. (1977) Microbial Transformation of Inorganic Nitrogen. *Prog. Wat. Technol.*, **8**, 3.

9. LAWRENCE, A.W. AND McCARTY, P. L. (1970) Unified Basis for Biological Treatment Design and Operation. *J. Sanit. Engng Div. Am. Soc. Civ. Engrs*, **96**, 757.

10. METCALF AND EDDY, INC. (1979) *Wastewater Engineering: Treatment, Disposal and Reuse.* New York: McGraw-Hill Inc.

11. WATKIN, A. T. AND ECKENFELDER, W. W. (1985) A New Design Procedure for Activated Sludge based on Active Mass. *Envir. Technol. Lett.* **6**, 421.

12. HALL, E. R. AND MURPHY, K. L. (1980) Estimation of Nitrifying Biomass and Kinetics in Wastewater. *Wat. Res.*, **14**, 297.

13. SHEINTUCH, M. (1987) Steady-state Modelling of Reactor-settler Interaction. *Wat. Res.*, **21**, 1463.

14. VERSTRAETE, W. AND VAN VAERENBERG, E. (1986) Aerobic Activated Sludge, *Biotechnology, (H.J. Rehm, and G. Reeds, eds.)*, **8**, 44. Weinheim: VCH Verlagsgesellschaft.

15. STENSTROM, M. K. AND PODUSKA, R. A. (1980) The Effect of Dissolved Oxygen Concentration on Nitrification. *Wat. Res.*, **14**, 643.

EXPERIMENTAL DATA FOR EACH RUN OBTAINED DURING THE ASSUMED STEADY-STATE PERIOD

Parameter	Feed			Anoxic reactor			Oxidation ditch		
	Mean	cv	n	Mean	cv	n	Mean	cv	n
Run 1									
pH	7.10	2.1	14	7.89	6.2	14	6.14	7.9	14
SS	–			–			658	16.6	13
VSS	–			–			553	16.2	13
COD	2 756	6.6	14	329	45.1	14	51	23.4	14
BOD	2 101	9.9	14	222	43.1	14	7	70.3	14
TOC	891	24.3	13	236	36.2	13	16	34.8	13
TKN	501	18.3	14	265	16.7	14	85	22.3	14
AN	353	23.0	14	223	15.2	14	65	16.7	14
NO_3N	0.4	77.8	14	0.3	79.7	14	86.5	22.0	14
NO_2N	ud	–	14	ud	–	14	6.5	214	14
P	12.5	37.8	13	6.6	21.0	13	5.5	19.0	13
Alk	968	46.1	14	893	18.7	14	24.7	115	14
SO_4	1 237	23.7	14	864	31.5	13	1 201	8.8	14
DO	–			0.2	0.1	14	1.1	36.4	14
Run 2									
pH	7.03	0.7	7	8.21	3.6	7	6.81	6.4	7
SS	–			–			177	32.3	7
VSS	–			–			127	53.5	7
COD	3 010	10.6	7	283	21.4	7	79	24.8	7
BOD	2 072	17.5	7	132	45.5	7	11	99.0	7
TOC	1 069	21.7	7	165	28.4	7	24	42.1	7
TKN	621	23.5	18	121	47.6	18	8	78.8	18
AN	404	33.0	18	87	49.8	18	4	108	18
NO_3N	ud		17	2.9	152	15	71.8	13.2	17
NO_2N	ud	–	17	ud	–	16	6.1	56.5	17
P	17.0	30.0	18	3.0	34.3	18	2.0	35.0	18
Alk	790	28.6	17	538	27.4	18	93	65.6	17
SO_4	1 242	23.8	18	1 272	27.2	18	361	25.4	18
DO	–			–			2.1	69.5	12
Run 3									
pH	$4.28/7.02^a$	0.2	8	8.26	2.2	8	7.10	2.0	8
SS	–			–			452	79.9	7
VSS	–			–			379	69.8	7
COD	2 990	5.1	8	144	36.6	8	40	22.2	8
BOD	2 458	8.5	8	60	75.2	8	7	130	8
TKN	517	13.7	8	209	29.1	8	85	24.3	8
AN	371	15.5	8	149	25.7	8	62	22.8	8

EXPERIMENTAL DATA FOR EACH RUN OBTAINED DURING THE ASSUMED STEADY-STATE PERIOD

Parameter	Feed			Anoxic reactor			Oxidation ditch		
	Mean	cv	n	Mean	cv	n	Mean	cv	n
Run 3									
NO$_3$N	0.8	99.9	8	1.6	194	8	123.5	14.3	8
NO$_2$N	ud	–	8	ud	–	8	1.1	74.2	8
P	14.7	20.7	7	3.3	29.0	7	5.1	38.0	7
Alk	813	13.8	8	680	25.6	8	18.3	40.6	8
SO$_4$	1 002	20.9	8	1 479	20.9	8	1 773	9.1	8
DO	–			–			4.2	25.4	8
Run 4									
pH	5.95/7.07[a]	0.9	14	8.13	1.2	14	7.06	1.3	14
SS	–			–			227	54.5	14
VSS	–			–			168	40.9	14
COD	2 750	12.7	14	92	34.4	14	39	29.3	14
BOD	2 230	11.0	14	15	74.5	14	3	59.6	14
TKN	657	11.6	12	128	33.7	12	15	63.9	12
AN	460	24.6	12	76	22.3	12	5	63.6	12
NO$_3$N	ud		14	0.3	254	14	118	17.9	14
NO$_2$N	ud	–	14	ud	–	14	ud	–	14
P	12.6	52.9	14	4.1	94.1	14	2.4	62.0	14
Alk	780	29.1	14	458	41.8	14	9	42.6	14
SO$_4$	977	30.9	13	1 350	33.5	14	1 401	37.1	14
DO	–			0.2	0.0	2	6.1	2.3	2
Run 5									
pH	7.07	1.1	18	7.89	2.3	18	7.02	3.1	18
SS	–			–			453	17.6	18
VSS	–			–			331	22.2	18
COD	2 988	14.4	18	153	53.6	18	62	28.1	18
BOD	2 501	15.1	18	69	92.3	18	11	59.6	18
TKN	621	23.5	18	121	47.6	18	8	78.8	18
AN	404	33.0	18	87	49.8	18	4	108	18
NO$_3$N	ud		17	2.9	152	15	71.8	13.2	17
NO$_2$N	ud	–	17	ud	–	16	6.1	56.5	17
P	17.0	30.0	18	3.0	34.3	18	2.0	35.0	18
Alk	790	28.6	17	538	27.4	18	93	65.6	17
SO$_4$	1 242	23.8	18	1 272	27.2	18	1 361	25.4	18
DO	–			–			2.1	69.5	12

All analyses except pH are expressed in mg/litre.
cv = coefficient of variation (standard deviation/mean), percent
n = number of samples
[a]pH values before and after batch addition of NaOH

A Modified Procedure for Foliar Sampling of Hevea brasiliensis

C. H. LAU*, C. B. WONG* AND H. C. CHIN*

The current procedures of foliar sampling and laboratory preparation of samples for chemical analysis were examined. A modified approach in which the foliar samples were collected and analysed without further sub-sampling in the laboratory was studied. Statistical analysis of results obtained shows that the modified procedure is comparable to the existing procedure and can be adopted for determining the nutritional status of Hevea *leaves.*

The reliability of foliar data to assess the fertiliser requirement of *Hevea* depends on the choice of foliar sampling technique. The current sampling procedure[1,2] consists of taking one composite leaf sample from thirty trees randomly selected over an area of 15–20 ha. For mature trees, four basal leaves (triplets) of a terminal whorl which constitute the low shade leaves are sampled. The total number of leaflets (three leaflets per leaf) for each composite sample will thus be 360 (30 trees × 4 leaves per tree × 3 leaflets per leaf). To reduce the bulk of a sample, sub-sampling before drying and grinding for chemical analysis is necessary.

The factors affecting accuracy and precision of routine field sampling and analysis had been extensively studied[3-6]. In general, the variability of foliar data is attributed to two major sources of errors, *viz.* laboratory errors and field sampling errors. While field sampling errors can be reduced by increasing the number of leaves per unit area, laboratory errors can be minimised by further simplifying the procedure for plant analysis.

In recent years, the total area under rubber on which soil and foliar nutrient surveys for discriminatory fertiliser recommendations were carried out had increased to more than 115 000 ha a year and the number of foliar samples collected for analysis had exceeded 13 000 samples[7]. As a result of this increase,

the workload in leaf sampling has increased. To cope with the increase, there is a need to re-examine the current procedure of foliar sampling and laboratory analysis.

This paper attempts to determine whether modifications to the existing procedure can be made without affecting the precision and accuracy of results, especially the nutrient composition of the major elements. The benefits derived from the modification are also discussed.

EXPERIMENTAL

Field Sampling

Leaf samples from mature rubber were collected according to the established procedure reported by Chan[1]. The established procedure *(Procedure I)* and the modified procedure *(Procedure II)* are described below.

Procedure I. In each composite leaf sample, low shade leaves were sampled from thirty trees randomly selected over an area of 15–20 ha. From each tree, the four basal leaves from the terminal whorls on any low branch in the shade, excluding spurs of limited growth, were taken. The number of leaflets (three leaflets per leaf) from each tree was twelve and the total number of leaflets for each composite sample amounted to 360. The leaves, packed in paper bags, were sent immediately for analysis.

*Rubber Research Institute of Malaysia, P.O. Box 10150, 50908 Kuala Lumpur, Malaysia

Procedure II. The procedure for collecting leaf samples was similar to that described in *Procedure I.* Instead of taking all the basal leaves, only the centre leaflet of each of the four basal leaves was sampled. When the centre leaflet was not suitable, one of the other leaflets within the same whorl was taken. At four leaflets per tree, the total number of leaflets in each composite sample was 120.

Preparation of Samples for Analysis

After removing the petioles, the leaves were cleaned with a moist linen, dried at 75°C–80°C and ground to pass through a 0.55 mm screen. To reduce the bulk of leaf samples collected by *Procedure I,* sub-sampling for drying and grinding was required. Precautions were taken to ensure that the composite sample was thoroughly mixed before it was sub-sampled.

To estimate the errors due to sub-sampling and chemical analysis, each of ten composite samples obtained by *Procedure I* was divided into four sub-samples of ninety leaflets each. The sub-samples were dried, ground and analysed in triplicates for major elements. Estimates of errors were obtained from analysis of variance according to the scheme given in *Table 1.*

Chemical Analysis

The leaf samples were analysed according to the standard procedure of the Rubber Research Institute of Malaysia[8]. About 2 g of milled leaves were charred on a hot plate and then ignited in a muffle furnace for 2 h at about 580°C. The ashed material was treated with concentrated hydrochloric acid and then digested with 20% volume/volume nitric acid. The leaf extract was analysed for phosphorus, potassium, calcium, magnesium and manganese. Nitrogen in the leaf sample was determined by the Kjeldahl digestion method followed by semi-micro distillation in a Markham apparatus. In all cases, the nutrient composition was adjusted to those at optimum leaf age[9].

The relationship between nutrient composition in leaves obtained by *Procedures I* and *II* was assessed by chemical analysis of 330 samples simultaneously collected by the two procedures. The samples were from trees of different clones, age and exploitation and grown on different soils. In addition, to test the precision and reproducibility of results, twenty-nine composite samples collected by the two procedures were analysed in triplicates. All the results were statistically analysed and examined.

RESULTS

Sub-sampling and Analytical Errors

Procedures I and *II* for sampling leaves for chemical analysis are technically similar. The only difference is that *Procedure II* does not require sub-sampling before drying and grinding. Assuming that errors attributed to operator, day-to-day operation and chemical analysis are identical for the two procedures, the major source of error in *Procedure I* is sub-

TABLE 1. ANALYSIS OF VARIANCE TO ESTIMATE THE VARIOUS SOURCES OF ERRORS

Source of variation	Degrees of freedom	Mean squares expressed as components of variance
Bulk samples	1	
Between different bulk samples	9	$\sigma_r^2 + 3\sigma_{ss}^2 + 12\sigma_s^2$
Between sub-samples within samples	30	$\sigma_r^2 + 3\sigma_{ss}^2$
Between triplicate chemical analysis	80	σ_r^2
Total	120	

sampling error. The scheme for determining sub-sampling error as well as error in chemical analyses in *Procedure I* is given in *Table 1* in which mean squares, are expressed as components of variance. From the mean squares, the errors arising from sub-sampling and chemical analyses can be computed and expressed as coefficients of variation(%) through the following equations:

$$\text{Analytical error} = \frac{100}{\text{Mean}} \sqrt{\sigma_r^2}$$

$$\text{Sub-sampling error} = \frac{100}{\text{Mean}} \sqrt{\frac{(\sigma_r^2 + 3\sigma_{ss}^2) - \sigma_r^2}{3}}$$

where σ_r^2 and σ_{ss}^2 are variance associated with chemical analyses, and sub-sampling, respectively.

The estimates of sub-sampling and analytical errors expressed as coefficients of variation (CV) are shown in *Table 2*. The sub-sampling errors for nitrogen, phosphorus, potassium, calcium, magnesium and manganese as determined by the CV ranged from 3.2% to 8.6% whereas the analytical errors were within the range of 3.9% to 7.2%. Except for nitrogen and potassium, errors for sub-sampling and chemical analyses were much larger and exceeded the CV value of 5%. These relatively large errors were consistent with the CV values of 5%–10% in plant analyses cross-checks among Malaysian laboratories held in the 1983–85 period[10]. Additionally, the inter-laboratory cross-checks also showed that the number of 'rogue' values (analytical results that had deviated by more than twice the standard deviation from the overall mean) had increased tremendously in the participating laboratories. In this study, 'rogue' values as defined were not omitted when statistical computations were made. All analyses were carried out in a routine manner with no special emphasis given or precaution taken. Further to this, the sampling and analysis were done to coincide with the peak season of soil and foliar survey.

Relationship between Procedures I and II

In an attempt to determine whether there were significant differences in foliar data when the leaves were sampled by the two procedures, the analytical results of 330 composite samples were studied. Significant correlations between the results of samples collected by *Procedures I* and *II* were obtained. These correlations as given in *Table 3* were significant at $P < 0.001$. The regression equations as obtained for each element were also shown in *Table 3*. For all the major elements, the slopes of the regression lines were significantly different and so were the regression coefficients. The regression lines in all cases did not originate from the origin.

Comparing the nutrient composition of twenty-nine foliar samples collected by the two procedures, it was observed that samples collected by *Procedure II* had higher values. In *Table 4*, pairwise t-test showed that there were significant differences in the nitrogen, phosphorus, potassium, calcium and magnesium concentrations of the leaves. Nitrogen and phosphorus registered the most significant diference at the 0.1% level whereas there was no significant difference in the manganese values. The difference in leaf values is anticipated since it is not possible to sample leaves of the same age and position for this study. Although there are significant differences in leaf values, a study of the mean of each composite sample showed that the differences seldom exceed by more than 5% of the overall mean values. Furthermore, these differences were reduced when provisions were made for the leaf age.

The precision and accuracy of *Procedures I* and *II* in determining the leaf nutrient status of rubber were assessed. In *Table 5, F*-values to determine whether there was any significant difference in precision between the two procedures were given. With the exception of phosphorus, no significant differences in nitrogen, potassium, calcium, magnesium and manganese determinations were noted.

DISCUSSION

Apart from some minor changes, the two foliar sampling procedures are generally similar. In *Procedure I,* the bulk samples require sub-

TABLE 2. COMPONENTS OF ERRORS IN PROCEDURE 1: STANDARD DEVIATION AND COEFFICIENTS OF VARIATION

Sources of variation	Overall mean C.V.(%)	Nitrogen Mean = 3.15%		Phosphorus Mean = 0.230%		Potassium Mean = 1.21%		Calcium Mean = 1.121%		Magnesium Mean = 0.291%		Manganese Mean = 130 p.p.m.	
		s.d.	CV(%)	s.d.	CV(%)	s.d.	CV(%)	s.d.	CV(%)	s.d.	CV(%)	s.d.	CV(%)
Analytical error	5.83	0.123	3.90	0.0160	6.96	0.0605	4.88	0.0652	5.82	0.0181	6.22	9.3980	7.22
Sub-sampling error	5.77	0.094	3.16	0.0121	5.26	0.0494	4.08	0.0757	6.75	0.0196	6.74	11.1800	8.60
Total error	8.28	0.160	5.09	0.0201	8.74	0.0782	6.46	0.1000	8.92	0.0267	9.18	14.66	11.28

Total error is made up of analytical and sub-sampling errors.

TABLE 3. CORRELATION COEFFICIENTS AND REGRESSION EQUATIONS
BETWEEN THE TWO SAMPLING PROCEDURES

Nutrient	Overall mean (%)	Regression equation	Correlation coefficient (r)
Nitrogen	Y = 3.38 X = 3.25	Y = 0.506 + 0.811X (±0.026) (±0.043)	0.72***
Phosphorus	Y = 0.234 X = 0.244	Y = 0.046 + 0.843X (±0.002) (±0.035)	0.96***
Potassium	Y = 1.55 X = 1.59	Y = 0.115 + 0.955X (±0.007) (±0.026)	0.89***
Calcium	Y = 0.943 X = 1.001	Y = 0.182 + 0.870X (±0.010) (±0.086)	0.80***
Magnesium	Y = 0.385 X = 0.389	Y = 0.102 + 0.748X (±0.006) (±0.057)	0.58***

Y = Procedure I; X = Procedure II; all values are adjusted for leaf age.

Number of composite samples is 330.

Figures within brackets are standard errors.

*** P < 0.001

TABLE 4. PAIRWISE T-TESTS FOR DIFFERENCES BETWEEN THE MEANS OF THE TWO PROCEDURES

Item	Nutrient composition					
	N(%)	P(%)	K(%)	Ca(%)	Mg(%)	Mn(p.p.m.)
Mean value Procedure I	3.36 (3.63)	0.266 (0.223)	1.35 (1.37)	1.050	0.378	119
Mean value Procedure II	3.23 (3.58)	0.239 (0.241)	1.38 (1.39)	1.106	0.394	120
t-value	-6.55***	6.25***	2.52*	3.56**	2.09*	0.54NS
n	29	29	29	29	29	29

***P < 0.001; **P < 0.01; *P < 0.05

NS – Not significant

Figures within brackets are values after adjustment for optimum leaf age.

sampling for drying and grinding. Unless steps are taken to ensure that all the sampling trees are adequately represented, the sub-sampling errors could be large as shown in *Table 2*. It is interesting to note that the sub-sampling errors for all the nutrient elements contributed as much as the analytical errors to the total error. Particularly during the peak sampling period between May and October, the need to prepare and analyse the large number of samples daily can affect the quality of results. Under these circumstances, the day-to-day operators' errors as studied by Middleton *et al.*[4] would tend to become significant.

TABLE 5. F-TESTS FOR SIGNIFICANCE OF DIFFERENCES IN PRECISION
BETWEEN THE TWO PROCEDURES

Item	Nutrient element					
	N	P	K	Ca	Mg	Mn
Within group error variance						
Procedure I	0.0151	0.0897×10^{-3}	0.0030	0.0054	0.0004	125.59
Procedure II	0.0102	0.0483×10^{-3}	0.0028	0.0034	0.0003	124.06
F-value	1.48NS	1.86*	1.07NS	1.57NS	1.33NS	1.01NS

*$P < 0.05$
NS: Not significant

In *Procedure II,* the sub-sampling step in the laboratory is omitted and all the materials that are required for analysis have already been carefully selected and bulked together in the field. The question that all the sampling trees are not represented does not arise. The samples are immediately dried and ground. The problem of storage in a refrigerator is also minimised when the samples can not be dried and ground immediately upon arrival. Furthermore, it is more convenient to transport samples from the field to the laboratory as the number of cardboard boxes required to contain the same number of samples would be reduced. A normal cardboard box would then contain about thrice the number of samples compared to *Procedure I.*

Foliar results of samples collected by the two procedures were highly related to each other. There was no significant difference in the level of precision and accuracy in the two procedures. In view of this and coupled with the high correlation of the results, the current interpretation of foliar data for manurial purposes is unlikely to be affected if the foliar samples were collected by *Procedure II.*

CONCLUSION

Considering that the number of foliar samples for laboratory analysis had increased significantly over the years, it is pertinent that the current field sampling procedures be modified to reduce the various sources of errors. One of these sources of errors is sub-sampling in the laboratory for drying and grinding. The modified procedure does not require further sub-sampling and the samples thus collected truly represent the area. In addition to this, the procedure also minimises the cost of transporting samples to the laboratory, storage problems and space in the oven for drying. In view of the reduced volume, the samples collected would be easier to handle in smaller cardboard boxes both in the field and subsequent collection from the transport station. Additionally, the size of leaf bags can be smaller for convenience in handling and storage in the field as well as in the laboratory.

REFERENCES

1. CHAN, H.Y. (1971) Soil and Leaf Nutrient Surveys for Discriminatory Fertiliser Use in West Malaysian Rubber Holdings. *Proc. Rubb. Res. Inst. Malaya Plrs' Conf. Kuala Lumpur 1971*, 201.

2. SHORROCKS, V.M. (1962) Leaf Analysis as a Guide to the Nutrition of *Hevea brasiliensis*. V. A Leaf Sampling Technique for Mature Trees. *J. Rubb. Res. Inst. Malaya*, **17(5)**, 167.

3. SHORROCKS, V.M. (1964) Some Problems related to the Choice of a Leaf Sampling Technique for Mature *Hevea brasiliensis, Plant Analysis and Fertiliser Problems, IV (Bould, C.* et. al. *eds.)*, 306. Michigan: American Society of Horticultural Science.

4. MIDDLETON, K.K., CHIN, P. T. AND IYER, G.C. (1966) Accuracy and Precision in Routine Leaf Analysis *J. Rubb. Res. Inst. Malaya*, **19(4)**, 189.

5. LANCASTER, LAI AIM (1971) Accuracy and Precision in Routine Plant Analyses. *Proc. 3rd Meet. Standardisation of Soil and Plant Analysis in Malaysia, Kuala Lumpur, 1971*, 244.

6. LAU, C.H. AND CHAN, H.Y. (1989) Effect of Sampling Intensity on Precision of Soil and Foliar Data I. Paleudults derived from Granite *J. nat. Rubb. Res.*, **4(4)**, 239.

7. RUBBER RESEARCH INSTITUTE OF MALAYSIA (1989) *Rep. Rubb. Res. Inst. Malaysia 1988.*

8. RUBBER RESEARCH INSTITUTE OF MALAYSIA (1980) *Methods of Plant Analysis.*

9. PUSHPARAJAH, E. AND TAN, K.T. (1972) Factors influencing Leaf Nutrient Levels in Rubber. *Proc. Rubb. Res. Inst. Malaysia Plrs' Conf. Kuala Lumpur 1972*, 146.

10. CHOOI, S.Y. AND GOH, K.H. (1985) Report on Plant Analysis Cross-checks between Malaysian Laboratories: 1983-1985. *Proc. Semin. and 8th Meet. Standardisation of Plant and Soil Analysis in Malaysia, 1985.*

Lutoids of Hevea *Latex:*
Morphological Considerations

J.B. GOMEZ*

Lutoids have been known for over forty years, but their functions and physiology are not fully understood. There is a strong school of thought which has identified lysosomal properties in these vesicular structures found in abundance in Hevea *latex. Earlier proposals that these organelles are vacuoles have also found acceptance. This paper considers some of the morphological aspects of the variability of lutoids and the physiological complexity of the organelle. Gaps in the knowledge of the physiology of lutoids have caused considerable delay in the progress of biochemical mechanisms controlling latex flow, yield-determining qualities of certain latex properties and progress towards control of these to overcome the latex vessel plugging phenomenon.*

Homans and van Gils[1,2] reported in 1948 that in undiluted latex, there is a microscopic body distinct from the Frey Wyssling (F.W.) particles identified earlier by Frey Wyssling[3] in 1929. These particles or organelles could be separated as a lower layer or bottom fraction when latex is centrifuged at low speed. These bodies were named lutoids ('yellow bodies') as it was not suspected at that time that the yellow colour of the lower layer is due to the presence of trapped or co-sedimenting F.W. particles or F.W. complexes. Ruinen[4] revealed the presence of well defined spherical particles in the lutoid aggregates. The individual lutoids were considerably larger than most rubber particles and she concluded that they consisted of fluid material bounded by a membrane.

Schoon and Phoa[5] reported the presence of particulate inclusions in Brownian motion inside the lutoids and were of the opinion that lutoids were polymerisation vessels for rubber. These inclusions were later studied by Southorn[6] who observed that many lutoids in some latices contained particles in Brownian motion. As the latex aged, the motion ceased as well. By phase-contrast microscopy of fresh, chilled latex, Southorn[7] detected the presence of two different types of lutoids, one with an opaque membrane which was more frequent in younger trees but was also frequently observed in older trees during the wintering period. Lutoids from trees in regular tapping had fewer inclusions.

Of the prominent organelles in *Hevea* latex the lutoids are the most numerous after rubber particles. In centrifuged fresh latices, the bottom fraction consisting mainly of lutoid particles with numerous other co-sedimenting particles occupy volumes of 18%–36% of latex[8]. In size they vary from 0.5 – 3 μm and are bounded by a unit membrane about 80 Å thick[9,10]. A study of the ultrastructure of the lutoid membrane and its reaction to various surface-active chemicals has been published[11]. The osmotic sensitivity of lutoids which swell and may disrupt under hypotonic conditions was evident in the first descriptions of them[1,4]. This was emphasised by Wiersum[12] and much studied since then[13,14,15]. Pujarniscle's identification of lutoids as lysosomes because they contain characteristic hydrolases is noteworthy[15,16]. According to these researchers, lutoids fit the properties of vacuo-lysosomes.

MATERIALS AND METHODS

Latex was collected under chilled conditions from ten trees per clone from a number of

---

*Rubber Research Institute of Malaysia, P.O. Box 10150, 50908 Kuala Lumpur, Malaysia
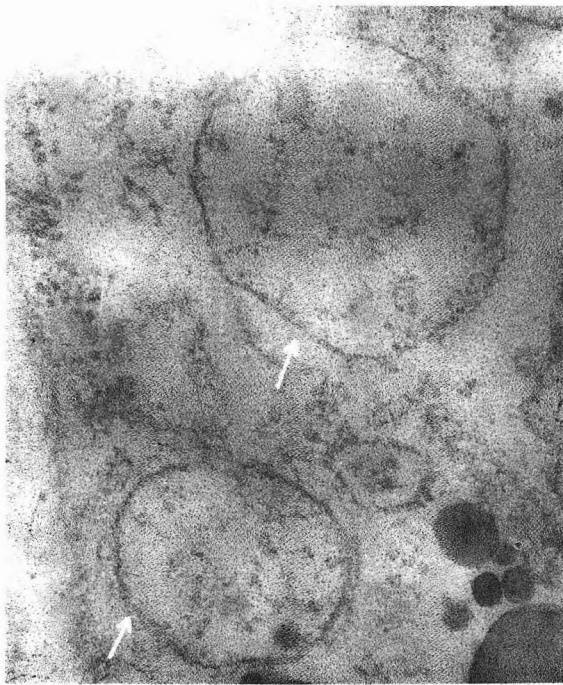
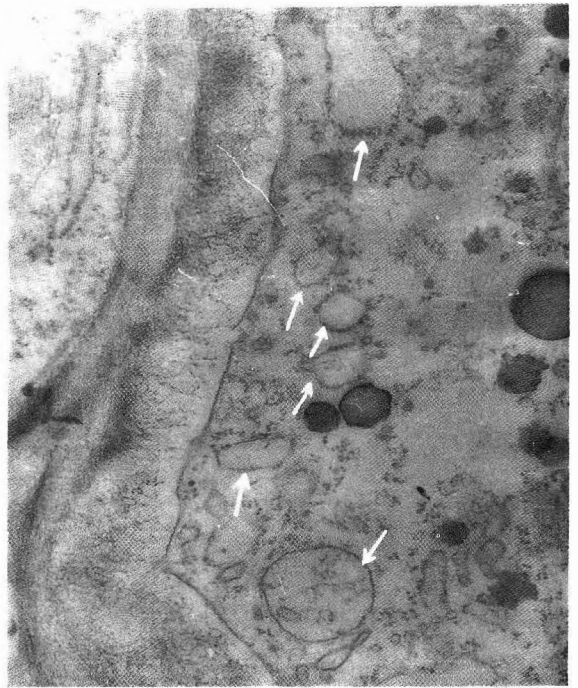*Figure 1. Prolutoids in young latex vessel in green stem. Magnification 61 000 X.*

Figure 2. Prolutoids in young latex vessel from month-old seedling. Magnification 13 000 X.
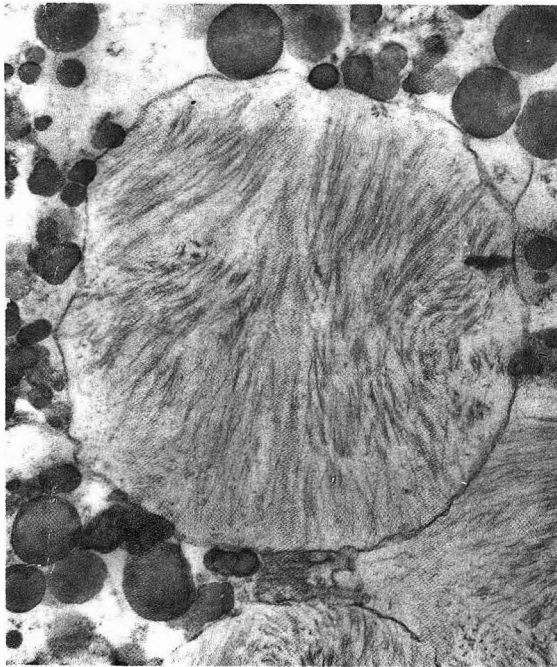

Figure 3. Lutoid with fibrillar component from green stem. Magnification 30 000 X.
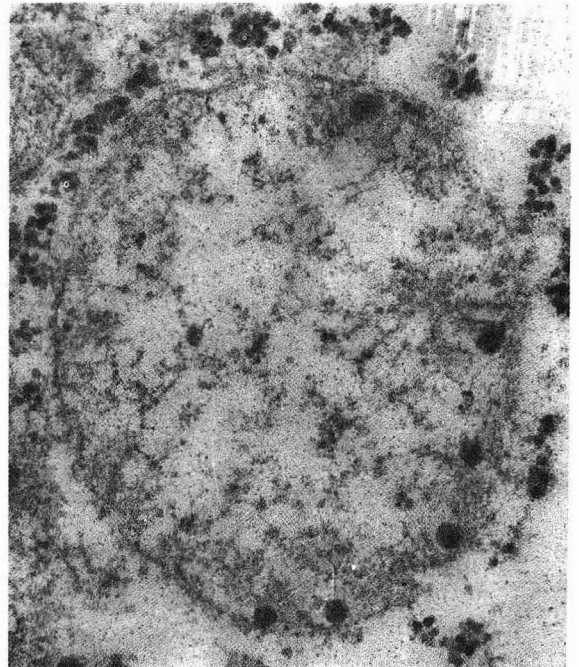

Figure 4. Young lutoid from ethephon-treated mature bark. Magnification 58 000 X.

clones selected for this study. The clones were RRIM 501, RRIM 600, GT 1, PB 86 and Tjir 1. During the study, the trees were in tapping on *Panel BO-1* under the 1/2S d/2 system. Samples for electron microscopy were secured every three months for more than one year for the observations reported in this study.

The latices were subjected to ultra-centrifugation in the Spinco L ultracentrifuge for 1 h at 59 000 g max. The latex was always kept chilled prior to centrifugation. The tubes were cut after centrifugation to secure the samples for fixation in chilled fixatives.

Each sample was fixed in a tube containing 1% osmium tetroxide buffered with phosphate at pH 7.0 and with addition of 0.35 M sucrose for tonicity control. Fixation was for a period of 2 h at 0°C–5°C after which samples were dehydrated in graded ethanol series before infiltration and embedding in styrene/methacrylate using low speed centrifugation when necessary. Sections were stained with uranyl acetate and lead citrate before examination with a Philips EM 300.

Whenever tissue sections were used for the study, soft tissues having green colour were fixed as described earlier[10]. Occasionally, soft bark tissue from mature bark was also studied for clarification of certain ultrastructural features.

Negative staining with phosphotungstic acid (PTA) was according to methods described earlier[11].

RESULTS

Figure 1 shows a section from a young latex vessel in a green stem with several lutoid-like structures close to the plasmalemma of the cell. These may be termed prolutoids. *Figure 2* shows several prolutoids from another developing laticifer in a month-old seedling tissue.

At a slightly more developed stage the prolutoids exhibit numerous protein crystals in them *(Figures 3* and *4)*. Some of this protein material is in the form of squiggles. More mature lutoids in seedling tissue contain another form of protein inclusions abundantly in stimulated tissue *(Figure 5)*.

Studies on ultracentrifuged fractions which are rich in lutoids display some characteristic differences in sedimentation pattern depending on the variety of their inclusions. *Zone 8A* often contained lutoids which had inclusions of globular osmiophilic particles[10] resembling rubber particles. Micro-helices were also easy to detect in such lutoids. *Figure 6* shows such an example from *Zone 8A* containing micro-helices and osmiophilic particles. *Figure 7* shows lutoid containing a large number of osmiophilic particles. *Figure 8* shows osmiophilic particles included in vesicles inside lutoids, almost resembling a multi-vesicular body.

Figure 9 shows a number of lutoids from *Zone 8B* with relatively few proteinaceous inclusions. Many of them are electron-transparent whereas an occasional particle contains osmiophilic inclusions.

Figure 10 is a rare example of a lutoid-like organelle retrieved from *Zone 4*, the characteristic zone of the Frey Wyssling complexes and components. However, the unit membrane surrounding the organelle merits its inclusion in this study. The occurrence of a large number of osmiophilic particles inside these organelles is exceptional.

Lutoids with finger-like extensions *(Figure 11)* are very rarely observed in tapped latex prepared by negative staining techniques. *Figure 12* shows thread-like material isolated from the same fraction containing lutoids. *Figure 13* is a lutoid with tentacles observed in negative stained preparations from the lutoid fraction.

DISCUSSION

Unit membrane-bound vesicles like lutoids appear to be the equivalent of vacuoles dispersed in a polydisperse manner[12]. However, modern biochemical techniques have revealed the presence of many acid hydrolases characteristic of lysosomes[15,16] in the lutoid fraction. It is possible therefore to consider lutoids as vacuoles with lysosomal properties.
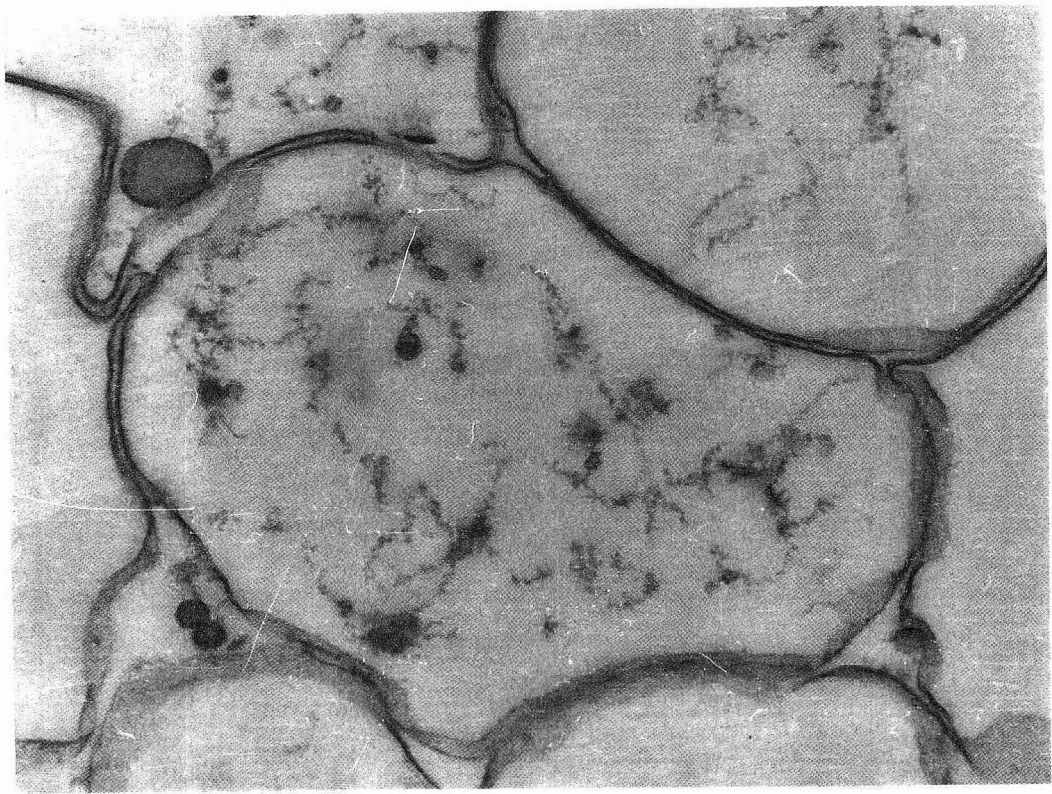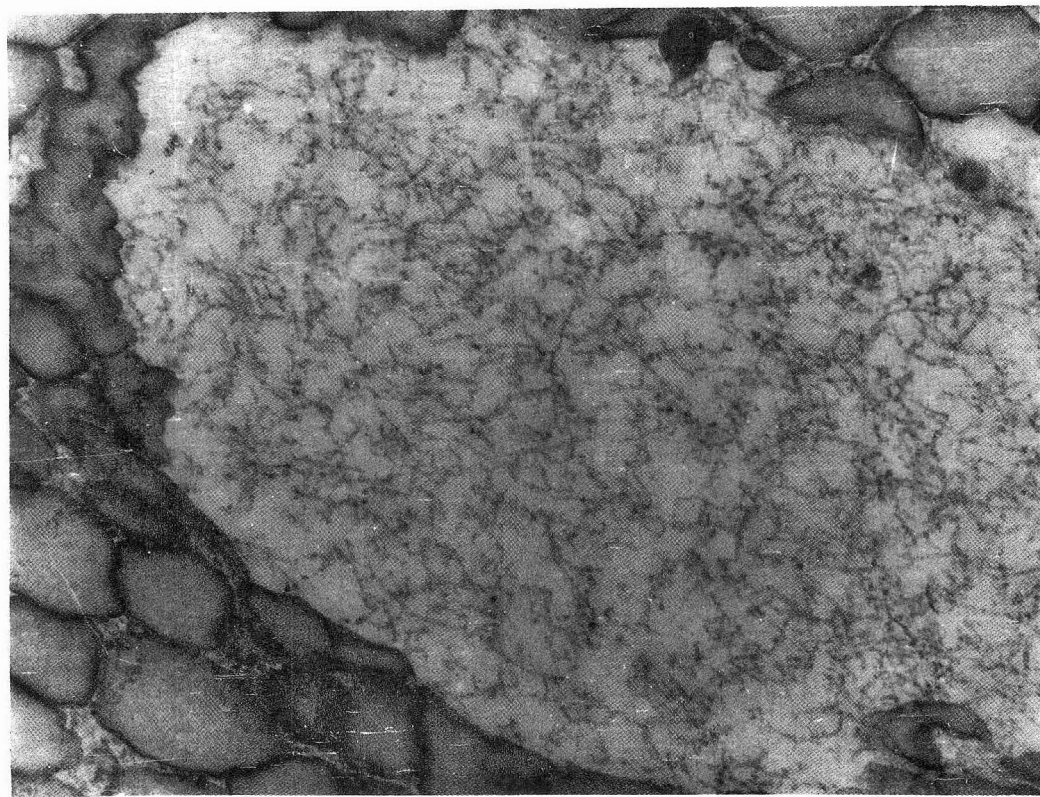
Figure 5. Lutoid from ethephon-treated seedling tissue showing micro-micro-helical content. Magnification 58 000 X.

Figure 6. Lutoid from centrifuged latex (Zone 8A) showing micro-helical material. Magnification 58 000 X.

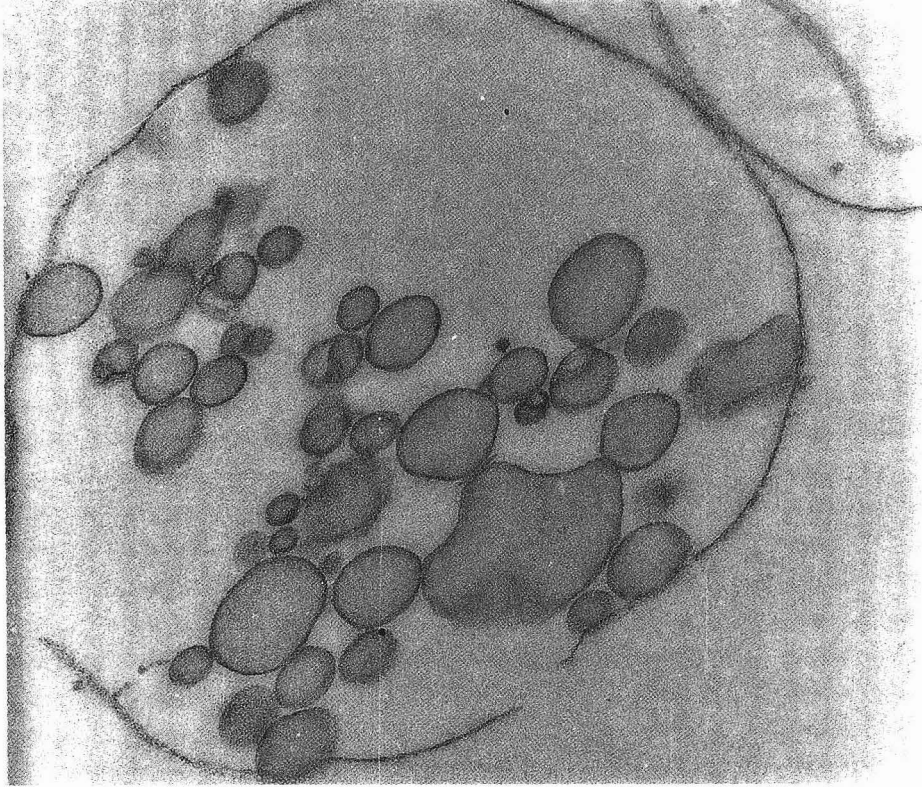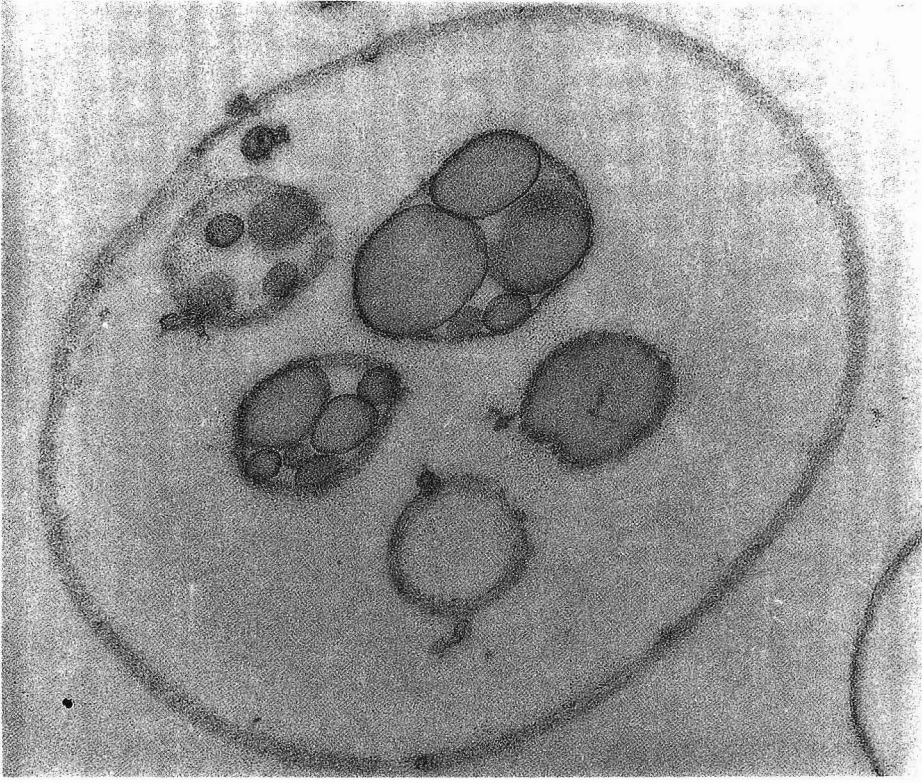*Figure 8. Lutoids from centrifuged latex (Zone 8A, PB 86) showing multi-vesicular inclusions. Magnification 55 000 X.*

Figure 7. Lutoid from centrifuged latex (Zone 8A, PB 86) with a large number of osmiophilic particles. Magnification 55 000 X.
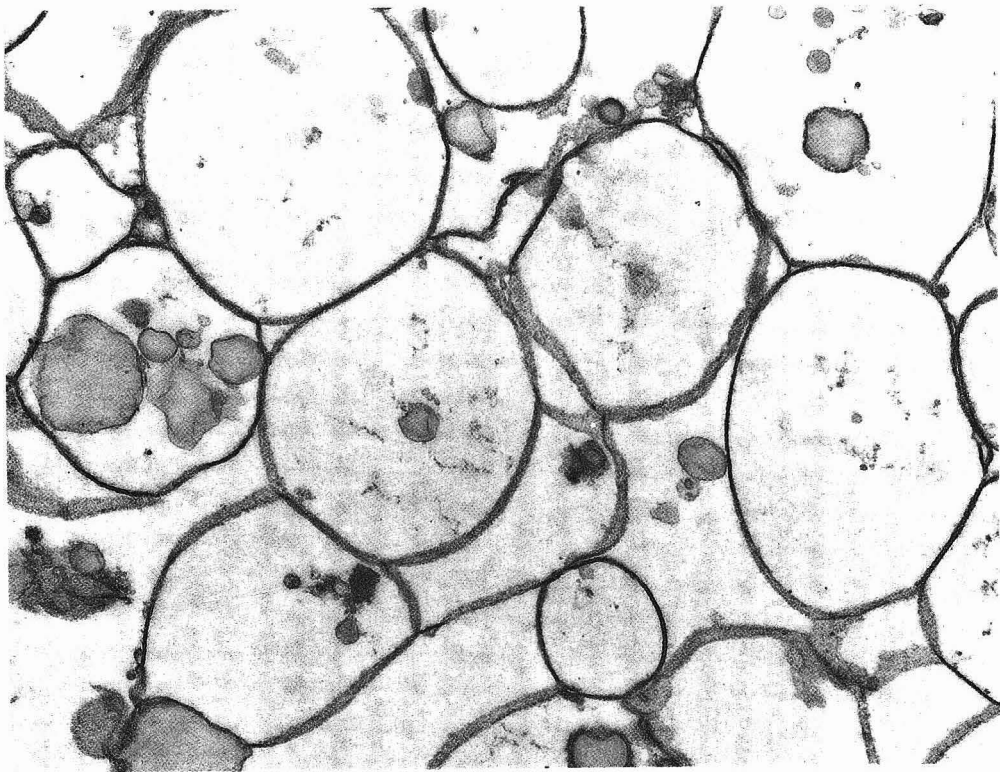
Figure 9. Lutoids from centrifuged latex (Zone 8B) containing micro-helices and osmiophilic particles. Magnification 36 000 X.
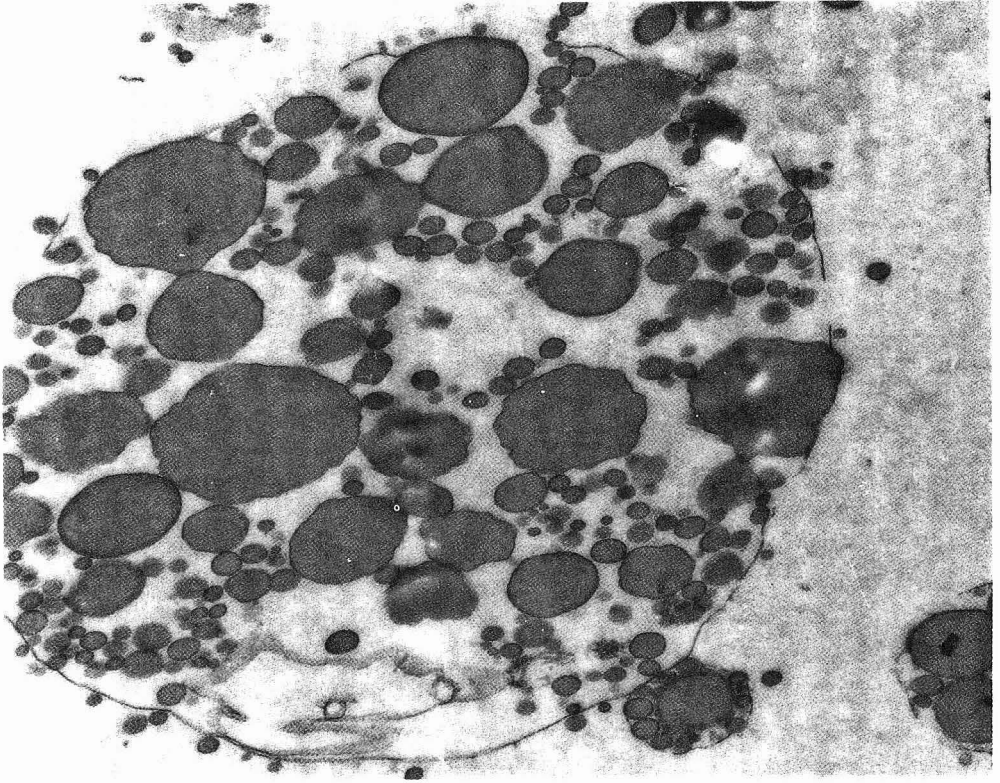

Figure 10. Lutoids from centrifuged latex (Zone 4, RRIM 501) with a large number of osmiophilic particles. Magnification 27 000 X.
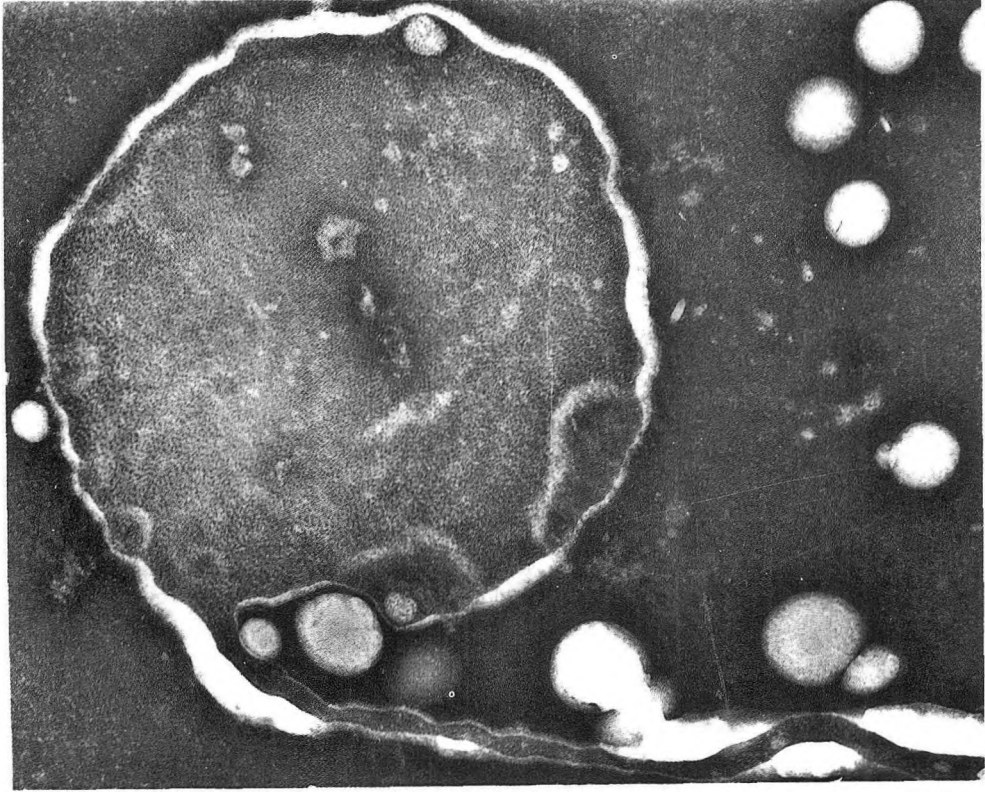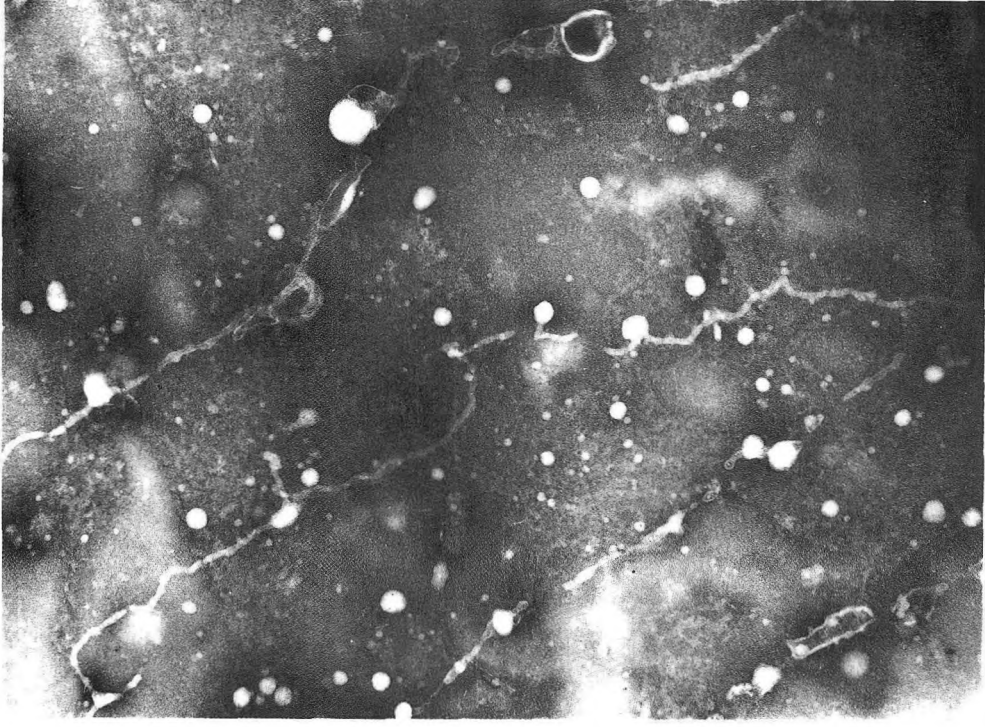
Figure 12. Thread-like material from bottom fraction of latex negatively stained with PTA. Magnification 25 000 X.

Figure 11. Thread-like extension of a PTA stained lutoid. Magnification 71 000 X.
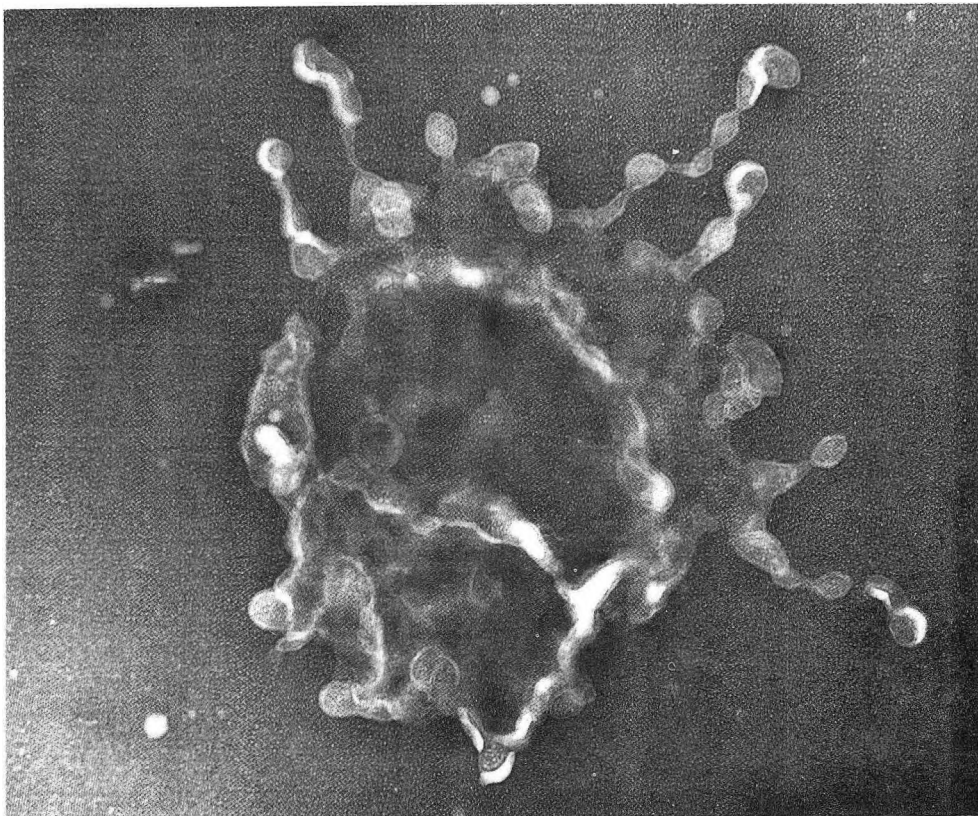
Figure 13. Tentacles in a lutoid after negative staining. Magnification 31 000 X.

The variety of developmental states of lutoids shown by electron microscopic investigation in this paper reveals a morphological complexity hitherto unsuspected. Proteins of various structural configurations are present in lutoids, sometimes depending on their state of development. Thus, prolutoids seem to be devoid of a large concentration of electron microscopically visible proteins showing remarkably striking crystalline features, which are observed in later stages of development. Microfibrillar protein from lutoids have been studied and characterised in detail by Audley[17].

Another protein obtainable from mature lutoids by methods of dialysis of latex had been studied by Gomez and Yip[18] who showed that it has a micro-helical configuration. Neither of these proteins visualised by the electron microscope in large quantities has been clearly identified to be associated with any of the enzymatic activities reported in the bottom fraction or lutoid particles.

Studies reported here also show many lutoids containing osmiophilic particles resembling rubber particles. When this was first noticed[5], lutoids were described as polymerisation vessels for rubber. However, keeping in mind the possibility that vacuoles often merge, the possibility that these osmiophilic particles are accidental inclusions in the lutoids cannot be ruled out. Furthermore, many of these electron micrographs were prepared from centrifuged material which increases the chances of coalescence of smaller lutoids into bigger lutoids probably also enclosing particles in the surrounding medium rather readily. Even the multi-vesicular bodies noted in this study could

be explained in this manner. However, such lutoids have been noticed in tissue sections as well. So perhaps a phagocytic function may be attributed to some lutoids. Analysis of the bottom fraction after ultracentrifugation indicates about 5%-7% rubber[19] some of which are present in the sedimented particles.

Southorn[20]'s observation of thread-like reticulum in fresh latex several years ago has not received much further attention. In this study of lutoids from centrifuged preparations examined by the negative staining method, often thread-like materials are observed. Whether they are aspects of lutoid membranes reflecting physical changes during latex flow or associated endoplasmic reticulum is still not clear.

Students of biochemical mechanisms in *Hevea* latex often deal with fractions of mixed origin or heterogeneous populations of lutoids and/or Frey Wyssling complexes. There is a need therefore to develop and refine more exact separation methods of particles to increase our knowledge of the site of various enzyme activities found in latex fractions. As demonstrated in this study, lutoids occur in various morphological types perhaps reflecting their degree of maturity and/or functional differences. Existing biochemical information does not account for the morphological differences observed. It is perhaps necessary to resolve this question through correlated biochemical and electron microscopical studies.

The segregation of cations in latex by the lutoids is well known. The lutoid membrane must therefore have special capacity for selective solute transport at the boundary. Chrestin[16] has thrown some light on the biochemistry of transport of ions at the lutoid membrane barrier. It would appear that further progress in the control or prevention of tree dryness will have to await development of techniques to influence the transport properties of lutoid membranes or the coagulation mechanisms existing in latex to prevent pre-coagulation at the cut, and *in situ* coagulation in latex vessels.

Lutoids occur in various morphological forms and it is difficult to believe that all of them have the same function. Although some of these states are developmental states, the mature lutoids display different metabolic states as inferred from their morphological variety. More research is necessary to resolve these questions.

REFERENCES

1. HOMANS, L.N.S., VAN DALFSEN, J.W. AND VAN GILS, G.E. (1948) Complexity of Fresh *Hevea* Latex. *Nature,* **161,** 177.

2. HOMANS, L.N.S. AND VAN GILS, G.E. (1948) Fresh *Hevea* Latex: a Complex Colloidal System. *Proc. 2nd Rubb. Technol. Conf. London,* 292.

3. FREY-WYSSLING, A. (1929) Microscopic Investigations on the Occurrence of Resins in *Hevea* Latex. *Archf. Rubbercult.,* **13,** 394.

4. RUINEN, J. (1950) Microscopy of the Lutoids in *Hevea* Latex. *Archf. Rubbercult.,* **27,** 255.

5. SCHOON Th. G.F. AND PHOA, K.L. (1956) Morphology of the Rubber Particles in Natural Latices. *Archf. Rubbercult.,* **33,** 195.

6. SOUTHORN, W.A. (1960) Complex Particles in *Hevea* Latex, *Nature (Lond.)* **188,** 165.

7. SOUTHORN, W.A. (1961) Microscopy of *Hevea* Latex. *Proc. nat. Rubb. Res. Conf. Kuala Lumpur 1960.*

8. RESING, W.L. (1955) Variability of *Hevea* Latex. *Archf. Rubbercult.,* **32,** 75.

9. DICKENSON, P.B. (1965) The Ultrastructure of the Latex Vessel of *Hevea brasiliensis. Proc. MRPRA Jubilee Conf. Cambridge 1964,* 52.

10. GOMEZ, J.B. AND MOIR, G.F.J. (1979) The Ultracytology of Latex Vessels in *Hevea brasiliensis. MRRDB Monograph No. 4.*

11. GOMEZ, J.B. AND SOUTHORN, W.A. (1969) Studies on Lutoid Membrane Ultrastructure. *J. Rubb. Res. Inst. Malaya.,* **21(4),** 513.

12. WIERSUM, L.K. (1975) Enkele Latexproblemen. *Vakbl. Biol.,* **3,** 17.

13. SOUTHORN, W.A. (1969) Physiology of *Hevea* (Latex Flow). *J. Rubb. Res. Inst. Malaya,* **21(4),** 494.

14. GOMEZ, J.B. (1983) Physiology of Latex (Rubber) Production. *MRRDB Monograph No. 8.*

15. PUJARNISCLE, S. (1968) Caractere lysosomal des lutoides due latex d'*Hevea brasiliensis.* Mull. Arg. *Physiol. Veg.,* **6.** 27.

16. CHRESTIN, H. (1989) *Physiology of Rubber Tree Latex. (d'Auzac, J., Jacob, J.L. and Chrestin, H. eds.),* p. 431. Raton, Florida: CRS Press Boca.

17. AUDLEY, B.G. (1964) Studies of an Organelle in *Hevea* Latex containing Helical Protein Microfibrils. *Proc. MRPRA Jubilee Conf. Cambridge 1964.* London: Maclaren & Sons.

18. GOMEZ, J.B. AND YIP, E. (1975) Microhelices in *Hevea* Latex. *J. Ultrastruc. Res.,* **52,** 76.

19. GOMEZ, J.B. AND YONG, W.M. (1989) Unpublished Results.

20. SOUTHORN, W.A. (1961) Thread-like Reticulum in Latex from *Hevea brasiliensis* and its Relation to Latex Particles. *Nature (Lond.),* **189(4769),** 1000.

ORDER FORM
JOURNAL OF NATURAL RUBBER RESEARCH

Please send to
    The Secretary
    Editorial Committee
    Journal of Natural Rubber Research
    Rubber Research Institute of Malaysia
    P.O. Box 10150, 50908 Kuala Lumpur, Malaysia

Name: _____
(Please print)

Address: _____

_____

_____

_____

No. of copies: _____

Volume/Issue: _____

_____

_____

_____

Form of Remittance: Cheque/Bank Draft/Postal Order/Money Order payable to 'Rubber Research Institute of Malaysia' (please include postage charges)

Amount: M$/US$ _____

Date: _____   Signature: _____

Journal Price

	Overseas rate			Local rate
Per issue	Per volume (4 issues)		Per issue	Per volume (4 issues)
US$15	US$50		M$30	M$100

Postage

	By sea			By air
Per issue	Per volume (4 issues)		Per issue	Per volume (4 issues)
US$1	US$4		US$5	US$20

กำหนดส่ง

17. ก.ย. 2534

25. ต.ค. 2537

2 2 ธ.ค.

JOURNAL OF NATURAL RUBBER RESEARCH

Scope

The Journal of Natural Rubber Research is one of the most renowned publications in the world on natural rubber. It publishes results of research and authoritative reviews on all aspects of natural rubber.

Contributions are welcome on any one of the following topics: Genetics, Breeding and Selection; Tissue Culture and Vegetative Propagation; Anatomy and Physiology; Exploitation: Tapping Systems and Stimulation; Agronomic Practices and Management; Nutrition and Fertiliser Usage; Soils: Classification, Chemistry, Microbiology, Use and Management; Diseases and Pests; Economics of Cultivation, Production and Consumption and Marketing; Mechanisation; Biochemistry and Biotechnology; Chemistry and Physics of Natural Rubber; Technology of Dry Rubber and Latex; Natural Rubber Processing and Presentation, Product Manufacture, End-uses and Natural Rubber Industrialisation; Tyres; NR and SR Blends; and, Effluent Treatment and Utilisation.

The Editorial Committee, in accepting contributions for publication, accepts responsibility only for the views expressed by members of the MRRDB and its units.

Best Paper Award

Papers submitted to each volume of the **Journal** will be considered for the annual **Best Paper Award** which carries a cash prize of 1000 ringgit and a certificate. The decision of the Editorial Committee and publisher of the **Journal** on the award will be final.

Submission of Articles

General. Manuscripts should be typewritten double-spaced throughout on one side only of A4 (21.0 × 29.5 cm) paper and conform to the style and format of the **Journal of Natural Rubber Research.** Contributions, to be submitted in four copies (the original and three copies) should be no longer than approximately ten printed pages (about twenty double-spaced typewritten pages). Intending contributors will be given, on request, a copy of the journal specifications for submission of papers.

Title. The title should be concise and descriptive and preferably not exceed fifteen words. Unless absolutely necessary, cientific names and formulae should be excluded in the title.

Address. The author's name, academic or professional affiliation and full address should be included on the first page. All correspondence will be only with the first author, including any on editorial decisions.

Abstract. The abstract should precede the article and in approximately 150–200 words outline briefly the objectives and main conclusions of the paper.

Introduction. The introduction should describe briefly the area of study and may give an outline of previous studies with supporting references and indicate clearly the objectives of the paper.

Materials and Methods. The materials used, the procedures followed with special reference to experimental design and analysis of data should be included.

Results. Data of significant interest should be included.

Figures. These should be submitted together with each copy of the manuscript. Line drawings (including graphs) should be drawn in black ink on white drawing paper. Alternatively sharp photoprints may be provided. The lettering should be clear. Half-tone illustrations may be included. They should be submitted as clear black-and-white prints on glossy paper. The figures should be individually identified lightly in pencil on the back. All legends should be brief and typed on a separate sheet.

Tables. These should have short descriptive titles, be self-explanatory and typed on separate sheets. They should be as concise as possible and not larger than a Journal page. Values in tables should include as few digits as possible. In most cases, more than two digits after the decimal point are unnecessary. Units of measurements should be SI units. Unnecessary abbreviations should be avoided. Information given in tables should not be repeated in graphs and *vice versa.*

Discussion. The contribution of the work to the overall knowledge of the subject could be shown. Further studies may also be projected.

Acknowledgements. These can be included if they are due.

References. References in the text should be numbered consecutively by superscript Arabic numerals. At the end of the paper, references cited in the text should be listed as completely as possible and numbered consecutively in the order in which they appear in the text. No reference should be listed if it is not cited in the text. Abbreviations of titles of Journals should follow the **World List of Scientific Periodicals.**

Reprints. Twenty-five copies of Reprints will be given free to each author. Authors who require more reprints may obtain them at cost provided the Chairman or Secretary, Editorial Committee is informed at the time of submission of the manuscript.

Correspondence

All enquiries regarding the **Journal of Natural Rubber Research** including subscriptions to it should be addressed to the Secretary, Editorial Committee, Journal of Natural Rubber Research, Rubber Research Institute of Malaysia, P.O. Box 10150, 50908 Kuala Lumpur, or 260 Jalan Ampang, 50450 Kuala Lumpur, Malaysia.

Institut Penyelidikan Getah Malaysia

Rubber Research Institute of Malaysia